Université catholique de Louvain

Faculté des Sciences Appliquées

Département de Sciences de Matériaux et Procédés

Electrochemically template-grown multi-segmented metal-conjugated polymer nanowires

Décembre 2009

Jury Members

Prof. S. Demoustier-Champagne (UCL, supervisor)

Prof. J.-F. Gohy (UCL)

Dr. J.-L. Duvail (Université de Nantes, France)

Prof. R. Lazzaroni (Université de Mons)

Prof. B. Nysten (UCL)

Prof. C. Bailly (UCL, president)

A mes parents

Acknowledgements

J'aimerais exprimer ma sincère reconnaissance envers toutes les personnes qui ont contribué, directement ou indirectement, à la réalisation de ce travail de thèse.

Tout naturellement, je tiens d'abord à remercier chaleureusement ma promotrice Sophie Demoustier-Champagne pour l'encadrement exemplaire dont j'ai bénéficié au cours de ces cinq années. Je la remercie pour sa disponibilité permanente, ses conseils éclairés, pour la confiance qu'elle m'a accordée, ainsi que pour le temps passé dans l'amélioration de ce manuscrit. Je tiens par ailleurs à souligner combien j'apprécie ses qualités humaines.

Je remercie Christian Bailly, Jean-Luc Duvail, Jean-François Gohy, Roberto Lazzaroni et Bernard Nysten d'avoir accepté d'être membre de mon comité de Jury. Je leur sais gré du sérieux dont ils ont fait preuve dans l'évaluation du manuscrit, de l'intérêt qu'ils ont manifesté pour mon travail au cours de ma soutenance privée, ainsi que des remarques et conseils constructifs qui ont contribué à rendre cet ouvrage plus complet.

Je remercie nos collègues physiciens, en particulier Loïk et Sorin, pour la collaboration fructueuse qui nous a liés dans ce travail. Je leur suis pleinement reconnaissant d'avoir accepté que l'aspect « Mesures électriques des nanofils » figure dans cet ouvrage, et d'avoir grandement aidé le chimiste que je suis dans l'écriture de cette partie.

Je tiens à remercier plus personnellement Loïk pour son enthousiasme communicatif, sa rigueur dans le travail, mais aussi et surtout pour son amitié fidèle et sa fibre épicurienne à l'extérieur du labo. Je m'excuse pour les éventuels cheveux blancs que mes « nano-progénitures » auraient fait apparaître chez lui. Je lui souhaite le meilleur pour sa fin de thèse.

J'adresse à présent mes remerciements à Cédric, que la Franche-Comté a bien voulu nous prêter. De sa parenthèse belge, je n'ai que de bons

souvenirs, faits de rafales voire de SUPER-RAFALES, de cascades, de duels épiques au badminton, …mais pas de festivals de musique.

Je le remercie lui ainsi que Delphine d'avoir sollicité mon aide pour des analyses XPS dans leurs travaux respectifs. Je souhaite qu'ils sachent que les publications qui ont découlé de ces recherches ont pour moi une grande valeur symbolique car elles me lient à deux personnes que j'apprécie.

Il m'est impossible d'oublier dans tous ces remerciements la personne qui a débuté ce projet il y a six ans, Olivier. Je le remercie d'abord pour sa contribution capitale dans la mise au point des premiers nanofils multi-segmentés. Je lui suis, par ailleurs, extrêmement reconnaissant pour tous les conseils qu'il m'a donnés pendant les quelques semaines où nous nous sommes croisés, pour son coaching,… en bref, pour le relais efficace entre le post-doc et le doctorant débutant dont il fut l'auteur. Je le remercie enfin pour la très grande sympathie dont il a fait preuve à mon égard.

Je tiens à remercier également les deux mémorants que j'ai eu le plaisir d'encadrer, Nicolas et Ouassima. Les assister dans la réalisation de leur stage fut pour moi une expérience enrichissante.

J'aimerais saluer l'ensemble des personnes dont j'ai sollicité l'aide pour des techniques ou des domaines pour lesquels elles sont plus qualifiées que moi. Ainsi, je remercie Pascale pour le TEM/EDX, Michel Genet pour l'XPS, Xavier et Gaëtan pour la RMN. Je remercie Etienne, Colette, Julien et Laurent pour l'approvisionnement en membrane, ainsi que Maria pour leur métallisation. Je remercie également Etienne et John pour l'usinage des cellules en Téflon.

Je souhaite remercier Luc Piraux pour les éclaircissements qu'il m'a apportés concernant la spintronique.

Je remercie également Xavier pour les réponses qu'il a apportées à mes quelques questions de chimie organique.

Je tiens à saluer l'ensemble des membres du laboratoire POLY que j'ai eu le plaisir de côtoyer pendant ces cinq années. Par souci de concision, je ne les citerai pas.

Je remercie les créatrices du COGF, Halima et Françoise, ainsi que celles qui ont brillamment repris le flambeau afin que cette belle initiative perdure: Anne-Christine, Colette, Cécile et Alexandra. Merci à Pierre Godard d'avoir permis que toutes ces « guindailles et festivités » se réalisent.

Je remercie Aurore pour l'ensemble des services qu'elle m'a rendus.

Je remercie Dimitri pour les petits dépannages informatiques, et Anne-Christine pour son aide dans mes conflits avec WORD.

Je tiens aussi à remercier toutes les personnes que j'ai vu défiler dans le bureau. J'adresse un grand merci à mes « secrétaires personnels » d'avoir toujours scrupuleusement réceptionné et transmis les appels de Loïk.

Je remercie tous les sportifs du POLY pour les séances de volley, de badminton et de foot.

Je voudrais remercier également les gens du PCPM pour les « vendredis Brasse-Temps » que j'ai eu le plaisir de partager avec eux.

Je termine ce difficile exercice en remerciant de tout cœur mes proches.

Je remercie en particulier mes parents pour la confiance et le soutien sans faille qu'ils m ont accordés durant ces longues études.

Enfin, merci de tout cœur à Anne-Christine pour avoir su pendant ces derniers mois de thèse dissimuler ses soucis pour soulager les miens, pour m'avoir supporté, …et supporté. A charge de revanche.

Contents

List of main abbreviations and symbols

1D	one-dimensional
CP	conjugated polymer or conducting polymer
PPy	polypyrrole
PEDOT	poly(3,4-ethylenedioxythiophene)
PANI	polyaniline
PA	polyacetylene
PSS	poly(styrenesulfonate)
σ	electrical conductivity
VRH	variable range hopping
XPS	X-ray photoelectron spectroscopy
BE	binding energy
SDS	sodium dodecylsulfate
PC	polycarbonate
AAO	anodized aluminum oxide
Φ	diameter
SEM	scanning electronic microscopy
TEM	transmission electronic microscopy
CV	cyclic voltammetry
RE	reference electrode
L_j	length of the polymer junction
S_a	adhesion surface
L_m	gold meniscus length
L_{PPy}	polypyrrole segment length
R	(L_m/L_{PPy}) ratio
SAM	self-assembled monolayer
MUA	11-mercaptoundecanoic acid
MPA	3-mercaptopropionic acid
T_c	critical temperature
R	electric resistance
F	electric field
T_0	Mott temperature
k_B	Boltzmann constant
α^{-1}	localization length

$N(E_F)$	density of states at the Fermi Energy
F_0	critical electric field
$R(B)$	magnetoresistance
B_c	critical magnetic field
$\hbar$	Planck constant
NW	nanowire
EDX	energy-dispersive X-ray
R_c	contact resistance
R_p	resistance of the polymer segment
3DIN	three-dimensional instantaneous nucleation
3DPN	three-dimensional progressive nucleation
3PPA	3-(Pyrrol-1-yl) propanoic acid
L_{Ni}	length of Ni segment
L_{Co}	length of Co segment
$[\ ]$	molar concentrations

Overview of the Thesis

During the last decade, one-dimensional (1D) nanostructures (e.g. nanowires and nanotubes) have received a growing attention due to their potential use in many applications such as (bio-) sensors, electronic components, data storage, photovoltaic cells, field emission displays, actuators, surface protection, ... 1D nanostructures are defined as fibers with a diameter of sub-100 nm size. This nanoscopic dimension, negligible compared to the length, is known to be responsible of their exciting new properties. For about five years, there is an increasing interest into the design and synthesis of multi-component nano-objects, capable of performing several functions simultaneously. In this respect, multi-segmented nanowires including inorganic and organic materials are of special interest for improving our fundamental understanding of electrical transport at the nanoscale and for technological development of novel electronic devices. However, the development and use of low diameter multi-segmented wires is still hampered by the difficulties of building, at the nanoscale, strong interfaces between the different co-existing materials.

In this context, the main objective of our thesis was to develop and optimize synthesis processes allowing the preparation of a wide range of mechanically robust hybrid multi-segmented nanowires including inorganic (metal) and organic (conjugated polymer) materials, presenting potential applications in nanoelectronics.

The synthesis process used throughout this research work for producing the different multi-striped 1D nanowires is based on the electrochemical template method, using home-made polycarbonate membranes as templates. The technique, depicted in Scheme 1, consists in coating one face of the template with a metallic layer, used as working electrode for the sequential electrodeposition of the different materials within the nanopores of the template. Then, the resulting multi-segmented nanowires can be freed by successively removing the metal coating and the template. In order to obtain nanowires with the best possible structural quality, we developed an electrochemical method based on cyclic voltammetry. For all the studied systems, a special attention was paid to the structural characterization, by electronic microscopies, of the different metal/polymer interfaces created along the long axis of the nanowires.

Besides their many potential applications, such 1D anisotropic nanostructures are providing ideal systems to investigate the effect of the

confinement on the electrical properties. Therefore, the electrical transport properties of a large number of electrosynthesized multi-segmented nanowires were studied in collaboration with Loïk Gence and Sorin Melinte from UCL-DICE laboratory.

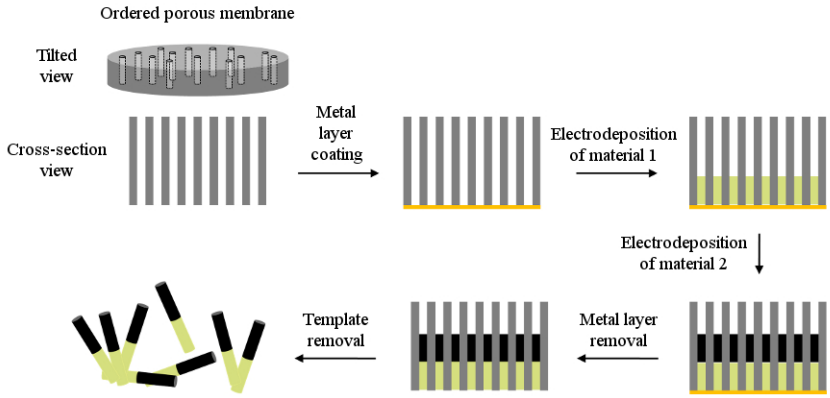

Scheme 1 *Schematic representation of the template electrochemical synthesis process used for the preparation of multi-segmented 1D nanostructures.*

The first chapter of this manuscript is a literature survey and is divided into three parts. The first one gives a presentation of the synthesis and main properties of conjugated polymers (CPs). The second part briefly discusses the genesis of nanotechnology. The third one gives an overview on 1D CPs and hybrid metal-CP multi-segmented nanostructures, by briefly presenting the different routes to prepare 1D nanostructures and their various potential applications.

In Chapter II, we report on the all-electrochemical template preparation of hybrid noble metal-polypyrrole(PPy) multi-segmented nanowires, their structural characterization and the study of their electrical transport properties.

Chapter III is devoted to the development of the synthesis of hybrid multi-segmented nanowires based on poly(3,4-ethylenedioxythiophene) (PEDOT). Among these systems, the tetra-segmented nanowires containing a PEDOT-PPy heterojunction exhibit original electrical characteristics that will be presented to the reader.

The fourth chapter presents a careful study of the impact of several electrosynthesis parameters on the resulting morphology of polyaniline (PANI) nanostructures. We will further discuss the synthesis and characterization of hybrid multi-segmented nanowires based on PANI.

Finally, Chapter V reports on the synthesis of hybrid multi-segmented nanowires containing one or two magnetic blocks. The developed process allowing the electrodeposition of CP segments on oxidizable magnetic nanowires and the improvement of the strength of the resulting interface will be finally described.

Chapter 1

Introduction

1.1 Conducting polymers

1.1.1 Introduction to conducting polymers: some basics

Traditionally until the middle of the 70s, polymers were only regarded as insulator plastics with their so appreciated features such as mechanical properties and processability. But among them, a material group exhibiting electrical properties, which is generally characteristic of metals and semiconductors, was discovered. Because they have in common an extended π-electron system, consisting of alternating single and double bonds along the polymer backbone, they are called conjugated polymers. The terms synthetic metals, name of a journal almost exclusively dedicated to this new class of materials, and conducting polymers are equally used, with reference to the unexpected high conductivity values reached for some of them. With the exception of polyacetylene (PA), typical conjugated polymers are based on a straight chain of repeated aromatic units consisting of five or six-membered rings. Figure 1.1 shows the ideal chemical structures of some intensely studied conjugated polymers. The represented neutral structures on no account explain that these polymers conduct electricity. If the conjugated polymers are insulators in their native state, an oxidation or a reduction of their chain, respectively referred to as p-type and n-type doping, causes a conductivity enhancement (See § 1.1.4).

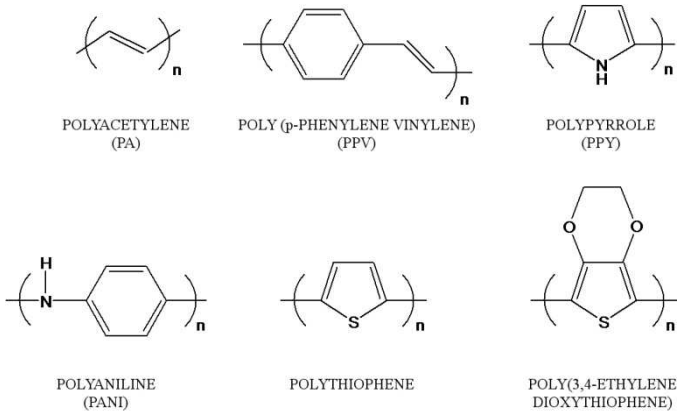

Figure 1.1 *Scheme representing ideal chemical structures of some intensely studied conjugated polymers.*

1.1.2 Historical background

The story of conducting polymers begins in 1973 when an inorganic polymer, the polysulfur nitride $(SN)_x$, was found metallic.[1] The discovery of its superconductivity two years later[2] encouraged chemists to understand its physicochemical properties[3,4] in order to find analogous polymeric systems exhibiting still more interesting electrical properties, but $(SN)_x$ remained a unique exception to conventional polymeric behavior. In 1977, even when a ten times greater level of conductivity in crystalline $(SN)_x$ modified with bromine was reported[5], the discovery of metallic to semiconducting properties adjustable by chemical doping in polyacetylene (PA) derivatives $(CHX_\alpha)_x$[6,7] was memorable as for the first time, an organic material was considered as an electricity conductor. Although to date levels of conductivity of doped $(CH)_x$ are still the highest recorded in the class of organic materials, PA has the disadvantages of being insoluble and instable in contact with oxygen.[8] Parallel to the efforts provided to improve the stability properties of PA to air[9], new conducting systems appeared in the late 70s. Among them, the heterocyclic polypyrrole (PPy), firstly reported in 1979[10], was considered as a significant advance in the development of stable organic conducting materials. Moreover, with these pioneers works, the electrochemical preparation of conducting polymers appeared as an alternative way of synthesis to the classical chemical strategy (See § 1.1.3). According to this new approach, the synthesis of many organic conducting polymers rapidly followed[11,12] in the early 80s. At the same time, increasing number of works on the physicochemical characterization were carried out in order to understand the chemistry governing the electrical transport [13,14] (See § 1.1.4 and 1.1.5). From the early 90s, the advent of materials with nanoscopic dimensions gave to the field a new considerable outburst as it was shown that by altering the size and shape of conducting polymers, it was possible to adjust their fundamental properties.[15]

1.1.3 Synthesis routes

Synthesis of conductive polymers generally uses one of the two main following ways: the chemical or the electrochemical process. Each of this process has advantages and disadvantages summarized in Table 1.1.

Table 1.1 *Comparison of the advantages and disadvantages of chemical and electrochemical conducting polymer synthesis.*

Polymerization process	Advantages	Disadvantages
Chemical Polymerization	Large-scale production More options to modify conducting polymer backbone covalently	Thin films cannot be prepared
Electrochemical polymerization	Doping occurs simultaneously Wide choice of dopant ions by selecting the appropriate electrolyte Thin film synthesis possible Straightforward synthesis	Low amount of produced polymer Difficulties in removing polymeric material from electrode surface

a) Chemical synthesis

Various chemical methods have been successfully developed for preparing conducting polymers, but establishing a general route is difficult. Nevertheless, a classical method, common to polyheterocyclic polymers, consists in employing oxidizing agents such as $FeCl_3$, $Fe(OTs)_3$, $Cu(ClO_4)_2 6H_2O$ or $(NH_4)_2S_2O_8$[16,17,18,19] (Figure 1.2). The corresponding anion is incorporated in the polymer chains as dopant ions. Many chemical strategies have been developed to produce conducting polymers with highly interesting properties. Some of them have leaded to applications, as the famous BAYTRON P synthesis of PEDOT/PSS, developed by Bayer AG[20] and used for the antistatic treatment of photographic films[21] and other plastics[22].

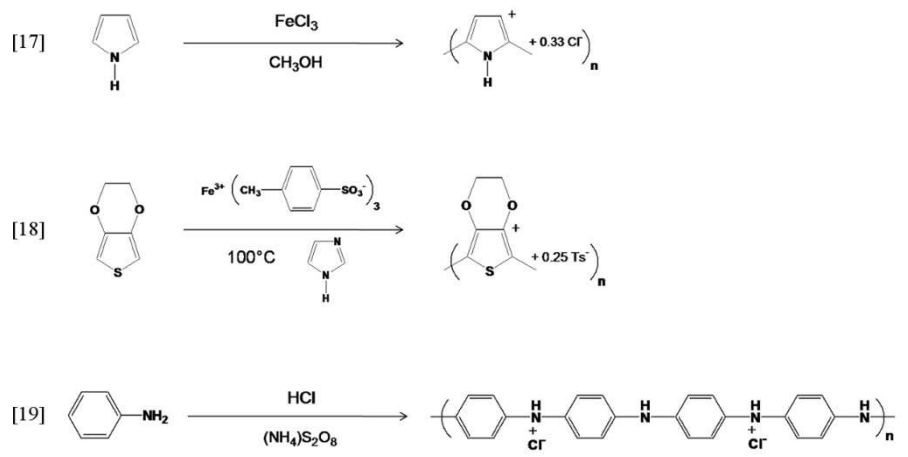

Figure 1.2 *Some oxidative chemical polymerizations of common conducting polymers. The resulting products correspond to the ideal expected structures.*

b) Electrochemical synthesis

When A. F. Diaz and K. Kanazawa[10] reported in 1979 their work on PPy, it was not only the discovery of polyheterocycles as new organic conducting polymers, but the popularization of the electropolymerization technique, first reported by A. Dall'Olio *et al*[23] in 1968. With the electrochemical polymerization, the fast developing field of electrochemistry triggered the era of easily processable polymer. Electrochemical polymerization[24] is classically carried out using a three-electrode configuration (working, counter and reference electrodes) in a bath consisting of the monomer and an electrolyte (playing the role of dopant) dissolved in an appropriate solvent (Figure 1.3). When current passes through the solution, electrodeposition occurs at the positively charged working electrode or anode. At the surface of this latter one, insoluble polymer chains progressively increases resulting from a mechanism with a sequence of three steps "oxidation (a), coupling (b), deprotonation (c)" firstly described in 1983 by Diaz and its co-workers[25] for the PPy and applicable to other polyheterocycles (Figure 1.4).

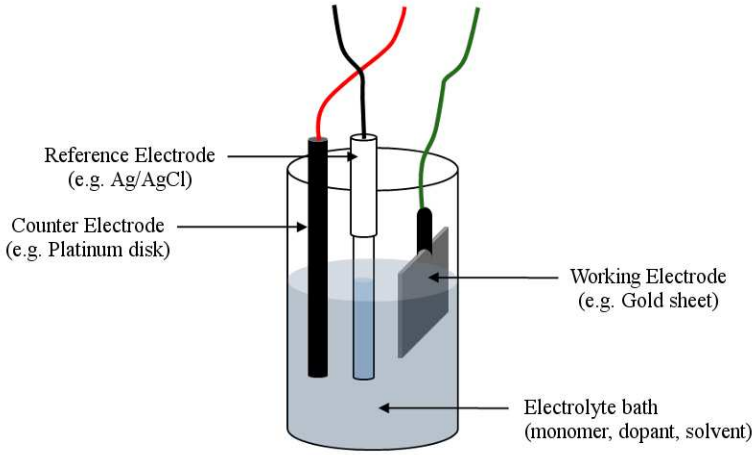

Figure 1.3 *Typical three electrode electrochemical set up.*

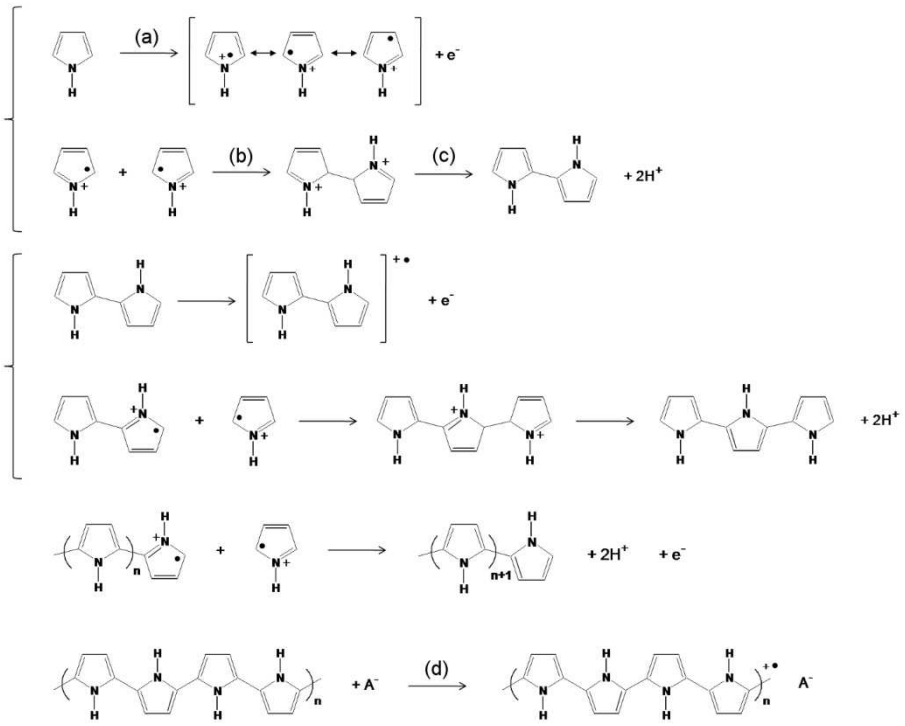

Figure 1.4 *Scheme representing the mechanism of the PPy electrochemical polymerization (based upon Diaz's mechanism[25]).*

The properties of the resulting conducting polymer and then its utility for possible further applications depend on an important number of parameters such as solvent, electrolyte, temperature, deposition time or deposition technique. For example, poorly nucleophilic aprotic solvents are preferred to generate stronger and more conductive polymer because nucleophilic protic solvents can lead to side reactions with radical cations, disrupting chain growth. Electrosynthesis at low temperature are equally known to generate conducting polymers with better physical characteristics.[26] Different levels of conductivity are obtained for a same polymer depending on the used dopant.[27] The electrochemical way of synthesis is generally preferred to chemical polymerization for many reasons. Electrochemical polymerization rapidly produces from small amounts of monomer a directly conducting polymeric film with a thickness easily controllable by the charge used during polymerization and with shapes and dimensions defined by the electrode characteristics. The possibility to work in aqueous solution reduces the environmental impact and allows to make interact the electrodeposited polymeric materials with biomolecules for applications such as in biosensing. In spite of these attractive features, the electrogeneration of conductive polymers presents two main defaults. The first disadvantage concerns the low amounts of produced polymer. The second disadvantage is linked to the fact that our knowledge of the electrochemical mechanism remains incomplete. The optimization of electrogenerated polymer properties requires that the interdependent effects of all the different involved variables are controlled, which will be possible achieved after a considerable fundamental research.

1.1.4 Conductivity and doping of conducting polymers

The extended π-electron system, common characteristic of conducting polymers and described in physics as a delocalized charge-density wave, allows charge mobility along and between the polymer chains, but the phenomenon is limited by disorder and Coulombic interactions between electrons and holes. Electrical conductivity σ, expressed in Siemens per unit of distance ($S.cm^{-1}$), measures the ability of a material to pass a current. In terms of σ, three categories of materials are distinguishable. Generally, insulators exhibit a conductivity less than 10^{-8} $S.cm^{-1}$, conductors (metals)

exhibit conductivity greater than 10^3 S.cm^{-1}, and semiconductors have intermediate conductivities. The electrical conductivity is logically the quasi-systematically investigated property in organic conjugated polymers. The one of heterocyclic polymers can be considerably enhanced passing from 10^{-10} S.cm^{-1} to 10^2 S.cm^{-1} in their neutral and oxidized states, respectively. Figure 1.5 shows the fields of conductivity of the most common conducting polymers, comparing them with some reference materials.

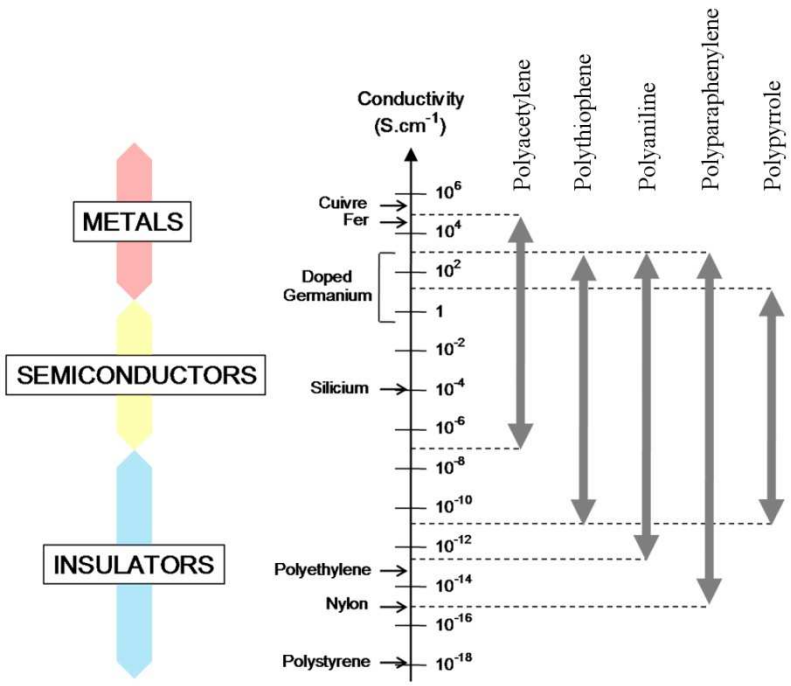

Figure 1.5 *Conductivity ladder locating the common conducting polymers.*

In the presence of "adapted" oxidizing or reducing species (which means capable of oxidizing or reducing the polymer without leading side reactions that would make it lose its ability to conduct electricity), an electron is removed from or added to the π-electron system. This charge injection leads to a free radical and a positive or negative charge and inserts a counter anion or cation in the conjugated backbone to maintain charge neutrality. These processes of oxidizing or reducing a neutral polymer are called p-doping or n-doping respectively and the counterion (resulting of electrolyte in the case of electrochemical polymerization) is known as dopant. The p-doping

process of neutral polypyrrole is showed in Figure 1.4.d. Upon doping process, polymer chains undergo deformations around the charge. The localized charges combined with the local chain distortions are known as charged polarons (i.e. radical ions) or bipolarons (i.e. dications or dianions)[28] (Figure 1.6). These particles are considered at the origin of charge mobility along and between the chains, proceeding by attraction of electrons in one repeating-unit to the nuclei in neighboring units. The ordered movement of these charge carriers, comparable with the mobility of electron-hole pairs created in conventional semiconductors, generates electrical conductivity.

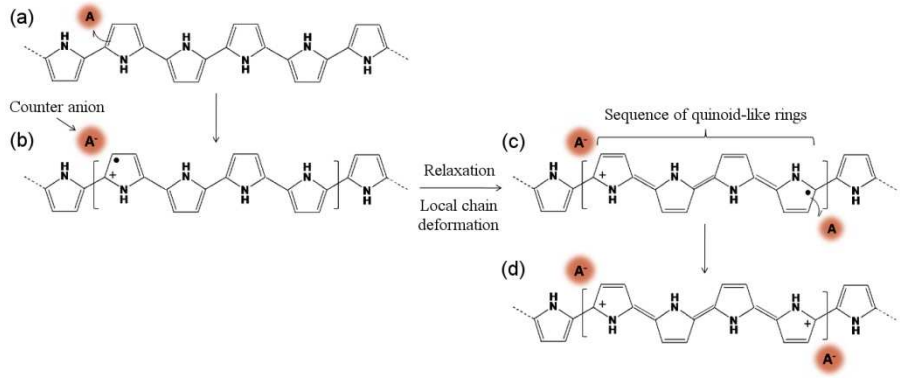

Figure 1.6 *Introduction of polaron and bipolaron lattice deformation upon p-doping in PPy. (a)→(b) Oxidation products a free radical and a positive charge coupled to each other via a local resonance. (b)→(c) To separate the two created defects, a chain deformation of higher energy than the non-affected part of the conjugated framework takes place along the sequence of quinoid-like rings. The resulting delocalized positive charge is in a lower electronic state. The considerable amount of energy consumed during this distortion process limits the number of quinoid-like cycles involved in the resonance linking the two defects together. This number of quinoid-like units depends on the polymer. In the case of PPy, four pyrrole rings may involve in the chain deformation around the charge. (c)→(d) Upon further oxidation, formation of a bipolaron by removing the unpaired electron of the polaron.*

Energetically, conducting polymers distinguish themselves from metals by the existence of a band gap, corresponding to the distance between their empty conducting band and their fulfilled valence band. The smaller their

band gap, the more conductive they are. Figure 1.7 presents the modification in energy band structure of PPy subsequent to doping. Depending on doping level, localized electronic states or bands are introduced in the band gap. By increasing doping level, band gap decreases and then conductivity is enhanced. Besides the oxidation level/doping, many other parameters such as nature of the dopant, synthesis temperature and electrodeposition technique influence the resulting conductivity of the polymer.

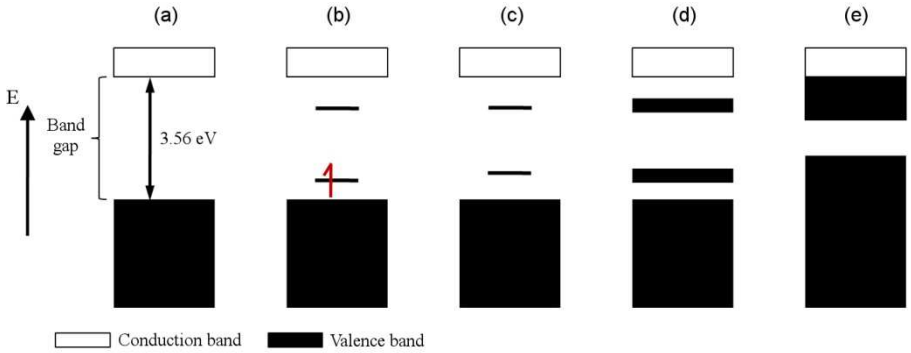

Figure 1.7 *Energy band structure evolution of PPy upon doping. (a) Neutral polymer. (b) Polymer containing a polaron. (c) Polymer containing a bipolaron. (d) High doping level (≈ 33%) resulting from electrochemical doping. Formation of bipolaron bands. (e) Theoretical doping level of 100%. Bipolaron bands merges with conduction and valence band, decreasing the band gap (adapted from Guimard et al.[29]).*

As we have previously seen conductivity in a conjugated polymer results from doping which simultaneously consists in chemically or electrochemically injecting a charge and inserting a counterion in the conjugated backbone. We have equally seen that the main source of charge carriers in heterocyclic polymers consists in entities based on the polarons and bipolarons particles. Although these basic principles are known for a long time, detailed knowledge of charge transport in these highly disordered materials (89 to 100% of amorphous structure in PPy) is still quite limited insofar as trailing the path of the charge carriers through the polymer still cannot be achieved. This generally encountered high degree of disorder increases the number of parameters involved in charge transport as interchain interactions, anisotropic diffusion of charge carriers or still the role of dopant counterions and the individual contributions of these different

parameters are difficultly quantifiable. Consequently, the extreme complexity of the conducting polymer structure makes the theoretical modeling of transport properties a true challenge. Among the different proposed theoretical models to predict the electric conduction process in conducting polymers, the Mott's variable range hopping (VRH)[30] remains the most used. It describes the low temperature behavior of the conductivity in materials where states are localized and its predictions are generally found to be in correlation with the experimental results. However, the VRH model mainly concerns the strongly disordered conducting polymers. The already old case of highly conducting PA and the more recent progresses accomplished in the preparation of other conjugated polymers with strongly reduced disorder made that other more adapted theories had to be invoked to describe the transport mechanism occurring in weakly disordered conducting polymers. For theses polymeric materials in which extensive conduction regions are separated by small insulating gaps, the firstly proposed Sheng's fluctuation-induced tunneling (FIT) model[31] was successfully applied to some systems such as PA. Later, disorder-induced metal-insulator transition was found to interpret the behavior of electrical conductivity in highly conducting PANI and PPy.[32,33] Currently, finding a general behavior for charge transport in conducting polymers is not easy, but it is known that structural heterogeneities, common characteristic to all the polymers, play a predominant role in their electronic properties.[34]

1.1.5 Chemical structure, a view by XPS

Concerning the characterization of a typical conducting polymer, efforts essentially focused on the understanding of the structure, charge transfer and degradation processes. X-ray photoelectron spectroscopy (XPS) proved to be an adapted tool to characterize electroactive polymers since it yields simultaneous chemical and electronic structural information without material destruction.

This is usually by this technique that the electronic structure of the polyheterocycles was studied. Indeed, a very convenient method for determining the doping ratio of the polymer is to analyze the core level spectrum of the heteroatom. The doping of the polymer, which consists in the introduction of counterions between the polymeric chains, leads to a

broadening of the peak relative to the heteroatom. A percentage of these heteroatoms located in the neighborhood of doping species present a shift of their binding energy (BE). By peak decomposition, it is possible to calculate the proportion of heteroatoms affected by charge injection, and thus to determine the doping ratio. Pfluger and Street[35] and Skotheim *et al.*[36] were the first to find *N1s* spectra with a strong asymmetry on the high BE side for PPy/ClO_4 samples (see Figure 1.8.a). These pioneering works suggested delocalized positive charges or partially charged nitrogens. Munro *et al.*[37] then succeeded first in quantitatively correlating the *N1s* high BE component with the doping level of the polymer by making the assumption that all oxidized nitrogen atoms bear a unit positive charge. The *N1s* peak generally develops another shoulder on its low binding energy side. Inganäs *et al.*[38] ascribed this component to deprotonated pyrrolylium or imine-like nitrogens (=N- structure) whose presence affects the conductivity of the polymer. All these studies revealed the co-existence of chemically different nitrogens, neutral and positively charged, in the *N1s* core-level spectrum. In Figure 1.8.b, the *N1s* XPS spectrum of a PPy/PF_6 sample reported by Joo *et al.*[39] is presented. It is possible to distinguish the neutral nitrogen atoms (BE < 400 eV) from doped nitrogen atoms (BE > 400 eV) and thus to determine the value of the doping ratio.

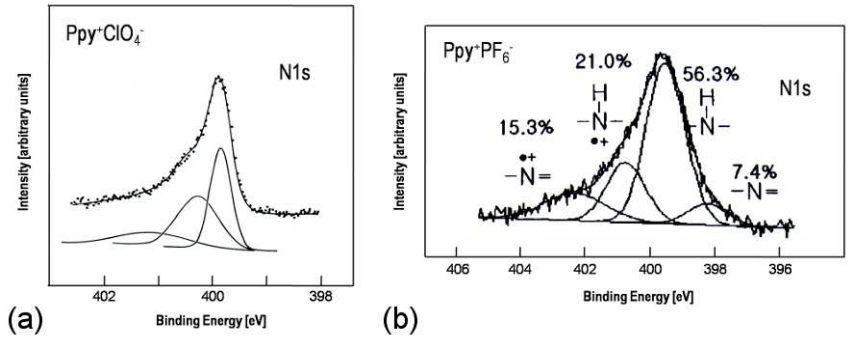

Figure 1.8 *(a) N1s XPS core level spectrum of polypyrrole perchlorate (Pfluger and Street[35]). (b) N1s core level spectrum of polypyrrole perfluorate (Joo et al.[39]).*

Few structural studies on the poly(3,4-ethylenedioxythiophene) (PEDOT) were reported until now. In these rare XPS works, the analysis of the sulfur heteroatom was conducted in accordance with previous works

done on polythiophenes.[40,41] Aaron *et al.*[42] considered that the *S2p* signal for PEDOT films electrochemically synthesized in a $LiClO_4$ acetonitrile solution can be deconvoluted in two doublets. That of lowest energy can be attributed to the sulfur atoms in the neutral state, and that of highest energy to the thiophene sulfur atoms with a positive partial charge ($S^{\delta+}$) due to the presence of a perchlorate dopant anion in the neighborhood. More recently, Duvail *et al.*[43] reported XPS studies done on PEDOT material electrochemically synthesized in a micellar $LiClO_4$ aqueous solution. In their analysis of the *S2p* spectrum, they took into account the contribution of the shake-up $\pi \rightarrow \pi^*$ transitions responsible for the broadening of the sulfur peak on its high binding energy side and suggested by Tourillon *et al.*[44]. Considering the two doublets due to the sulfur atoms of the dopant anion (dodecylsulfate), they obtained a *S2p* signal in five components as illustrated in Figure 1.9.a. They also showed that, under the same conditions of electropolymerization, the doping ratio for 35 nm PEDOT nanowires is reduced by about a factor of 2 in comparison with the film (Figure 1.9.b). These XPS results were in perfect agreement with electric transport measurements which indicate that the insulating behavior of PEDOT nanowires is larger when their diameter decreases. They showed that the confined synthesis induces competitive effects, a better alignment of polymer chains and the increase of conjugation length in favor of electrical conductivity on one side and the doping ratio decrease on the other side. This makes the description of electric transport at sub-100 nm scale more complex than it was before.

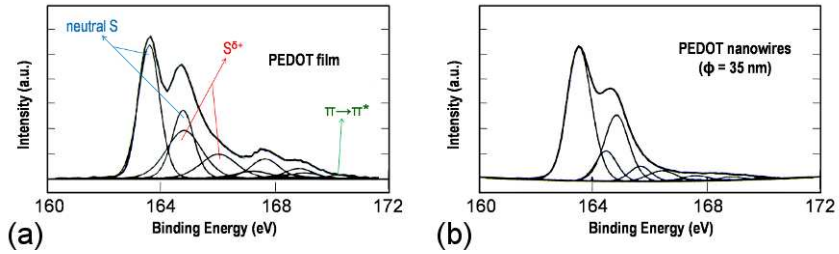

Figure 1.9 *(a) S2p XPS core level spectra for (a) a PEDOT film and (b) 35 nm PEDOT nanowires (Duvail et al.[43]).*

1.2 Genesis of nanotechnology

Generally, when speaking of the genesis of nanotechnology, two main symbolic dates are in priority reminded. The first one precisely goes back half of a century, in 1959, when Richard Feynman, on the occasion of the annual meeting of the American Physical Society, evoked in his famous talk entitled "There's plenty of room at the bottom"[45] the possibility of manipulating matter on the atomic scale. Feynman, remarkable visionary and pedagogue, imagined that writing the entire 24 volumes of the Encyclopedia Britannica on the head of a pin was conceivable. The second remembered date, 1974, corresponds to the year when the term "nanotechnology" was created by Norio Taniguchi to refer to the group of techniques intended for conceiving, fabricating, characterizing and applying structures on the nanoscale.[46] Parallel to theses anecdotic events, rapidly conscious that the efforts made to decrease the size of the electronic devices have their physics limits, the visionary minds envisaged a new paradigm, complementary or competing of the classical "top-down" strategy which aims to miniaturize objects, instruments and machinery. This approach is based on the assembling of the smallest elements, the molecules, which by opposition will be called "bottom-up". The electronics industry that launched the race to miniaturization in the early 50s can be considered as the main driving force in the race to the extremely small.

The electronics industry, motor of the miniaturization race

The different revolutions known by electronics were associated to steps of radical miniaturization linked to major inventions or discoveries. The invention of the transistor in 1947 by the American searchers John Bardeen, William Shockley and Walter Brattain,[47,48] Nobel prizewinners in Physics in 1956, and progress accomplished during the early 50s in the proceedings to refine the silicon,[49,50,51] semi-conductor material above all, led to the advent of electronics based on silicon transistors.[52] Then, as a result of the works on photolithography carried out by Jules Andrus and Walter Bond in 1955 allowing to improve the manufacturing of the semi-conductor substrates,[53] Jack St Clair Kilby permitted the second revolution of radical miniaturization when he invented the integrated circuit in 1958. This second essential invention allowed to still reduce the size and the cost of the

electronic machines by integrating on a same electronic circuit more and more transistors without using the electric wires. The World was precipitated into the microelectronics area. From that moment, the number of transistors that could be integrated inexpensively on silicon ships doubled approximately every 18 months until this day (from 64 in 1965 to 2300 transistors in 1971 for the most performing circuit). This long-term trend, expressed for the first time in 1965 and adjusted some years later by Gordon Moore (the famous Moore's Laws), very soon made the scientists community become conscious the all-silicon technology had its limits and it was necessary to find a complementary competing alternative by finding potential substitutes to the "King Silicon". In parallel of this miniaturization race, chemists, biochemists and molecular geneticists moved in the other direction by working with the smallest existing objects, the molecules. During the 70s, two famous isolated works envisaged organic components as conductors of current. In 1974, Mark A. Ratner and his graduate student were the first ones to suggest the idea that molecules could act as electronic circuit components.[54] These theoretical works, considered as a major contribution to the field of molecular electronics, gave an approach, certainly futuristic since the stage of commercialization is not yet reached today, but advantageous in term of cost, efficiency and reproducibility. In 1977, the pioneer investigations of Alan J. Heeger, Alan G. MacDiarmid and Hideki Shirakawa, Nobel laureates in 2000, showed that after some modifications, a conjugated polymer can conduct electricity.[55] Nevertheless, we will have to wait the early 80s to see the different fields such as chemistry, physics and engineering being concretely joined towards the knowledge of the extremely small.

Observe and manipulate the object at the nanoscale

In the 80s, two major inventions gave nanotechnology a fantastic outburst. With the Scanning Tunneling Microscope (STM) developed by Gerd Binnig and Heinrich Rohrer in 1981,[56] Nobel Prize in Physics in 1986, and the Atomic Force Microscope (AFM) invented by the same Binnig, Calvin Quate and Christoph Gerber in 1986,[57] it became possible to obtain atomic-scale images of metal surfaces and even to manipulate atoms and molecules. From that moment on searchers were capable of "seeing" atoms. During this decade two novel carbon structures were found. The fullerenes

in form of spherical "buckyballs" were discovered by Robert Curl, Harold Kroto and Richard Smalley in 1985.[58] Few years later in 1991, the carbon nanotubes, members of the fullerene structural family, were identified for the first time by Sumio Iijima[59] and constitute one of the two most essential development in nanotechnology with the discovery of conducting polymers.

New promising nano-objects

In 1989, Zhihua Cai and Charles R. Martin found that polyheterocycles synthesized in a confined environment have dramatically better electrical properties than their bulk counterparts. With this discovery, the "hard-template" method (see § 1.3.2 c) rapidly became one of the most commonly used synthetic route to produce quasi one-dimensional structures with submicrometer and sub-100 nm dimensions. The 80s were the decade of development of the first instruments to characterize small objects. With quasi one-dimensional conjugated polymers nanostructures and carbon nanotubes, researchers have now promising nano-objects to study. From the 90s, the development of synthetic strategies and analytical instruments for building and characterizing nanostructures, the identification of the consequences of the miniaturization on their electrical, magnetic, optical, mechanical and chemical features, and the use of such properties in the fabrication of new devices were the focus of numerous studies. These three areas of study were defined by Chad A. Mirkin in the late 90s to describe nanoscience and nanotechnology. 25 years later its symbolic birth, the field of nanoscience and technology had acquired sufficient credibility to receive massive financial support. In 2005, global investment was estimated at 9 billion dollars per year.

1.3 1D conducting polymer nanostructures

1.3.1 Overview

Nanostructures can be defined as objects having at least one dimension of less than 100 nm. Among these nanometer-sized structures, one-dimensional (1D) conducting polymers (CP) nanostructures comprising nanowires, nanorods and nanotubes have received the greatest attention. In

the late 80s, Martin and his co-workers reported that confinement 1D CP structures on a submicrometer scale exhibited unique and enhanced electrical properties in comparison with the equivalent bulk materials.[60] These pioneering works gave rise to a growing interest in this class of nanoscale objects during the following decade. Since about ten years, a wide variety of techniques suitable for many different important nanotechnology applications have been developed,[61,62] from the physical methods such as electrospinning[63] to the template-based chemical approaches in which "hard-template"[64] and "soft-template"[65] are classically distinguished. Today, the polymeric nanofibers and nanotubules have flooded the scene of research to such a point that they are considered as a possible candidate to oust silicon from semiconductor industry on which it has been reigning without partition during more half of a century.

In the following sections, we will describe the most commonly used methods for preparing 1D nanostructures and review the resulting various classes of 1D CP nano-objects. Finally, the interesting properties and potential applications in various fields of these nanostructures will be described.

1.3.2 Approaches for achieving 1D CP nanostructures

a) Physical methods

Electrospinning process has recently become the most used physical approach for synthesizing polymer 1D nanofibers. This method allows to produce very long continuous polymeric nanofibers with diameters ranging from micro-scale down to sub-30 nm. The first works on the electrospinning of CP concerned polyaniline (PANI),[66] but now studies on electrospun polypyrrole nanowires (PPy) have equally been carried out.[67] The electrospinning process principle, illustrated in Figure 1.10.a, is based on three main components: a high voltage supplier, a syringe with a needle of very small diameter and a metal collecting screen. A polymeric solution or melt placed in the syringe is charged by the high electrostatic field generated by the power supply between the needle of the syringe and the metal collector. When the repulsive electrostatic forces within the solution caused by the electric field overcome the surface tension which held the fluid, the polymeric liquid ejected from the needle stretches to form a very thin fiber

landing on the metal collector. By this way, polymer nanofibers which are, in principle, infinitely long, can be extremely rapidly formed (on a millisecond time-scale) and their properties can be controlled by adjusting the numerous process parameters including the applied potential, the distance between the anode and the cathode or the properties of the polymer solution.[63] However, even if the derived co-electrospinning process allows to prepare core-shell nanostructures[68,69] (Figure 1.10.b), the synthesis of multi-segmented nanowires with a control over segment length cannot be reached by this route. Moreover, this method does not suit for the transport phenomena study due to hard experimental conditions, particularly the high supplied voltage, susceptible of affecting the electrical properties of the resulting nanostructures.

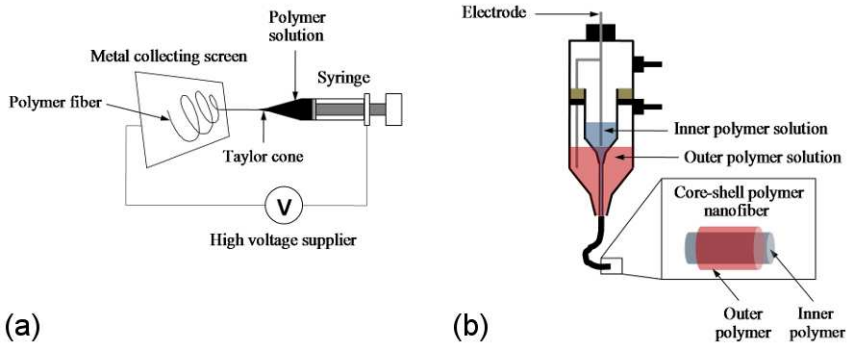

Figure 1.10 *Schematic set up for (a) the electrospinning of polymer nanofiber. (b) the co-electrospinning of core-shell polymer nanofiber (Greiner et al.[68]).*

Numerous lithographic techniques were equally successfully applied for the fabrication of 1D CP nanostructures. For instance, the scanning probe microscopy (SPM)-based techniques allow the production of directly positioned nanowires with controlled dimensions. One attracting feature, in comparison with the conventional patterning methods such as nanoimprint lithography (NIL) (Figure 1.11.a), is that no post-process step for removing residual layers is necessary, which avoid polymer properties degradation. Among this recent class of nonconventional lithographic methods, dip-pen lithography, developed in 1999 by Mirkin[70] is found. In 2002, Liu *et al.* reported in their pioneering investigations, the creation of poly(3,4-ethylenedioxythipohene) (PEDOT) nanowires in the sub-100 nm range by

electrochemical dip-pen nanolithography (E-DPN).[71] This technique uses an atomic force microscope (AFM) tip (the "pen") to deliver molecules (the "ink") and fabricate nanostructures of well-defined nanometer shape and size onto suitable substrate surfaces (the "paper") (Figure 1.11.b). Adding to its capability to direct-place nano-sized materials, this approach is relatively rapid (typical writing speed ranging from 10 $nm.s^{-1}$ to 0.8 $\mu m.s^{-1}$), and offers high spatial precision (down to 10 nm) without complicated steps. In the beam of disadvantages, once again the synthesis of multi-segmented heterostructures is difficult to achieve. Lastly, if the technique seems to perfectly suit to fields such as gas sensing (possibility to pattern high-density large areas of conducting polymer nanostructures) or electronics, the use of nanostructures in others fields as free individual functional nano-object is compromised due to the molecules anchorage on the substrate surface.

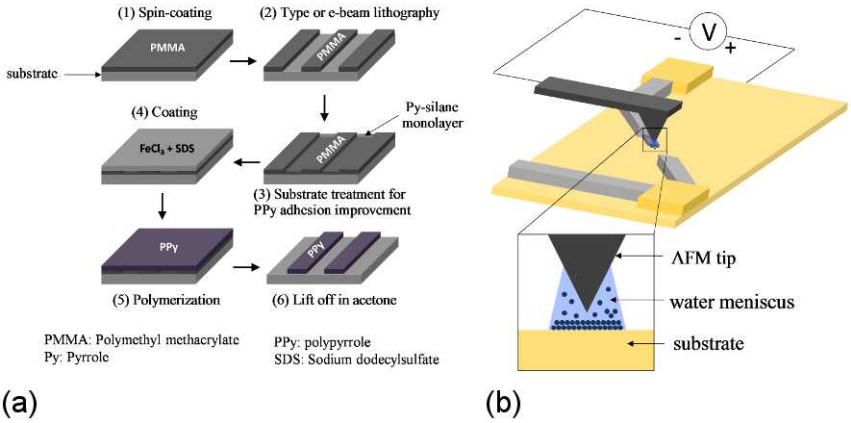

Figure 1.11 *(a) Schematic illustration of the NIL process (Chi et al.[72]). (b) Schematic illustration of the E-DPN process.*

b) "Soft-template" methods

One first class of chemical approaches includes the methods which involve structural directing molecules called "soft-templates" in the growth process of 1D polymer nanostructures. This type of technique is sometimes falsely named "template-free" method too because it avoids the use of the conventional external insoluble membranes (by opposition to the "hard-template" approach). Soft (organic) template techniques include the use of

large organic dopant anions and surfactant-based reverse microemulsion systems. Herein, the surfactant plays as template and doping function at the same time. The morphology and the diameter of the resulting 1D nanostructures are directly influenced by the size of the micellar template, consequently of the surfactant and equally depend on the concentrations of the surfactant and oxidant. There are about ten years ago, Wan *et al.* developed a self-assembly process using naphtalenesulfonic acid as organic "soft-template" to produce polyaniline nanotubes in the sub-micrometer and nanometer ranges.[73,74] Han and Foulger recently reported the synthesis of very thin PEDOT nanowires (down to 10 nm) with relatively high electrical conductivity (0.05 $S.cm^{-1}$) from an aqueous solution using sodium dodecylsulfate as surfactant/dopant[75] (Figure 1.12). "Nanofiber seeding", described in 2004 by Manohar *et al*., proposed an alternative soft-template approach using seed nanofibers such as V_2O_5 as the sacrificial template.[76] By this way, 1D polypyrrole hollow nanostructures in the 60-80 nm and 4-8 nm ranges (respectively outer and inner diameters) were produced.[77] Even if soft-template methods offer a bulk synthesis of 1D CP nanostructures, they are generally restricted to the preparation of monolithic polymer nano-cylindrical materials, with besides that, a relative poor control of their morphology and without control of length. Moreover, the impossibility of producing hybrid 1D nano-objects by most of the techniques reviewed up to now, bring us to discuss the most versatile approach to yield CP-based 1D nanostructures, the "hard-template" method, that we have used in our research work to synthesize various metal-CP multi-segmented nanowires.

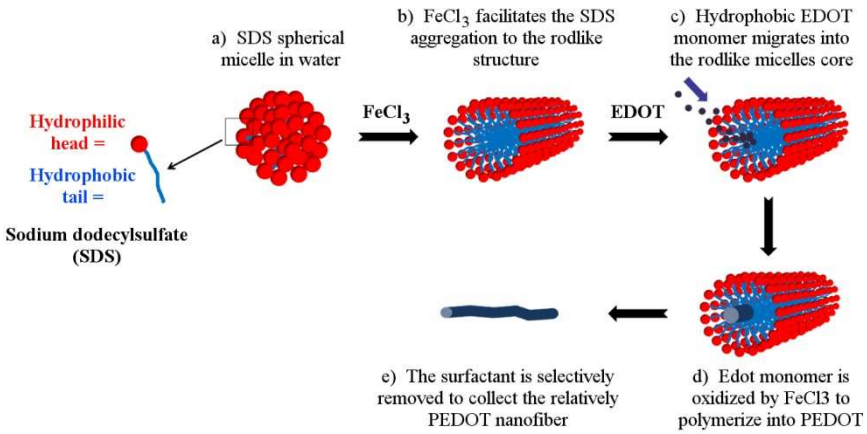

Figure 1.12 *Schematic illustration of the process for the synthesis of PEDOT nanofibers assisted by soft-template SDS cylindrical micelles (adapted from Han and Foulger[77]).*

c) "Hard-template" strategy

Among the many developed methods for preparing nano-objects, the "hard-template" or more easily termed "template" synthesis have been the most widely employed. The strategy consists in synthesizing the desired material within the pores of a host membrane. After removing this membrane, the resulting nanoscale sculptures with morphological and dimensional features related to those of the cavities can be released and collected. Historically, Possin[78] introduced the method 40 years ago by electro-filling the holes of etched nuclear damage tracks in a mica matrix with different metals. He obtained wires with diameters as small as 40 nm and about 15 µm long. In spite of this pioneering report, it was necessary to wait for the second half of the 80s, when Martin and his co-workers successfully explored the synthesis of conducting polymers in polymeric membranes,[60,79] to reveal the template approach being the most suitable way to produce 1D nanostructures of a wide variety of materials with controlled characteristics and enhanced properties.[80,81] Template synthesis is generally based on the use of two kinds of nanoporous materials, "track-etched" polycarbonate (PC) and anodized aluminum oxide (AAO) membranes. Their respective features are reported in Table 1.2. Various methods for filling the pores with a conducting polymer exist but by far the

most employed is electrochemical deposition.[82] Figure 1.13.a illustrates a typical template-based electrosynthesis process. Electrochemical deposition of a material within the pores is carried out by using a thin metal layer coated on one face of the membrane as a working electrode. By suitable treatments (e.g. use of dichloromethane or chloroform for PC dissolution), the template and the coated metal layer are removed and the 1D nanostructures of target materials are released (Figure 1.13.b). Alternatively, by only dissolving the membrane, a kind of "brush" of nanostructures protruding from the electrode is obtained (Figure 1.13.c).

Table 1.2 *Different track-etched PC and AAO template features.*

	Track-etched PC membranes	**AAO membranes**
Thickness range	6 to 50 µm	10 to 50 µm
Pore diameter range	10 nm to 10 µm	4 to 200 nm
Maximum pore density	5.10^9 pores/cm^2	10^{11} pores/cm^2
Removal treatment	Dichloromethane, chloroform	Alkaline solution
Pore distribution	Random but relatively homogeneous in size	Highly ordered hexagonal porous arrangement
Advantages	Possibility to choose the density of pores regardless of their diameter	More suitable for mass-production of nanostructures by the template method
Disadvantages	Hydrophobicity, so potential difficulty for working in aqueous media	Very limited number of available pore diameters

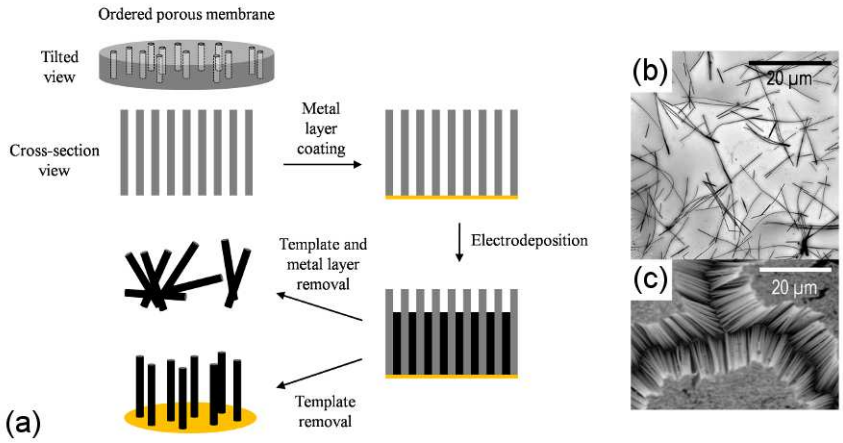

Figure 1.13 *(a) Schematic representation of electrochemical synthesis of 1D nanostructures within a cylindrical nanoporous template. (b) Transmission electronic microscopy picture of 110 nm diameter hybrid Au-PEDOT nanowires freed from a track-etched PC membrane. (c) Scanning electronic microscopy picture showing a "bristle" of gold nanowires protruding from a gold/chromium surface after removal of the template.*

Another easy to put in practice method consists in using a nanoporous membrane as a dividing wall in a two-compartment cell as shown in Figure 1.14.[83] An aqueous monomer solution is placed in the first compartment and allowed to diffuse through the complete thickness of the template prior to the introduction of an oxidant in the second compartment which in its turn will diffuse along the entire length of the pores. So, both species diffuse toward each other through the pores and react to yield the polymer.

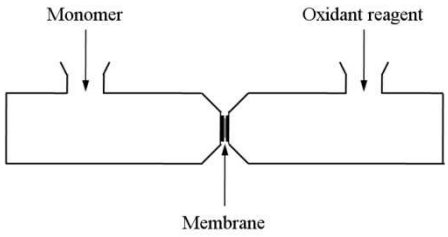

Figure 1.14 *Schematic representation of the two-compartment cell set up to perform the template chemical polymerization (adapted from Demoustier-Champagne et al.[83]).*

An interesting observation was done concerning the template polymer synthesis in track-etched PC membrane achieved by these both quoted methods. The polymer preferentially nucleates and grows on the pore walls[84] to give tubular morphologies. Martin suggested solvophobic and electrostatic effects to explain this tendency.[85] Reynes and Demoustier-Champagne showed that potentiodynamic electrochemical polymerization of pyrrole can lead either to solid nanowires or to hollow nanotubes as a function of certain parameters such as monomer concentration and sweep rate.[86] Lee and his co-workers proposed a mechanism describing the morphological transition between PEDOT nanowire and nanotube as a function of monomer concentration and applied potential.[87] As for the chemical synthesis, it was reported that a structural transition from the completely hollow nanotube with a thin wall to the completely filled nanowire was achieved by running successive syntheses.[83]

Template method offers many attracting advantages, among which some have no equivalent in other previously quoted techniques. Firstly, the deposit materials present remarkable morphological and mechanical features. Indeed, due to the well-defined nanoarchitectures of the actual porous materials, the generated 1D nanostructures are strong, smooth and uniform, just like the pores within which they grow. Then, another key asset is the template approach allows to obtain segments of the target material with controlled shape, dimension and morphology. Last but not least, template synthesis represents the unique route to easily prepare multi-segmented nanowires.

1.3.3 Hybrid metal-CP multi-segmented 1D nanostructures

The bottom-up strategy naturally drove chemists and nanoscientists to design and synthesize nanostructures performing more than one function, and consequently consisting of more than one material. Among multi-component nano-objects, multi-segmented nanowires, built with different materials piled along the long axis of the structure, were very early the object of a deep attention. We saw in the previous section that the “hard-template” approach was the most adapted way of synthesis of multi-segmented nanowires. They can be produced by changing the plating solution and, accordingly adapting parameters of deposition at defined

intervals. 1D nanostructures with stripes of controlled length result from this sequential electrochemical process. During the last two decades, entirely metallic and mixed metal-semiconductor multi-segmented nanowire systems were intensely investigated.[88,89,90] On the other hand, because the synthesis which is behind is more problematic, works on multi-striped nanowires based on organic polymer components were much less reported. The purpose of this section consists in reviewing the works on multi-segmented hybrid metal-polymer mesoscopic and nanoscopic wires published during these last years.

a) Mesoscopic bi-segmented gold-PPy wires

Mirkin *et al.*[91] reported on the synthesis in AAO hard template (with pores of about 400 nm diameter) of bi-segmented wires consisting of one hard hydrophilic area based on gold (Au) and one soft hydrophobic area based on polypyrrole (PPy). They studied the assembly properties of these pseudo-conical amphiphilic structures once they are released from the template. They observed that the bi-segmented objects assemble into microscale arrangements whose shape and size depend on the ratio of Au-PPy segment lengths (Figure 1.15).

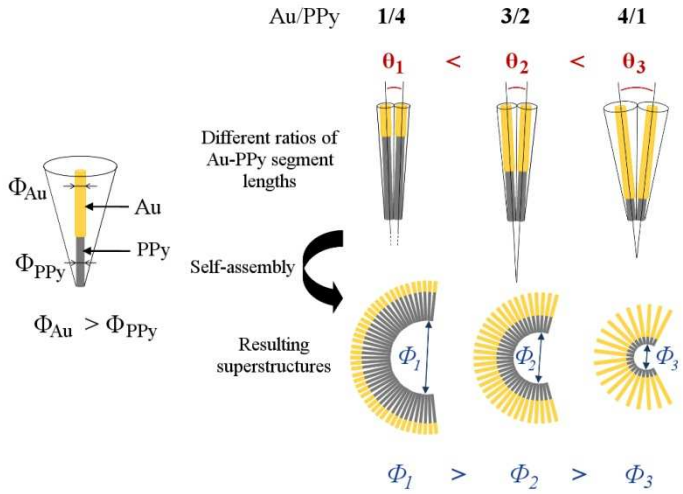

Figure 1.15 *Schematic representation of one influence of the Au-PPy segment lengths ratio on the self-assembly of the bi-segmented Au-PPy wires. Here, the dependence of the superstructure size is represented (adapted from Mirkin et al.[91]).*

Mirkin and his co-workers[92] more recently used in a theoretical model the exactly same type of mesoscopic two-segment Au-PPy structure as unit of curved superstructures exhibiting reversible actuation properties. This time, the diameter of the curved superstructures built by self-assembly should dramatically change (up to 20%) under the influence of the small change (c.a. 3%) in the diameter of individual PPy sections of every bi-segmented unit (Figure 1.16). This small contraction or expansion of the PPy segment could be caused by using external stimuli such as humidity, temperature and light.

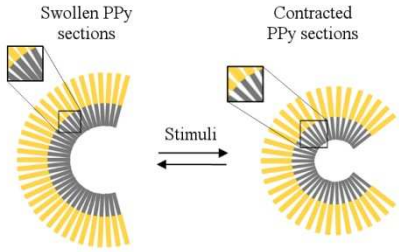

Figure 1.16 *Schematic representation of "C-shaped" curved superstructures based on two segment Au-PPy wires and exhibiting a reversible actuating behavior under an external stimulus (Mirkin et al.[92]).*

Wang *et al*.[93] recently developed the first example of sub-micrometer (≈ 250 nm in diameter) actuator base on the same binary Au-PPy segments. By alternately applying potential values corresponding to the doped and undoped states of the PPy segment, the polymer part shrinks and swells with incorporation and withdrawing of the charge-compensating doping counter-anion, respectively. As a result, this electrochemically stimulated actuation makes the "nanowire" bend as a "nanofinger" (Figure 1.17).

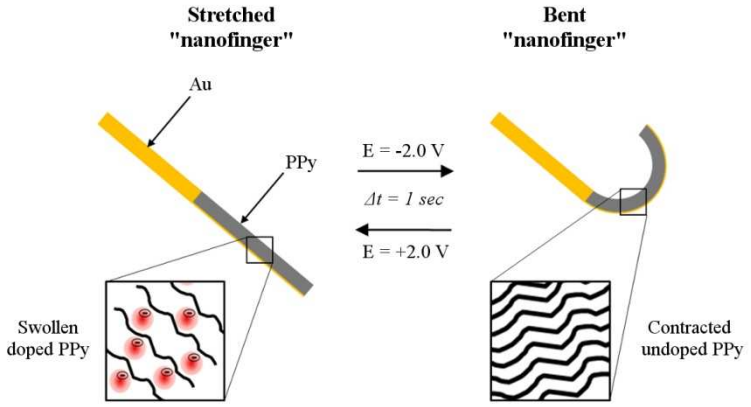

Figure 1.17 *Schematic figure representing the principle of the bending actuator based on a bi-segmented Au-PPy "nanowire" (adapted from Wang et al.*[93]*).*

b) Multi-segmented metal-conducting polymer nanowires

In most cases, research on nanowires concern the study of their electronic properties and their integration as systems with various functionalities into nanoscale devices.[94] Unfortunately, one-component nanowires are not ideal nanostructures to these approaches for several reasons, in particular the difficulty of their positioning on electrodes and the existence of contact resistances which are large enough to interfere with the actual measurement of the nanoscale device. In this respect, tri-segmented nanowire configuration in which the functional material of interest is "sandwiched" between two metallic segments appears to be much more efficient. In fundamental electronics, these multi-segmented nanowires offer the potential for elucidating transport mechanisms and structure-property relationships. Some isolated works focused on the synthesis of multi-component metal-conducting polymer nanowires. Within these hybrid multi-segmented 1D nanostructures, inorganic blocks can consist in a noble metal insuring contact conductance to allow the organic polymer to exhibit its actual electronic features, or/and in a magnetic component to help positioning.

Mirkin *et al.*[95] made resistors and diodes from Au-PPy-Au and Au-PPy-Cd-Au "nanowires" (≈ 300 nm in diameter), respectively. The multi-segmented nanostructures were classically prepared by a template

electrochemical synthesis into an AAO membrane. The tri-segmented Au-PPy-Au nanowires, deposited onto microelectrodes exhibited an ohmic behavior at room temperature and nonlinear I-V curves at low temperature, which is typical for semiconducting behavior in conducting polymers (Figure 1.18.a). The four-segment Au-PPy-Cd-Au nanowires were characterized by a non-ohmic asymmetric diode behavior at room temperature due to the PPy-Cd junction nature. By adding a Cd block, they succeeded in producing an organic nanodiode (Figure 1.18.b).

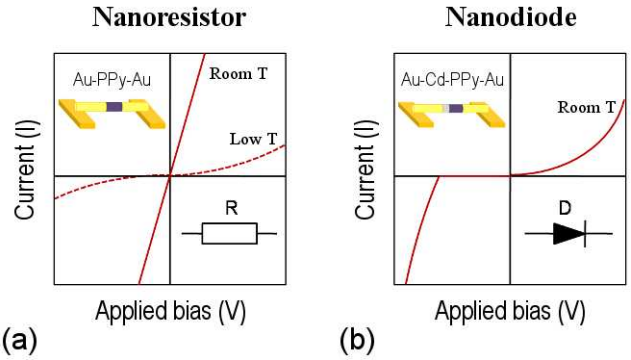

Figure 1.18 *Schematic I-V characteristics for (a) a single Au-PPy-Au wire at room and low temperature (T) (b) a single Au-PPy-Cd-Au wire at room temperature (adapted from Mirkin et al.[95]).*

Kuk and co-workers[96] achieved to fabricate the first example of organic field-effect transistor (FET) based on hybrid multi-segmented nanowires by using tri-segmented Co-PPy-Co nanowires electrochemically synthesized in AAO membranes, dispersing them on a silicon wafer and patterning three electrodes (as source, channel and drain) on one side of the wire. Beyond the physical aspect, this example is still a feat unique in terms of synthesis. The nanowires are first the smallest hybrid nanostructures encountered in the literature (Φ= 35 nm). Then they contain materials which are difficult to link them, metal oxides and conjugated polymers (see chapter 5).

Multi-striped nanowires also showed their potential in detection and sensing of biological or chemical analytes. Mallouk *et al.*[97] investigated the template synthesis of tri-segmented Au-PPy-Au "nanowires" (300 nm in diameter) with physically entrapped proteins into the polymer segment. Myung *et al.*[98] recently prepared multi-functional four-segmented Au-PPy-

Ni-Au "nanowires" (200 nm in diameter). The conducting polymer, magnetic metal and noble metal segments were used for chemical sensing, for controlled placement on prefabricated electrodes and for ensuring good electrical contacts, respectively (Figure 1.19). Mallouk *et al.*[99] prepared tri-segmented Au-PEDOT-Au "nanowires" (> 300 nm in diameter) with two kinds of PEDOT segments (PEDOT/PSS and PEDOT/ClO_4). By comparing their respective vapor sensing abilities, they showed that different charge transport mechanisms influence the resulting properties (e.g. sensing mechanism) for a material.

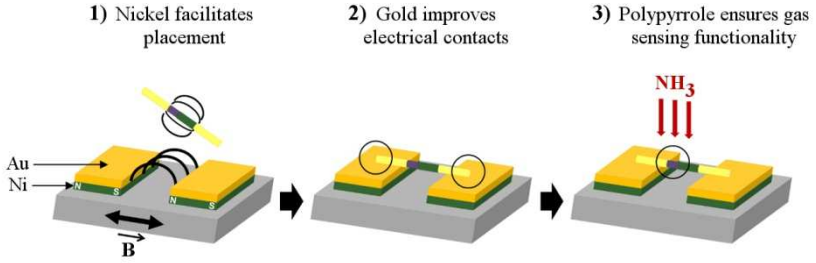

Figure 1.19 *Schematic illustration representing the respective role of three components within the four-segmented Au-PPy-Ni-Au nanowires (adapted from Myung et al.*[98]*).*

1.3.4 CP 1D nanostructures: properties and applications

Behind the attractive examples of nano-sized systems that were presented in the previous section, a great activity around their possible applications is growing. Once the fundamental aspect will be cleared, the researchers hope to build on the unique properties of nanostructures to make new devices more efficient than the already existing ones. The purpose of this last section is to provide a brief review of potential device applications of CP nanowires and nanotubes in various sectors and to highlight the properties required.

a) Sensing

Bio-sensing

In comparison with other nanomaterials, conducting polymer nanowires and nanotubes have emerged as attractive candidates for fabricating sensor devices because of their large surface-to-volume ratio, binding affinities for various biomolecules, chemically tailorable physical properties and biocompatibility. An effective biosensor exhibits a significant change in its physical and chemical properties provided by a target binding. In biosensor fabrication, the ability to tune the physical properties of nanomaterials is a first key for their application in biodetection. This is now possible with the development of new synthesis, fabrication and characterization methods for nanostructures. A second challenge is the immobilization of biomolecules and retention of their bioactivity. The two commonly used strategies for biofunctionalizing conducting polymer are the entrapment during polymerization and covalent attachment post-polymerization. Although it allows to incorporate biomolecules in a single step, the first method has the major disadvantages of loss of biological activity during polymerization and inaccessibility of the biomolecule that largely does not emerge from the polymer matrix. Finally, the change for one property of the biosensor caused by the interaction with the target must be measurable. For example, if the response is electrical as in most cases, the device must be put in contact with electrodes. Until recently, the use of conducting polymer nanowires as biosensors has been limited. Nevertheless, some publications may be cited. They give an overview of different ways to proceed to immobilize the recognition element on the CP 1D nanostructure.

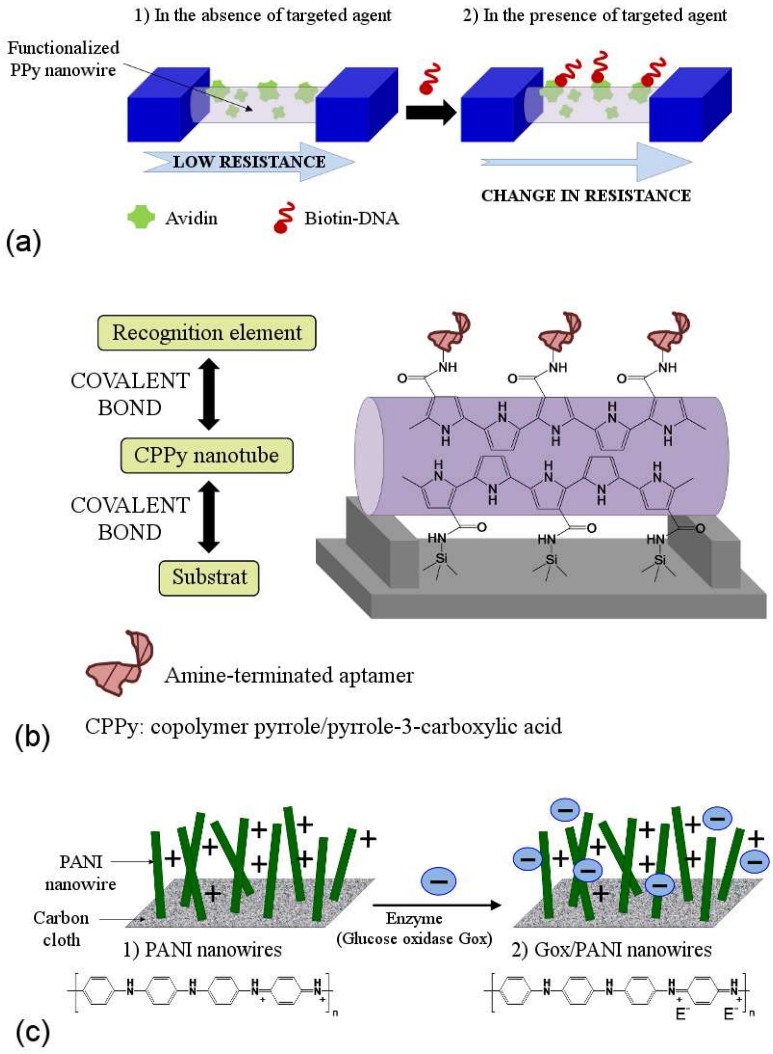

Figure 1.20 *Some examples of biosensor models based on 1D conducting polymer nanostructures: (a) The resistance of a 200 nm diameter avidin-functionalized PPy nanowire increases upon addition of the target (biotin-DNA conjugate) (Mulchandani et al.[101]). The recognition element is entrapped during polymerization. (b) The copolymer CPPy nanotube covalently bonded both to the substrate and to the recognition units is able to recognize a target protein (human α-thrombin) (Jang et al.[102]). (c) Schematic illustration of glucose oxidase immobilization on oxidized PANI nanowires via electrostatic interaction for the fabrication of a glucose sensor (Chen et al.[103]).*

Mulchandani *et al.*[100] reported a pioneering example of functionalized CP nanowires as sensors. By entrapping a model protein, avidin, during electrochemical polymerization, resulting functionalized PPy nanowires (Φ = 200 nm) exhibit changes in resistance upon addition of a biotin-DNA conjugate (Figure 1.20.a). Jang *et al.*[101] proposed another sensor device model based on carboxylic acid-functionalized PPy nanotubes fabricated by copolymerization. Bonding of the molecular recognition element to the nanotube surface and nanotube immobilization onto the microelectrode substrate were both covalently achieved. They chose the aptamer-protein interaction to demonstrate the applicability of the system (Figure 1.20.b). Chen *et al.*[102] reported the synthesis of a glucose sensor based on polyaniline (PANI) nanowires on which glucose oxidase (GOx) enzymes were immobilized via electrostatic interaction (Figure 1.20.c). Other studies recently demonstrated applicability of biosensors based on PPy nanowires in the diagnosis of various diseases such incipient renal disease or cancer.[103,104] In these papers, the molecular recognition element was covalently grafted by N-substitution, on the monomer or on the polymer before or after polymerization, respectively.

Chemical sensing

In comparison with their bulk counterparts, the fact that the 1D nanostructures have a high surface-to-volume ratio is very interesting in terms of sensing. On the one hand, if we consider a surface and the same surface covered with 1D nanostructures of the same material, it is clear that the "brush" of nanostructures has much higher surface area than the smooth surface. The second advantage of this geometry is that the smallest dimension permits a rapid diffusion of analytes into and out of the material. The sensing efficiency of 1D nanostructures is particularly proved when they are found in well-ordered configuration. As for biosensors, PANI and PPy nanowires are the most frequently encountered for developing new chemical sensor devices. PANI nanowires have been employed to detect various chemical species. McDermott and co-workers[105] synthesized large arrays of uniform and well-aligned PANI nanowires (50 to 70 nm in diameter, 800 nm in length) on various substrates using a templateless growth (Figure 1.21). They showed that PANI nanowires supporting iron (III) hexacyanoferrate nanoparticles can be used as chemical sensor for H_2O_2. Craighead *et al.*[106]

observed that upon exposure to NH_3 gas the conductivity of (PANI/polyethylene-oxide) nanowires (100-500 nm in diameter) decreases. The gas acts as electron-supplying and so eradicates charge-carrier in polymer backbone. PPy nanowires have equally been abundantly applied in sensing. Wang *et al.*[107] described the highly toxic nitrite electro-reduction by PPy nanowires modified electrode as chemical sensing. Although poly(3,4-ethylenedioxythiophene) (PEDOT) nanotubes was early considered as a matrix in a glucose sensor,[108] little work has been devoted on the development of sensors based on PEDOT nanowires. However, we can cite the recent paper by Yu and co-workers[109] demonstrating the efficiency as NH_3 and HCl gas sensor of a well arranged PEDOT nanowire film produced by a template synthesis coupled with Langmuir-Blogett technique. Lin and co-workers[110] studied the electrical properties of PEDOT nanowires synthesized by dip-pen lithography to develop NO gas sensors.

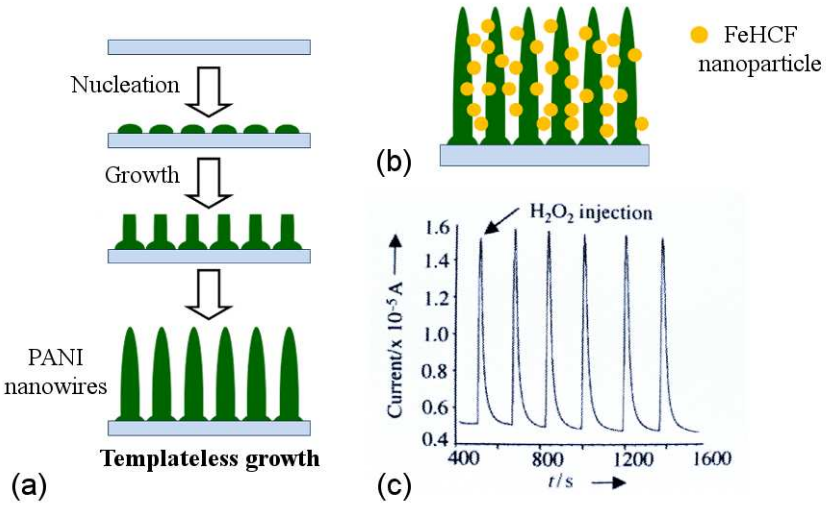

Figure 1.21 *Principle of a H_2O_2 sensor based on a large array of oriented PANI nanowires supporting FeHCF nanoparticles (McDermott et al.[105]). (a) Schematic illustration of the templateless growth of PANI nanowires. (b) Schematic representation of the PANI/FeHCF sensor. (c) Electrochemical response of the sensor to repetitive injections of 50 ppm H_2O_2.*

b) Nanoelectronics

In the mid-70s, conjugated polymers were discovered as materials that can conduct electricity. As such, the fact that they are at the scene in the field of molecular electronics is not a surprise. Indeed, in comparison with other molecules, polymers have many advantages. Their synthesis is relatively uncomplicated; they are relatively stable and low cost. Besides they exhibit enhanced mechanical, optical, magnetic and electronic features in confined environment. For all these reasons, the conjugated polymers have become the organic material of choice firstly for elucidating transport mechanisms in organic semiconductors. But beyond the fundamental, many electronic components based on conducting polymers nanoparticles have already been developed.[95,96] Along with improving the performance of these molecular components, another challenge for nanoelectronics is to develop techniques for controlling the positioning of these nanoparticles. The engineering for the self-assembling of electrical circuits requires particles with both interesting properties and convenient shapes. It is clear by its dimensions that the quasi 1D geometry is the only one to meet these two criteria. On one hand by nanoscale diameter, nanotubes and nanowires offer attractive properties related to the confinement, and on the other hand their third dimension of several micrometers long facilitates their observation and their positioning. Several methods were proposed for the assembly of rod-particle nanostructures on patterns as the prior chemical functionalization, alignment by a stream of solvent or by applying an electric or magnetic field.[111]

c) Other applications

Conjugated polymers having many others attracting properties, their use in the form of 1D nanostructures is considered in different other applications in a variety of fields such as energy storage, electrochromic display or data storage. Dou *et al.*[112] showed that the use of a carpet of PANI/$HClO_4$ "nanotubes and nanowires" (≈ 300 nm in diameter) as cathode in rechargeable Li/polymer batteries offers the advantage of improving system performance compared to commercial powder-based batteries, particularly due to high active surface areas of the nanostructures and faster diffusion of Li ions through their thin porous network. CP nanowires were also considered in the design of electrochromic displays for "electronic paper" development. Electrochromism is a property of a material defined as its

ability to reversibly change color under the influence of an electric field. Among electrochromic materials, conjugated polymers have many advantages such as easy processing, fast switching time, high contrast and coloration efficiency, and tunable band gap. Again nanostructured CP are more interesting than bulk counterparts since they are the seat of even faster switching times. PEDOT nanotubes (10 to 20 nm in diameter) in ordered alignment were proposed by Lee *et al.*[113] as ideal candidates for electrochromic technology development. The nanostructured PEDOT features have permitted to overcome the disadvantages of films. Indeed, the thin wall thickness of PEDOT nanotubes and their micrometric length have contributed to improve the diffusion of counterions during the redox process, so to decrease the switching time, and the coloration intensity, respectively.

References

[1] V. V. Walatka, Jr., M. M. Labes, J. H. Perlstein, *Phys. Rev. Lett.* **1973**, *31*, 1139.

[2] L. R. Greene, G. B. Street, L. J. Suter, *Phys. Rev. Lett.* **1975**, *34*, 577.

[3] G. B. Street, L. R. Greene, *IBM J. Res. Develop.* **1977**, *21*, 99.

[4] A. Wolmershäuser, C. R. Brulet, G. B. Street, *Inorg. Chem.* **1978**, *17*, 3586.

[5] W. D. Gill, W. Bludau, R. H. Geiss, P. M. Grant, R. L. Greene, J. J. Mayerle, G. B. Street, *Phys. Rev. Lett.* **1977**, *38*, 1305.

[6] H. Shirakawa, E. J. Louis, A. G. MacDiarmid, C. K. Chiang, A. J. Heeger, *J. C. S. Chem. Comm.*, **1977**, 578.

[7] C. K. Chiang, M. A. Druy, S. C. Gau, A. J. Heeger, E. J. Louis, A. G. MacDiarmid, Y. W. Park, H. Shirakawa, *J. Am. Chem. Soc.* **1978**, *100*, 1013.

[8] J. M. Pochan, D. F. Pochan, H. Rommelmann, H. W. Gibson, *Macromolecules* **1981**, *14*, 110.

[9] P. Benni, L. D'Ilario, M. Schwarz, *J. Mat. Sci. Lett.* **1988**, *7*, 1124.

[10] K. K. Kanazawa, A. F. Diaz, R. H. Geiss, W. D. Gill, J. F. Kwak, J. A. Logan, J. F. Rabolt, G. B. Street, *J. Chem. Soc. Chem. Comm.* **1979**, 854.

[11] G. Tourillon, F. Garnier, *J. Electroanal. Chem.* **1982**, *135*, 173.

[12] F. Garnier, G. Tourillon, M. Gazard, J. C. Dubios, *J. Electroanal. Chem.* **1983**, *148*, 299.

[13] W. R. Salaneck, R. Erlandsson, J. Prejza, I. Lundström, O. Inganäs, *Synth. Met.* **1983**, *5*, 125.

[14] S. A. Brazovskii, N. N. Kirova, *JETP Lett.* **1981**, *33*, 4.

[15] K. H. An, S. Y. Jeong, H. R. Hwang, Y. H. Lee, *Adv. Mater.* **2004**, *16*, 1005.

[16] S. Machida, S. Miyata, A. Techagumpuch, *Synth. Met.* **1989**, *31*, 311.

[17] D. M. De Leeuw, P. A. Kraakman, P. F. G. Bongaerts, C. M. J. Mutsaers, D. B. M. Klaassen, *Synth. Met.* **1994**, *66*, 263.

[18] A. G. MacDiarmid, J. C. Chiang, A. F. Richter, N. L. D. Somasiri, A. J. Epstein, *Conduct. Polym. Proc. Workshop* **1987**, 105.

[19] J. Stejskal, R. G. Gilbert, *Pure Appl. Chem.* **2002**, *74*, 857.

[20] Bayer AG, *Eur. Patent 440 957* **1991**.

[21] Agfa Gevaert, *Eur. Patent 564 911* **1993**.

[22] Bayer AG, *Eur. Patent 821 025* **1998**.

[23] A. Dall'Olio, G. Dascola, V. Varacca, V. Bocchi, *Compt. Rend.* **1968**, *C267*, 433.

[24] K. Gurunathan, A. Vadivel Murugan, R. Marimuthu, U. P. Mulik, D. P. Amalnerkar, *Mat. Chem. Phys.* **1999**, *61*, 173.

[25] E. M. Genies, G. Bidan, A. F. Diaz, *J. Electroanal. Chem.* **1983**, *149*, 101.

[26] C. Li, G. Shi, G. Xue, S. Jin, B. Yu, S. Yang, *J. Polym. Sci. Part B* **2003**, *33*, 2199.

[27] G. Zotti, G. Schiavon, N. Comisso, *Synth. Met.* **1991**, *40*, 309.

[28] *Handbook Of Organic Conductive Molecules And Polymers Vol. 2*, (Ed: H. S. Nalwa), Wiley, Chichester, UK **1997**.

[29] N. K. Guimard, N. Gomez, C. E. Schmidt, *Prog. Polym. Sci.* **2007**, *32*, 876.

[30] N. F. Mott, E. A. Davis, *Electronic Processes In Non-Crystalline Materials*, (Clarendon-Press), Oxford, UK **1979**.

[31] P. Sheng, *Phys. Rev. B* **1980**, *21*, 2180.

[32] R. Menon, C. O. Yoon, D. Moses, A. J. Heeger, *Phys. Rev. B* **1993**, *48*, 17685.

[33] A. J. Epstein, J. Joo, R. S. Kohlman, G. Du, A. G. MacDiarmid, E. J. Oh, Y. Min, J. Tsukamoto, H. Kaneko, J. P. Pouget, *Synth. Met.* **1994**, *65*, 149.

[34] J. P. Travers, *J. Chim. Phys.* **1998**, *95*, 1427.

[35] P. Pfluger, G. B. Street, *J. Chem. Phys.* **1984**, *80*, 544.

[36] T. A. Skotheim, M. I. Florit, A. Melo, W. E. O'Grady, *Phys. Rev. B* **1984**, *30*, 4846.

[37] J. G. Eaves, H. S. Munro, D. Parker, *Polym. Comm.* **1987**, *28*, 38.

[38] O. Inganäs, R. Erlandsson, C. Nylander, I. Lundström, *J. Phys. Chem. Solids* **1984**, *45*, 427.

[39] J. Joo, J. K. Lee, S. Y. Lee, K. S. Jang, E. J. Oh, A. J. Epstein, *Macromolecules* **2000**, *33*, 5131.

[40] G. Morea, L. Sabbatini, P. G. Zambonin, A. J. Swift, R. H. West, J. C. Vickerman, *Macromolecules* **1991**, *24*, 3630.

[41] E. T. Kang, K. G. Neoh, K. L. Tan, *Adv. Polym. Sci.* **1993**, *106*, 135.

[42] N. Sakmeche, S. Aeiyach, J.-J. Aaron, M. Jouini, J.-C. Lacroix, P.-C. Lacaze, *Langmuir* **1999**, *15*, 2566.

[43] J.-L.Duvail, P. Rétho, V. Fernandez, G. Louarn, P. Molinié, O. Chauvet, *J. Phys. Chem. B* **2004**, *108*, 18552.

[44] G. Tourillon, Y. Jugnet, *J. Chem. Phys.* **1988**, *89*, 1905.

[45] R. P. Feynman, *Engineering And Science*, **1960**, *XXIII*. Available on the web at http://www.zyvex.com/nanotech/feynman.html.

[46] N. Taniguchi, *Proc. ICPE Tokyo*, **1974**, *2*, 18.

[47] J. Bardeen, W. H. Brattain, *Phys. Rev.*, **1948**, *74*, 230.

[48] E. J. Ryder, W. Shockley, *Phys. Rev.*, **1948**, *75*, 310.

[49] H. C. Theurer, *U. S. Patent 3.060.123*, **1952**.

[50] P. H. Keck, M. J. E. Golay, *Phys. Rev.*, **1953**, *89*, 1297.

[51] R. Emeis, *Zeitschrift für Naturforschung 9a*, **1954**, 67.

[52] M. Tanenbaum, L. B. Valdes, E. Buehler, N. B. Hannay, *J. Appl. Phys.*, **1955**, *26*, 686.

[53] J. Andrus, W. L. Bond, *Transistor Technology*, **1957**, *III*, 151.

[54] A. Aviram, M. A. Ratner, *Chem. Phys. Lett.*, **1974**, *29*, 277.

[55] H. Shirakawa, E. J. Louis, A. MacDiarmid, C. K. Chiang, A. J. Heeger, *J. C. S. Chem. Comm.*, **1977**, 578.

[56] G. Binnig, H. Rohrer, *U.S. Patent # 4.343.993*, **1982**.

[57] G. Binnig, C. F. Quate, C. Gerber, *Phys. Rev. Lett.*, **1986**, *56*, 930.

[58] H. W. Kroto, J. R. Heath, S. C. O'Brien, R. F. Curl, R. E. Smalley, *Nature*, **1985**, *360*, 162.

[59] S. Iijima, *Nature*, **1991**, *354*, 56.

[60] Z. Cai, C. R. Martin, *J. Am. Chem. Soc.* **1989**, *111*, 4138.

[61] G. A. Ozin, *Adv. Mat.* **1992**, *4*, 612.

[62] S. V. N. T. Kuchibhatla, A. S. Karakoti, D. Bera, S. Seal, *Prog. Mat. Sci.* **2007**, *52*, 699.

[63] Z.-M. Huang, Y.-Z. Zhang, M. Kotaki, S. Ramakrishna, *Compos. Sci. Tech.* **2003**, *63*, 2223.

[64] C. R. Martin, *Science* **1994**, *266*, 1961.

[65] Z. X. Wie, M. X. Wan, T. Lin, L. M. Dai, *Adv. Mater.* **2003**, *15*, 136.

[66] A. G. MacDiarmid, W. E. Jones, I. D. Norris, J. Gao, A. T. Johnson, Jr., N. J. Pinto, J. Hone, B. Han, F. K. Ko, H. Okuzaki, M. Llaguno, *Synth. Met.* **2001**, *119*, 27.

[67] I. S. Chronakis, S. Grapenson, A. Jakob, *Polymer* **2006**, *47*, 1597.

[68] Z. Sun, E. Zussman, A. L. Yarin, J. H. Wendorff, A. Greiner, *Adv. Mater.* **2003**, *15*, 1929.

[69] Y. Dror, W. Salalha, R. Avrahami, E. Zussman, A. L. Yarin, R. Dersch, A. Greiner, J. H. Wendorff, *Small* **2007**, *3*, 1064.

[70] R. D. Piner, J. Zhu, F. Xu, S. Hong, C. A. Mirkin, *Science* **1999**, *283*, 661.

[71] B. W. Maynor, S. F. Filocamo, M. W. Grinstaff, J. Liu, *J. Am. Chem. Soc.* **2002**, *124*, 522.

[72] B. Dong, M. Krutschke, X. Zhang, L. Chi, H. Fuchs, *Small* **2005**, *1*, 520.

[73] H. Qiu, M. Wan, B. Mattews, L. Dai, *Macromolecules* **2001**, *34*, 675.

[74] L. Zhang, M. Wan, *Thin Sol. Films* **2005**, *477*, 24.

[75] M. G. Han, S. H. Foulger, *Small* **2006**, *2*, 1164.

[76] X. Zhang, W. J. Goux, S. K. Manohar, *J. Am. Chem. Soc.* **2004**, *126*, 4502.

[77] X. Zhang, S. K. Manohar, *J. Am. Chem. Soc.* **2005**, *127*, 14156.

[78] G. E. Possin, *Rev. Sci. Instrum.* **1970**, *41*, 772.

[79] R. Penner, C. R. Martin, *J. Electrochem. Soc.* **1986**, *133*, 2206.

[80] R. P. Burford, T. Tongtam, *J. Mat. Sci.* **1991**, *26*, 3264.

[81] A. Huczko, *Appl. Phys. A* **2000**, *70*, 365.

[82] (a) C. Schönenberger, B. M. I. Van Der Zande, L. G. J. Fokkink, M. Henny, C. Schmid, M. Krüger, A. Bachtold, R. Huber, H. Birk, U. Staufer, *J. Phys. Chem. B* **1997**, *101*, 5497. (b) M. Lai, J. Riley, *J. Coll. Int. Sci.* **2008**, *323*, 203. (c) J.-L. Duvail, P. Rétho, S. Garreau, G. Louarn, C. Godon, S. Demoustier-Champagne, *Synth. Met.* **2002**, *131*, 123. (d) Y. Cao, T. E. Mallouk, *Chem. Mater.* **2008**, *20*, 5260. (e) S. I. Cho, S. B. Lee, *Acc. Chem. Res.* **2008**, *41*, 699.

[83] J. Duchet, R. Legras, S. Demoustier-Champagne, *Synth. Met.* **1998**, *98*, 113.

[84] V. Ranjani, R. Parthasarathy, C. R. Martin, *Nature* **1994**, *369*, 298.

[85] C. R. Martin, *Science* **1994**, *266*, 1961.

[86] O. Reynes, S. Demoustier-Champagne, *J. Electrochem. Soc.* **2005**, *152*, D130.

[87] R. Xiao, S. I. Cho, R. Liu, S. B. Lee, *J. Am. Chem. Soc.* **2006**, *129*, 4483.

[88] J. C. Love, A. R. Urbach, M. G. Prentiss, G. M. Whitesides, *J. Am. Chem. Soc.* **2003**, *125*, 12696.

[89] R. Elnathan, R. Kantaev, F. Patolsky, *Nano Lett.* **2008**, *8*, 3964.

[90] D. J.Peña, J. K. N. Mbindyo, A. J. Carado, T. E. Mallouk, C. D. Keating, B. Razavi, T. S. Mayer, *J. Phys. Chem. B* **2002**, *106*, 7458.

[91] S. Park, J.-H. Lim, S.-W. Chung, C. A. Mirkin, *Science* **2004**, *303*, 348.

[92] J. K. Lim, J. W. Ciszek, F. Huo, J.-W. Jang, S. Hwang, C. A. Mirkin, *Nano Lett.* **2008**, *8*, 4441.

[93] V. A. Pedrosa, X. Luo, J. Burdick, J. Wang, *Small* **2008**, *4*, 738.

[94] A. L. Briseno, S. C. B. Mannsfeld, S. A. Jeneke, Z. Bao, Y. Xia, *Mater. Today* **2008**, *11*, 38.

[95] S. P. Park, S.-W. Chung, C. A. Mirkin, *J. Am. Chem. Soc.* **2004**, *126*, 11772.

[96] H.-J. Chung, H. H. Jung, Y.-S. Cho, S. Lee, J.-H. Ha, J. H. Choi, Y. Kuk, *Appl. Phys. Lett.* **2005**, *86*, 213113.

[97] R. M. Hernandez, L. Richter, S. Semancik, S. Stranick, T. E. Mallouk, *Chem. Mater.* **2004**, *16*, 3431.

[98] M. A. Bangar, C. M. Hangarter, B. Yoo, Y. Rheem, W. Chen, A. Mulchandani, N. V. Myung, *Electroanal.* **2009**, *21*, 61.

[99] Y. Cao, A. E. Kovalev, R. Xiao, J. Kim, T. S. Mayer, T. E. Mallouk, *Nano Lett.* **2008**, *8*, 4653.

[100] K. Ramanathan, M. A. Bangar, M. Yun, W. Chen, N. V. Myung, A. Mulchandani, *J. Am. Chem. Soc.* **2005**, *127*, 496.

[101] H. Yoon, J.-H. Kim, N. Lee, B.-G. Kim, J. Jang, *ChemBioChem* **2008**, *9*, 634.

[102] Y.-Y. Horng, Y.-K. Hsu, A. Ganguly, C.-C. Chen, L.-C. Chen, K.-H. Chen, *Electrochem. Comm.* **2009**, *11*, 850.

[103] S. B. Tolani, M. Craig, R. K. Delong, K. Ghosh, A. K. Wanekaya, *Anal. Bioanal. Chem.* **2009**, *393*, 1225.

[104] M. A. Bangar, D. J. Shirale, W. Chen, N. V. Myung, A. Mulchandani, *Anal. Chem.* **2009**, *81*, 2168.

[105] J. Liu, Y. Lin, L. Liang, J. A. Voigt, D. L. Huber, Z. R. Tian, E. Coker, B. McKenzie, M. J. McDermott, *Chem. Eur. J.* **2003**, *9*, 605.

[106] H. Liu, J. Kameoka, D. A. Czaplewski, H. G. Craighead, *Nano Lett.* **2004**, *4*, 671.

[107] Y. Tian, J. Wang, Z. Wang, S. Wang, *Synth. Met.* **2004**, *143*, 309.

[108] A. Kros, S. W. F. M. Van Howell, N. A. J. M. Sommerdijk, R. J. M. Nolte, *Adv. Mater.* **2001**, *13*, 1555.

[109] J. Xu, Y. Jiang, Y. Yang, J. Yu, *Mat. Sci. Eng. B* **2009**, *157*, 87.

[110] H.-H. Lu, C.-Y. Lin, T.-C. Hsiao, Y.-Y. Fang, K.-C. Ho, D. Yang, C.-K. Lee, S.-M. Hsu, C.-W. Lin, *Anal. Chim. Acta* **2009**, in press.

[111] (a) J. M. Tour, L. Cheng, D. P. Nackashi, Y. Yao, A. K. Flatt, S. K. St. Angelo, T. E. Mallouk, P. D. Franzon, *J. Am. Chem. Soc.* **2003**, *125*, 13279. (b) N. Kovtyukhova, T. E. Mallouk, *Chem. Eur. J.* **2002**, *8*, 4354. (c) Y. Huang, X. Duan, Q. Wei, C. M. Lieber, *Science* **2001**, *291*, 630. (d) Y. Cao, W. Liu, J. Sun, Y. Han, J. Zhang, S. Liu, H. Sun, J. Guo, *Nanotechnology* **2006**, *17*, 2378.

[112] F. Cheng, W. Tang, C. Li, J. Chen, H. Liu, P. Shen, S. Dou, *Chem. Eur. J.* **2006**, *12*, 3082.

[113] S. I. Cho, W. J. Kwon, S.-J. Choi, P. Kim, S.-A. Park, J. Kim, S. J. Son, R. Xiao, S.-H. Kim, S. B. Lee, *Adv. Mater.* **2005**, *17*, 171.

Chapter 2

Synthesis and characterization of hybrid noble metal-polypyrrole nanowires

Abstract:

This chapter deals with the all-electrochemical template synthesis of various narrow multi-segmented hybrid noble metal-polypyrrole nanowires (40 to 160 nm in diameter) of well-controlled dimensions. Typical well-shaped segmented metal (Au or Pt)-polypyrrole (PPy)-metal (Au or Pt) nanowires presenting different polymer in-wire junction lengths were prepared by an exclusively electrochemical process. A careful characterization of the metal/polymer interfaces of these tri-segmented nanostructures, performed by transmission electron microscopy, reveals that the structure and the strength of bottom and upper interfaces strongly depend on the nature of the consecutively deposited materials, on the diameter of the nanowires and on the synthesis conditions. Several strategies for improving the mechanical strength of metal/polymer interfaces were investigated and are reported here. XPS measurements were performed on PPy films and nanowires to evaluate their doping ratio. Variable temperature electrical transport measurements were performed on both multiple nanowires and single nanowires. The data show that the three-dimensional Mott variable range hopping model provides a complete framework for the understanding of transport in PPy nanowires, including non-linear current-voltage characteristics and magnetotransport at low temperatures. These results are in good agreement with the electronic structure determined by XPS experiments.

Two publications were extracted from this chapter:
"Structural and electrical characterization of hybrid metal-polypyrrole nanowires", L. Gence, S. Faniel, C. Gustin, S. Melinte, V. Bayot, V. Callegari, O. Reynes, S. Demoustier-Champagne, *Phys. Rev. B* **2007**, *76*, 115415.
"Size related transport mechanisms in hybrid metal-polymer nanowires", L. Gence, V. Callegari, S. Faniel, A. Vlad, C. Dutu, S. Melinte, S. Demoustier-Champagne, V. Bayot, *Phys. Stat. Sol. (a)* **2008**, *205*, 1447.

2.1 Introduction

One-dimensional (1D) conducting polymer (CP) nanostructures have been intensively studied during the last years. Due to the alignment of the polymer chains, conjugated polymers in the shape of nanowires exhibit better mechanical and electrical performances than their bulk counterparts. As a result, in addition to various potential applications, CP nanowires are ideal model systems for elucidating transport mechanisms and structure-property relationships in organic semiconductors. Hybrid multi-segmented nanowires in which one or more polymer junctions are sandwiched between metal blocks are particularly adapted for this fundamental study. The typical metal-CP-metal configuration facilitates positioning of the system and permits to obtain its actual electronic properties. Until now, very few investigations devoted to the synthesis and characterization of small diameter ($\Phi \leq 100$ nm) hybrid multi-segmented nanowires, particularly because of the interfacing matters between totally different materials.

Polypyrrole (PPy) (see Figure 2.1 for the ideal neutral chemical structure) has emerged as one of the most promising materials in nanodevice conception. This CP has been attracting a considerable attention for three decades due to its high conductivity, good environmental stability and ease of preparation. It offers tremendous technological potential such as electronic devices[1] chemical and biological sensors,[2,3] electrode in rechargeable batteries,[4] antistatic coating[5] and electrochemical muscles[6].

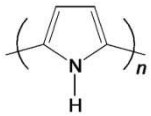

Figure 2.1 *Ideal structure of PPy under its neutral reduced state*

The "sandwich" configuration requires that the polymer does not have a tubular geometry. Indeed, the preferential formation of PPy nanowires (instead of nanotubes) is an essential condition to avoid short-circuits during the study of the transport properties of these hybrid nanowires. Different techniques exist to yield PPy 1D nanostructures[7,8,9,10,11] but the most suitable one for the fabrication of multi-striped nanowires remains the "hard template" strategy[12]. This classical method consists in alternately electrodepositing the different materials within the nanopores of a membrane. Filled as hollow nanostructures can be formed, the polymeric morphology being governed by the applied synthesis parameters. Martin and co-workers[13] were interested in the chemically or electrochemically performed synthesis of polypyrroles, polythiophenes and polyanilines using polycarbonate or alumina membrane as template. To explain the growth of nanotubes in a template, they suggested solvophobic and electrostatic interactions between conductive polymer and the template. This theory put us on the right track but was not enough to explain the growth of more or less partially filled nanotubes observed by carrying out electrochemical synthesis. We developed the synthesis of filled PPy nanostructures by using cyclic voltammetry as electrochemical method and lied to the conclusions that PPy nanowires were obtained in precise electropolymerization conditions depending on the choice of parameters such as monomer concentration, potential scanning range, pore diameter, and in the case of cyclic voltammetry the scanning rate[14] (see § 2.2.1). Lee and co-workers[15,16] recently investigated the mechanisms explaining the morphological transition between nanowire and nanotube. They deduced, from their experiments on PEDOT and polypyrrole synthesis by chronoamperommetry, a mechanism based on monomer diffusion and reaction kinetics (Figure 2.2). The polymer morphology could be controlled by fixing experimental parameters such as the applied potential, the monomer concentration and base electrode shape (Figure 2.3).

Our successful works on the synthesis of PPy nanowires paved the way to the possible synthesis of tri-segmented metal-PPy-metal nanowires. Among the rare studies performed on small diameter conjugated polymer-based hybrid nanowires, none of them reported on the structural

characterization of the metal/polymer interfaces, which could however, play an important role on the electrical properties.

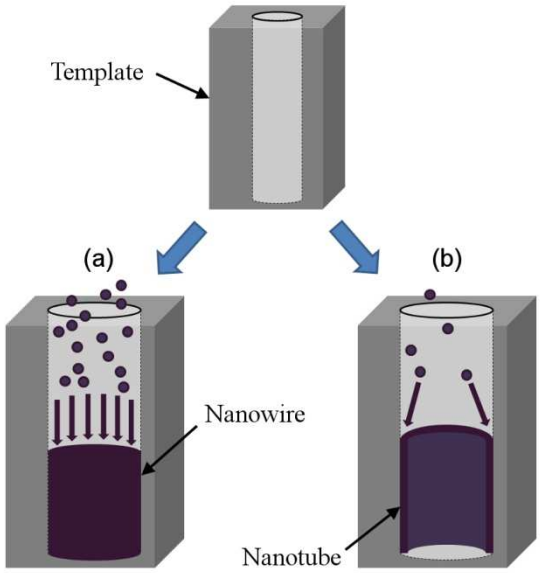

Figure 2.2 *Scheme of the growth mechanism of polymer nanostructures in nanoporous template based on Diffusion and Reaction Kinetics [15] (the small purple balls represent monomers). (a) Slow reaction rate and sufficient monomer supply lead to a polymer nanowire. (b) Fast reaction rate and insufficient monomer supply lead to a polymer nanotube. The insoluble polycations are formed at the pore periphery and interact with the anionic sites of the membrane. By combined solvophobic and electrostatic effects, the polymer preferentially nucleates and grows on the pore walls.*

In this chapter, the synthesis, the structural and electrical characterization of hybrid multi-segmented gold (or platinum)-PPy nanowires are presented. TEM observations of the resulting metal-PPy-metal hybrid nanowires revealed two morphologically different PPy/metal interfaces. The metal-onto-PPy interface is mechanically more robust than the PPy-onto-metal interface. Several strategies were considered to improve the mechanical strength of these weak zones, among which the change of noble metal, the use of an adapted organic self-assembly monolayer or the modification of the electrochemical growing parameters. Information on the doping level of PPy junctions were gathered by X-ray photoelectron spectroscopy (XPS).

The analysis of the nitrogen spectra shows that low doping ratios were reached in nanowires. This was attributed to the fact that during the deposition of the upper metallic segment, the polymer was partially reduced, resulting in a decrease of its doping rate, and thus its conductivity.

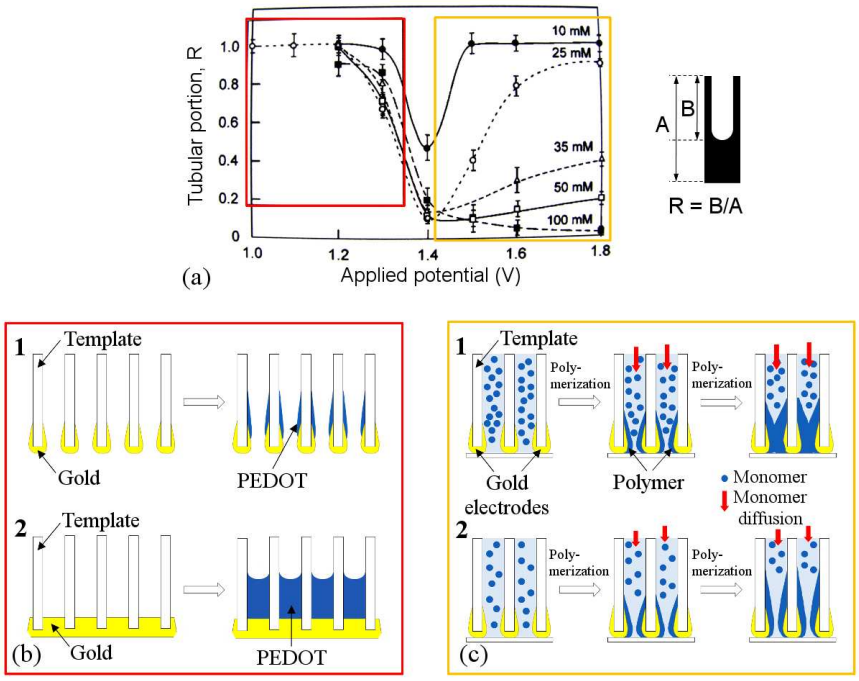

Figure 2.3 *(a) Potential dependence of the polymer tubular fraction R as a function of applied potential at given monomer concentrations in the electrochemical template synthesis on annular base electrode of PEDOT nanostructures. (b) At very low oxidation potentials (E ≤ 1.4 V), 1- for template electrosynthesis on annular base electrode, nanotubular structures are favored and become relatively insensitive to monomer concentrations, 2- for template electrosynthesis on flat-top electrodes, solid nanowires are produced; the potential and monomer concentration dependences of their tubular portions becomes explainable by the diffusion and reaction kinetics. (c) At high oxidation potentials (E ≥ 1.4 V), the diffusion and reaction kinetics determine the nanostructures geometry: 1- slow reaction rate under sufficient monomer supply gives filled nanostructures, 2- fast reaction rate under insufficient monomer supply gives hollow nanostructures(Lee et al. [16]).*

Finally, in collaboration with Loïk Gence and Sorin Melinte from DICE Lab, variable temperature electrical measurements were performed on tri-segmented nanostructures of diameters ranging from 40 nm to 160 nm to analyze their electrical transport. They were measured in both vertical (multiple-nanowire contained within polycarbonate template) and planar (single-nanowire deposited on gold electrical contacts) geometry. If the three-dimensional Mott variable range hopping (VRH) model provides a complete framework for the understanding of transport in PPy nanowires with diameters down to 50 nm, the 40 nm-diameter samples follow a power-law T-dependence of the resistance, indicative of the critical regime of disorder-induced metal-insulator transitions. These results are in correlation with those obtained for the poly(3,4-ethylenedioxythiophene) (PEDOT) nanowires,[17] where a transition from an insulating regime to a metallic one occurs too as the diameter of the nanowires decreases.

2.2 Results and discussion

2.2.1 Synthesis of PPy nanowires: general considerations

By tuning some electrochemical parameters and using cyclic voltammetry as non classical electrochemical deposition method, it was previously demonstrated that polypyrrole nanowires, instead of nanotubes, can be obtained.[14] In this work, we explored, into more details, the influence of some electrochemical growth conditions (pore size of the template, monomer concentration and potential sweep rate) on the resulting morphology of polypyrrole (PPy) nanostructures established within the pores of polycarbonate (PC) track-etched membranes with pore size ranging from 40 to 160 nm. The morphology and dimensions of the different PPy nanostructures were analyzed by scanning and transmission electronic microscopies (SEM and TEM respectively) after dissolution of the template. Typical SEM images (Figure 2.4.a) present PPy nanostructures gathered in bundles on their upper part preventing from distinguishing partially hollow nanowires from nanotubes. Therefore, complementary investigations shoud be done by TEM to fix that question (Figure 2.4.b).

Two first trends emerged from the study by SEM. The first one concerns the influence of the monomer concentration used in the electropolymerization bath. For fixed pore diameters of the template (Φ = 100 nm), we observed that decreasing the pyrrole concentration, from 0.1 to 0.005 M, leads to an increase of the filled portion of the PPy nanostructures (Figure 2.5.a-c). The second one concerns the influence of the potential scanning rate used for the electropolymerization of pyrrole by cyclic voltammetry. For fixed pore diameters of the template and monomer concentration, increasing the scanning rate from 100 to 300 $mV.s^{-1}$, also leads to an increase of the filled portion of the PPy nanostructures (Figure 2.5.d-f). Another general observed tendency is that the larger the pore diameters are, the higher the potential scanning rate should be. Finally, it should also be pointed out that a too high scanning rate (beyond 100 $mV.s^{-1}$) prevents from electropolymerizing into the narrowest nanopores. We can notice that the monomer concentration influence deduced from the SEM pictures is in contradiction with the works of Lee[16] mentioned in the introduction. Figure 2.6 shows that, by thinking in terms of nanotubular portion *R,* as Lee and his co-workers did, the series of pictures a, b and c is actually not necessarily in contradiction with the preceding cited literature. Indeed, despite the appearances, the so-called hollow nanostructures of Figure 2.5.a may be more solid nanostructures than those of Figure 2.5.c, as schematized in the insets of Figure 2.6. This confirms that SEM is not the most appropriate tool for achieving the morphological study of the polymer and, observations by TEM should be performed to remove any ambiguity.

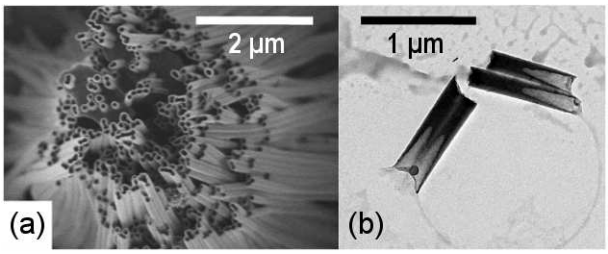

Figure 2.4 *(a) SEM image of PPy nanostructures after dissolution of the membrane. (b) TEM image of partially hollow PPy nanowires.*

From these preliminary works, it results that the morphology of the PPy nanostructures can be tuned from nanotubes to nanowires, passing through

partially hollow nanowires, by playing essentially on the pyrrole electropolymerization and diffusion rates. The monomer concentration, but also, specifically in cyclic voltammetry, the scanning rate, play important roles in determining the morphology of the PPy nanostructures. If the monomer concentration dependence has already been studied, that of the scanning speed should be discussed.

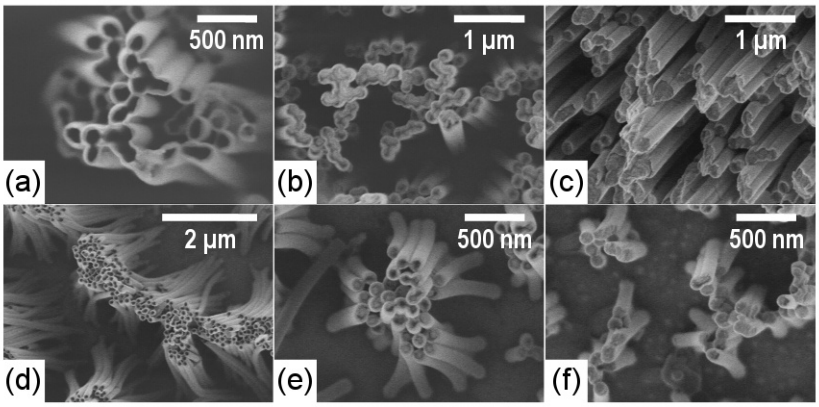

Figure 2.5 *SEM images of PPy nanostructures synthesized by cyclic voltammetry over the 0 to 0.85V potential range: (a,b,c) at a constant potential scanning rate of 300 mV.s^{-1} but for various pyrrole concentrations (a) 0.1 M (b) 0.01 M (c) 0.005 M and (d,e,f) at a constant monomer concentration of 0,01 M but for different scanning rates (d) 100 mV.s^{-1} (e) 200 mV.s^{-1} (f) 300 mV.s^{-1}.*

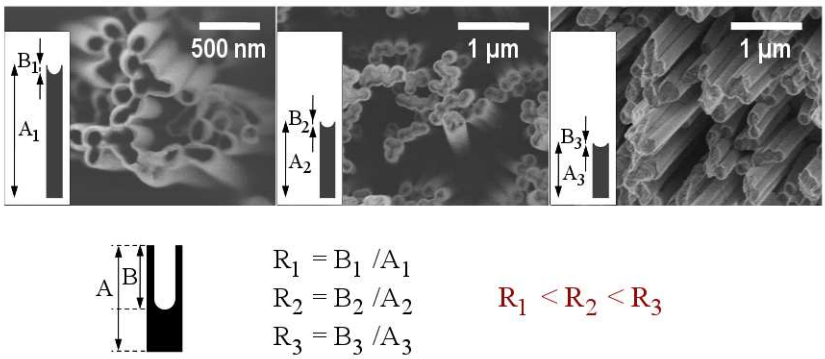

Figure 2.6 *Monomer concentration dependence of the tubular portion of PPy nanostructures: questioning about SEM pictures. The SEM images correspond to those of Figure 2.5 a, b and c. For each SEM image, insets show hypothetical schematic representation for PPy nanostructures of tubular portion B and length A.*

This plausible hypothetical case is in complete contradiction with what one could deduce a priori from the SEM images. It is possible that the most hollow nanostructures are actually the most filled ones.

A more detailed study of the influence of these electrochemical polymerization parameters on the polymer morphology will be presented further in the section dealing with the multi-segmented noble metal-PPy nanowires, as the TEM characterization of these nanostructures allows obtaining unambiguous images of the polymer, with a distinction between the nanotubular portion and the filled one.

2.2.2 Synthesis of multi-segmented noble metal-PPy nanowires

The possible electrosynthesis of filled PPy nanowires paved the way to the elaboration of hybrid metallic nanowires containing a polymer junction. In the following section, we will show that multi-segmented nanowires can be easily produced using an all-electrochemical process, by changing the plating solution and accordingly, adapting the electrochemical technique and the parameters of deposition. Whatever the nature of deposited metals and polymers, the same general scheme illustrates the synthesis of multi-striped nanowires through electrochemical way (Figure 2.7). One major advantage of the exclusively electrochemical process to prepare hybrid nanowires is that the length of each segment as well as the total length of the hybrid nanowires can be easily varied and adjusted at the desired length. The diameters of the nanowires are dictated by the pore size of the template, while their lengths are directly related to the amount of charge passed through the system according to Faraday's law. For the elaboration of metal-conjugated polymer-metal nanowires, we had to consecutively deposit metal and polymer stripes by connecting electrochemically opposite redox reactions. Indeed, metal segments are deposited by reduction of metal ions contained in the bath, while the conjugated polymer segment is synthesized by anodic oxidation of the monomer. Consequently, questions of compatibility between the processes used to successively deposit materials could arise. More precisely, the synthesis conditions of a material can partially damage the material previously deposited, which has an impact on the robustness of the interface between the two segments. The electropolymerization on an oxidizable metal is a classical case of

problematical interfacing between materials, for example the growth of polypyrrole directly on a nickel segment (see chapter 5). We therefore decided to start our research works dealing with the synthesis of hybrid nanostructures by using noble metals, such as gold or platinum for the fabrication of the metallic segment.

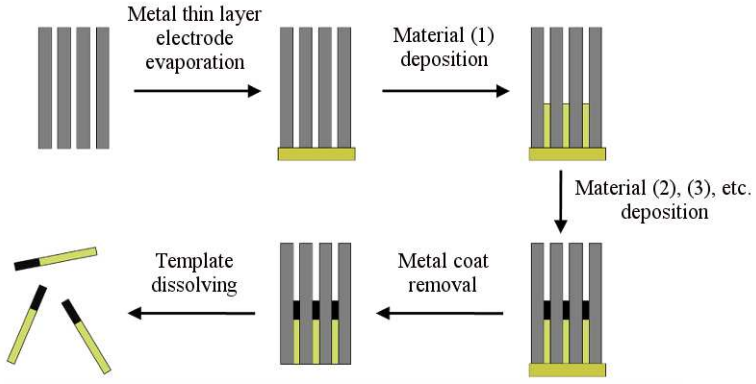

Figure 2.7 *General scheme for the synthesis of multi-segmented nanowires by the all-electrochemical template method.*

a) Synthesis of gold-PPy-gold nanowires

To start, we developed the electrochemical template method for preparing tri-segmented Au-PPy-Au nanowires of various diameters. The first step consisted in the electrodeposition of gold by cyclic voltammetry (CV) within the nanopores of a PC template under the electroplating conditions described in the experimental part. By adjusting the number of potential cycles accomplished at a scan rate of 200 $mV.s^{-1}$ over the 0 to initial potential E_i (about 0.7 V *vs.* Ag/AgCl RE) range during the electrodeposition, it was possible to control the length of the resulting Au nanowires. Figure 2.8 indeed shows that the gold nanowires length increases linearly with the number of potential sweeps. One can also notice that the gold electrodeposition rate decreases when the pore size of the template increases. The growth rates for diameters of 62, 110, and 147 nm are 7.5, 5.2 and 4 $nm.s^{-1}$, respectively.

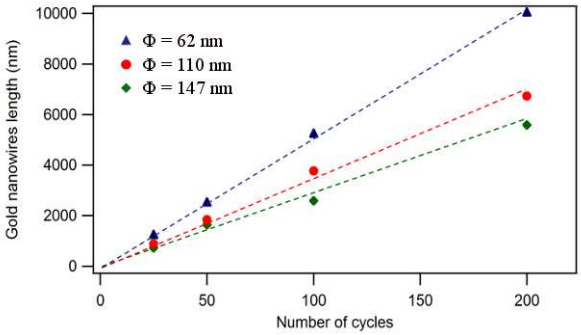

Figure 2.8 *Gold nanowires length as a function of the number of potential scans accomplished during the electrodeposition, for various diameters.*

Cyclic voltammograms recorded during this first step present a "sigmoidal" shape (Figure 2.9), characteristic of electrochemical reactions carried out on nanoelectrodes.

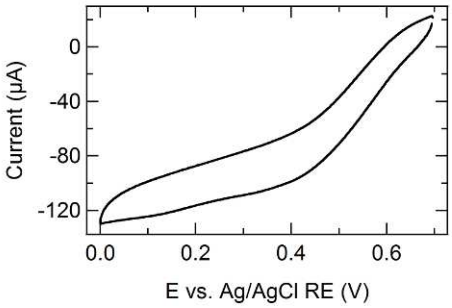

Figure 2.9 *Typical cyclic voltammogram recorded during the template growth of the first gold segment for the synthesis of tri-segmented Au-PPy-Au nanowires.*

The next step consisted in the electrodeposition of a PPy segment on the top of the Au segment. Electropolymerization of pyrrole was carried out using CV by repeating scans over the 0 to 0.85 V potential range. The length of the polymer junction (L_j) can be relatively well tuned by adjusting the number of electrochemical cycles. Figure 2.10 shows typical calibration curves for two selected pore diameters and synthesis conditions. Thanks to the values of sweep rate used for the polymer synthesis, it is possible to represent the evolution of *Lj* as a function of time. A linear regression made on the curves *Lj*(t) assesses the PPy growth rates. PPy average growth rates

of 1120 and 110 pm.s^{-1} were found for diameters of 62 and 110 nm, respectively. As generally observed by SEM, the polymer segment length is locally quite homogeneous (Fig. 2.11.a). However, when looking at hundreds of nanowires coming from different regions of the sample, an important disparity in length values appears for polymer segment lengths exceeding the micrometer. This disparity is particularly large in the case of the 62 nm diameter PPy nanowires where several micrometers polymer are grown in a few hundred cycles (faster growing rate). Differences in segment lengths are also sometimes observed between samples prepared under identical synthesis conditions, especially when the polymer growth rates are high. To explain the disparity of polymer nanowire lengths within the same sample, a purely technical reason can be invoked. In the electrochemical assembling we used (see Experimental Part), a Teflon cell is pressed against the sample through a rubber annular gasket. The sample, which consists of a gold coated polycarbonate thin membrane, does not connect perfectly and identically with the rigid plate of platinum used as working electrode on the entire active area. Therefore, depending on the location on the sample, the electrosynthesis takes place more or less rapidly. A picture of the top surface of a sample taken after the synthesis of tri-segmented Au-PPy-Au nanowires, reflects this inhomogeneity of the nanowire growth rates (Figure 2.11.b.) We can see on this image that the upper gold segments largely overflow from the membrane in some regions (light areas) while the overflow does not occur in other ones (dark areas). These differences in segment lengths in different regions of the sample as between samples synthesized in identical conditions does not pose a particular problem in our case since the majority of the electrical property measurements are performed on single nanowires fully characterized in terms of their structure. A possible improvement would be to work with supported membranes, but there will always be a difference between the growth rates in the sample center and periphery.

The relatively high disparity which we have discussed for the polymer is also valid for gold nanowires, even if it was not shown in Figure 2.8.

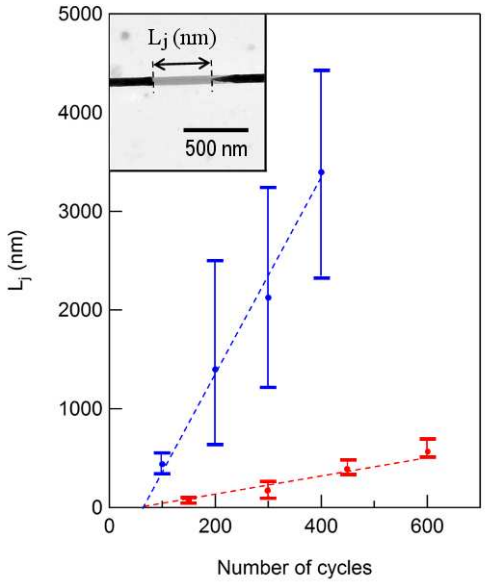

Figure 2.10 *PPy nanowires length (Lj) evolution with the number of performed electrochemical cycles for 62 nm and 110 nm diameters (blue and red dots, respectively). PPy was synthesized in the following conditions: the electropolymerization bath contained 0.02 M of pyrrole and 0.1 M of $LiClO_4$ (without surfactant); scans were repeated over the 0 to 0.85 V vs. Ag/AgCl RE potential range at 200 mV.s^{-1} and 400 mV.s^{-1} for the 62 nm and 110 nm diameters, respectively.*

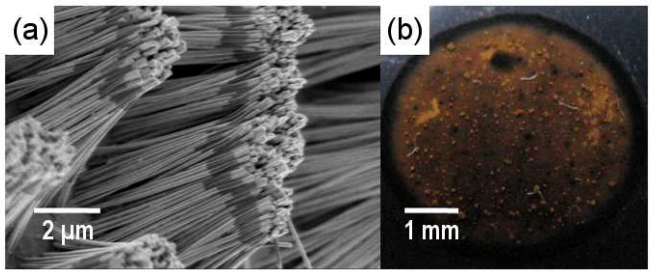

Figure 2.11 *(a) SEM picture of 90 nm diameter Au-PPy-Au nanowires. (b) Photo of the surface of a sample taken after the synthesis of nanowires.*

Figure 2.12 presents the evolution of the cyclic voltammogram for PPy nanowires of 62 nm in diameter grown at a scan rate of 200 mV.s^{-1}. In this case, the intensity of the irreversible pyrrole oxidation peak (starting at ~0.65

V) increases during the electrodeposition process (higher current value at the 200th cycle than at the first one).

Then, above the polymer junction, another gold segment was electrodeposited under similar conditions to those used in the first step of the process. A drastic change of the CV curve shape, accompanied by a strong increase of the current, indicates that deposition "overflows" the nanopores. So, the emergence of nanowires at the top surface of the template can be easily detected (Figure 2.13).

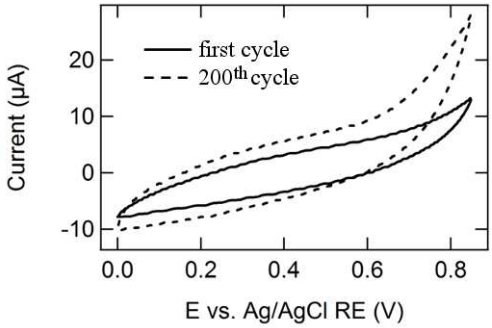

Figure 2.12 *Cyclic voltammograms recorded during the deposition of PPy nanowires of 62 nm in diameter.*

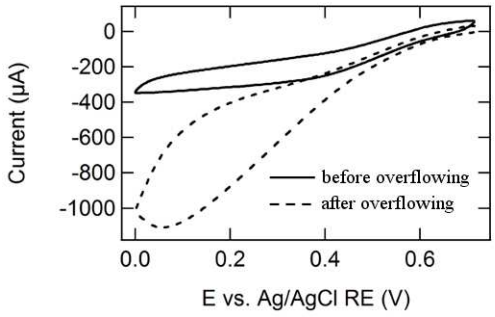

Figure 2.13 *CV curves characteristic of gold electrodeposition.*

b) Structural characterization of the tri-segmented Au-PPy-Au nanowires

The resulting nanowires have been observed by scanning electronic microscopy (SEM) and transmission electronic microscopy (TEM) after

dissolution of the PC template. The two types of materials are unambiguously distinguishable by SEM and TEM without any particular contrasting treatment. In a classic SEM picture, tri-segmented Au-PPy-Au nanowires appear as a dark polymer segment inserted between two bright metal segments (Figure 2.14.a). The other way round, by TEM, due to a lower electronic density, the polymer junction appears more transparent than the two metallic segments (Figure 2.14.b).

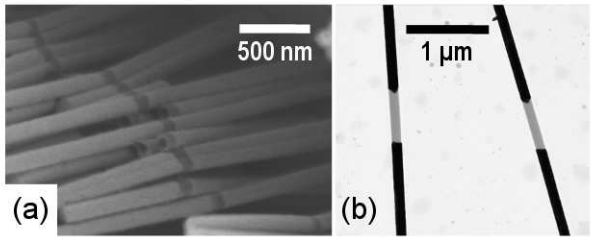

Figure 2.14 *(a) SEM picture of Au-PPy-Au nanowires of 90 nm in diameter. (b) TEM picture of Au-PPy-Au nanowires of 115 nm in diameter.*

Mechanical strength of the PPy/metal interfaces[18,19]

Tri-segmented Au-PPy-Au nanowires with various diameters (40 to 160 nm) and tunable PPy junction lengths from less than 10 nm to more than 3 micrometers were synthesized (Figure 2.15). The TEM pictures shown in Figure 2.15 demonstrate the absence of electrical short circuits (no physical contact between the two metallic segments), even for very short PPy junctions (down to 10 nm, Figure 2.15.a).

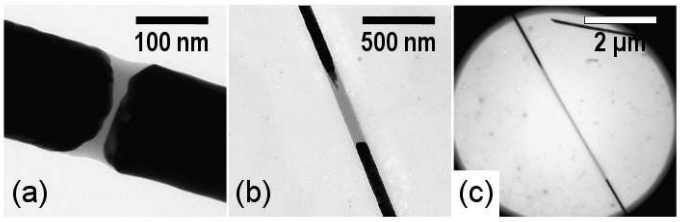

Figure 2.15 *TEM pictures of Au-PPy-Au nanowires after template dissolution. By adjusting the number of scans carried out during the electropolymerization step, a polymer junction of tunable length (Lj) is synthesized. (a) Lj < 10 nm; Φ = 150 nm. (b) Lj ≈ 400 nm; Φ = 62 nm. (c) Lj > 3 µm; Φ = 62 nm.*

However, once freed from the PC membrane, numerous Au-PPy-Au nanowires with one missing metallic segment were observed, particularly for the narrow diameters. Down to 40 nm in diameter, entire nanowires were rare (Figure 2.16).

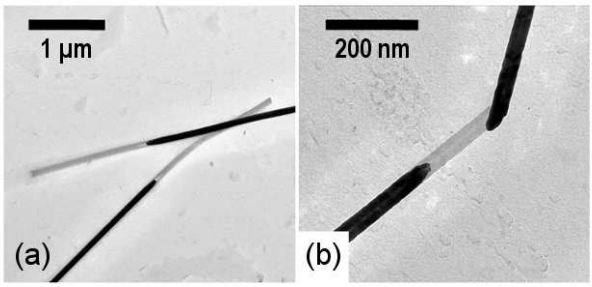

Figure 2.16 *TEM pictures of broken nanowires: (a) two 70 nm diameter nanowires with one missing metallic segment, (b) a 40 nm diameter nanowire with one broken metallic segment.*

This observation led us to investigate into more details the morphology and strength of both PPy/metal interfaces. Characterizations by TEM at high magnification, summarized in Figure 2.17, revealed that the polymer-onto-metal interface and the metal-onto-polymer one have quite different shapes. The relatively flat morphology of the bottom interface (Figure 2.17.b) indicates that the first metal section growth is homogeneous under our synthesis conditions. On the other hand, for the upper interface, a conical gold meniscus soars into the PPy section, ensuring a stronger link between the polymer and the upper metal section (Figure 2.17.c). This results in a larger adhesion surface (S_a) compared to that of the bottom interface, explaining why the metal-onto-polymer interface is mechanically more robust than the polymer-onto-metal interface. The presence of this meniscus could be explained by pore wall effects, similar to those leading to the formation of PPy nanotubes.[13,15] In the present work, the natural tendency of PPy to grow along the pore walls was thwarted by adjusting pyrrole electropolymerization rate. The creation of the meniscus seems to occur as soon as the electropolymerization is initiated and it has been observed in all investigated samples displaying various PPy junction lengths.

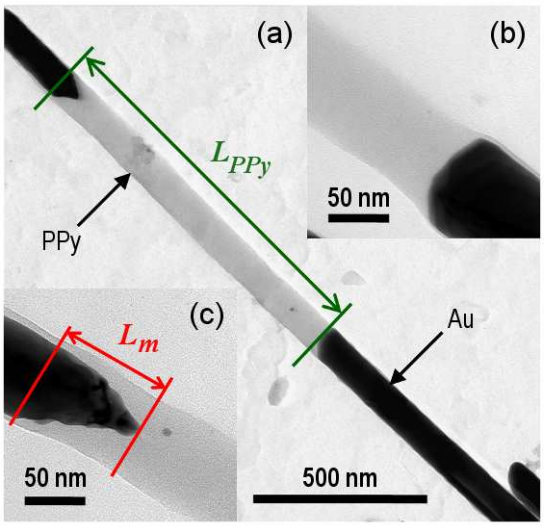

Figure 2.17 *TEM characterization of the two Au-PPy-Au nanowire interfaces. (a) TEM picture of a 70 nm diameter Au-PPy-Au nanowire. (b) The polymer-onto-metal bottom interface enlargement. (c) The metal-onto-polymer upper interface one. Lengths of the gold meniscus L_m and of the polymer segment L_{PPy} are indicated.*

The gold meniscus length (L_m) has been measured by TEM for several upper interfaces of 70 and 90 nm diameter Au-PPy-Au nanowires with different PPy segment lengths (L_{PPy}). The results are reported in the table of Figure 2.18. The corresponding adhesion surfaces (S_a) are also given in this table.

	Φ (nm)					
	70			90		
L_{PPy} (nm)	670	1680	3110	915	1440	3340
L_m (nm)	66	75	88	66	180	225
S_a (nm²)	9680	11000	12900	16400	33740	42600

(a)

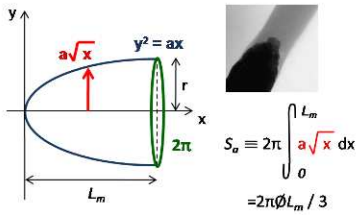

(b)

Figure 2.18 *(a) Length of the PPy segment for various Au-PPy-Au nanowires. For these nanowires, the gold meniscus length (L_m) and the corresponding calculated adhesion surface (S_a) of the upper interface are reported. (b) Principle of S_a calculation; the gold meniscus was considered as a parabola.*

For both nanowire sizes, Lm and the adhesion surface increase with the length of PPy segment. Considering meniscus length data (e.g. L_m = 66 nm) for both diameters, we find that the corresponding adhesion surface for the largest diameter is much higher (16400 nm^2 for Φ = 90 nm vs. 9680 nm^2 for Φ = 70 nm). Consequently, Sa values are generally smaller for all the 70 nm diameter nanowires compared to the 90 nm diameter nanowires. The adhesion surface roughly correlates with the percentage of observed unbroken nanowires and it is thus an important parameter in assessing the mechanical robustness of the nanowires.

Optimization of synthesis parameters to get the strongest upper interface

Concerning the metal-onto-polymer interface, we naturally thought that for a given diameter, there is an optimum value of electropolymerization rate at which the robustness of this upper interface is at the maximum. Therefore, we have systematically investigated the effects of the potential sweep rate on the morphology and mechanical strength of the PPy/Au interface. In Table 2.1, we report the results of this study for 62 nm diameter Au-PPy-Au nanowires. The meniscus length to polymer length ratios ($\mathcal{R} = L_m/L_{PPy}$) and the corresponding percentages of nanowires broken at the upper interface (ρ) were calculated from TEM observations for the three following potential scan rates 100, 200 and 400 $mV.s^{-1}$. From this study, it appears that 200 $mV.s^{-1}$ is the best value to obtain 62 nm diameter nanowires with the strongest upper interface.

Table 2.1 *L_m-PPy segment length ratios and percentages of broken nanowires (Φ = 62 nm) at the upper interfaces (ρ) for different potential scan rates.*

Scan rate **($mV.s^{-1}$)**	$\mathcal{R} = L_m/L_{PPy}$	ρ (%)
100	0.35	38
200	0.26	10
400	-	84

To understand why this intermediate value is the best one, we should consider the two extreme cases presented in Figure 2.19. When a too slow

scan rate is applied, there is a very long meniscus with at the upper part of the polymer tubular portion, very thin walls that are too fragile to maintain the top metal segment. On the other hand, when a too fast scan rate is applied, it results in a rather flat upper interface that strongly reduces its mechanical strength.

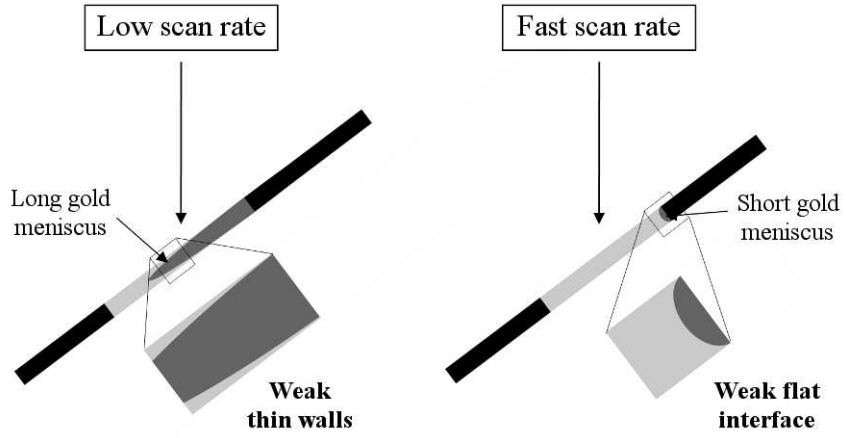

Figure 2.19 *Scheme illustrating the two extreme cases of obtained tri-segmented Au-PPy-Au nanowires depending on the scan rate used during the electropolymerization of pyrrole.*

The potential scanning speed, as well as the applied potential and the monomer concentration, has an influence on diffusion and electropolymerization kinetics. To explain why the polymer nanowire changes from a hollow to a nearly flat upper end with increasing the potential scan rate, the effect of a faster potential scan on the electropolymerization kinetics can be suggested. At high scan rate, the reaction undergoes disruption at high frequency, which probably reduces its speed. Slower electropolymerization rate obtained at faster potential scan rate could explain a more homogeneous growth in the pore and therefore un flatter top as observed. However, the potential scan rate has an influence on the diffusion phenomenon too. By scanning the potential faster, monomer supply occurring in the potential range where the reaction does not occur has less time to come about. Yet it seems that in this case increasing the potential scanning speed limits the electropolymerization rate for the benefit of more filled PPy nanostructures.

The optimization of the potential scan rate has been performed for nanowires presenting different diameters. The results of this study, presented in Table 2.2., show that the optimum scan rate increases with the pore diameter of the used template. This can be explained by the slower kinetics of monomer diffusion in smaller diameters. In that case, it is therefore required to sweep the potential more slowly in order to give more time for the reactants to diffuse into the nanopores during the reaction interruption.

Table 2.2 *Optimized potential scan rate according to template pore diameters to synthesize PPy nanowires. [pyrrole] = 0,02 M.*

Pore size (nm)	**Scan rate (mV s^{-1})**
30	100
50	200
70	300
100	400
160	500

Another important parameter playing on the polymer morphology is the monomer concentration in the electropolymerization bath. A study of the influence of this parameter was carried out for 62 nm diameter Au-PPy-Au nanowires. The $\mathcal{R}$ ratios (($\mathcal{R}$ = L_m/L_{PPy}) were calculated from TEM observations for pyrrole concentrations of 5.10^{-3}, $2.10^{-2,}$ 5.10^{-2} and 10^{-1} M at a given scan rate of 200 mV.s^{-1}. The results are listed in Table 2.3. First, for the lowest monomer concentration (5.10^{-3} M), no polypyrrole was formed. For the other concentrations, the following conclusions can be drawn: the higher the monomer concentration is, the higher the polymer junction length (and so, the electropolymerization rate) is, and the lower the $\mathcal{R}$ value and consequently, the corresponding meniscus size are. Thus, for this diameter, increasing the monomer concentration, lead to longer and more filled PPy nanostructures. These results are in good agreement with those recently published by Lee *et al*.[16]

Table 2.3 *The $\mathcal{R}$ ratios for the relative monomer concentrations. For each synthesis, scan rate was fixed at 200 mV.s^{-1}, and the number of cycles at 100.*

[Py] (M)	L_{PPy} *(nm)*	L_m *(nm)*	$\mathcal{R} = L_m/L_{PPy}$
5.10^{-3}	-	-	-
2.10^{-2}	560	150	0.26
5.10^{-2}	2760	315	0.11
10^{-1}	4895	430	0.09

Solutions to overcome the problem of the bottom interface weakness

In the case of the bottom interface, we could not control the shape of the interface by playing on electrodeposition parameters. We therefore tried to improve the mechanical strength of this interface by increasing the adhesion between the two different materials.

Among the different possible strategies, we first investigated the use of self-assembled alkylthiol monolayer onto gold. Self-assembled monolayers (SAM) of 11-mercaptoundecanoic acid (MUA) and 3-mercaptopropionic acid (MPA) were tested. They were inserted between the gold and PPy segment. By using this type of alkylthiol, we planned to create an electrostatic link between the negatively charged carboxylate groups of the chemisorbed monolayer and the positively charged growing polycation (Figure 2.20). On MUA monolayer, it was not possible to grow a polypyrrole segment. This is surely due to the presence of long aliphatic chains in MUA that passivated the Au electrode. Polymer formation occurred on the shorter chemisorbed MPA layer. However, no interface robustness improvement was brought by that chemical treatment. Moreover, in the presence of this short alkylthiol adsorbed onto the metallic segment, PPy nanowires had a different electrical transport signature. These samples, containing an additional insulating organic layer were logically more resistive than the classical tri-segmented nanowires.

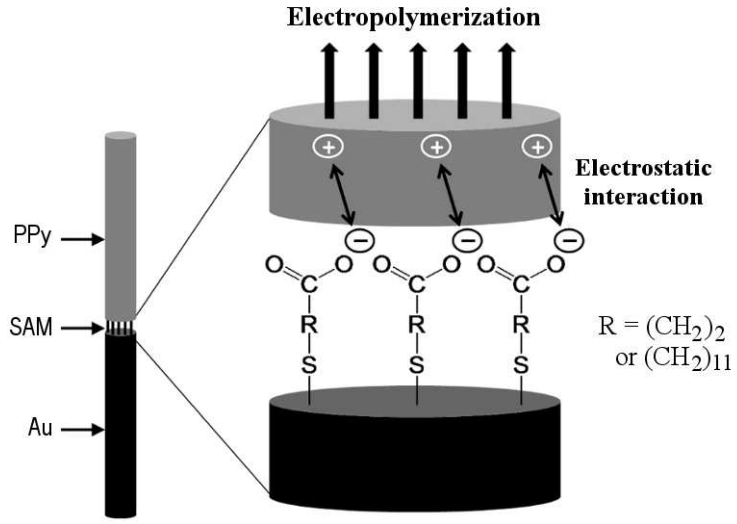

Figure 2.20 *Hypothetical scheme for the adhesion of the PPy to the metal throughout a bipolar molecule based on electrostatic interactions.*

We therefore tried another way for improving the adhesion between the first metal segment and the PPy. We decided to change the nature of the noble metal and used Pt for the bottom metallic segment. Interestingly, observations of Pt-PPy-Au nanowires show that stronger bottom polymer-onto-metal interfaces were obtained by this way (Figure 2.21). By optical observation, we estimated that the percentage of broken nanowires decreased by a factor of ~3 when preparing Pt-PPy-Au instead of Au-PPy-Au nanowires. It is possible that the nitrogen atom has a stronger interaction with platinum than with gold, which would explain a better adherence of PPy on the first one of the two metals. Thanks to that large robustness improvement of the polymer-onto-metal interface strength, synthesis of more elaborated structures presenting several PPy junctions has been carried out. Examples of such nanostructures, Au-PPy-Pt-PPy-Au nanowires and multi-segmented nanowires presenting six metal/polymer interfaces are illustrated in Figure 2.22.a and Figure 2.22.b, respectively.

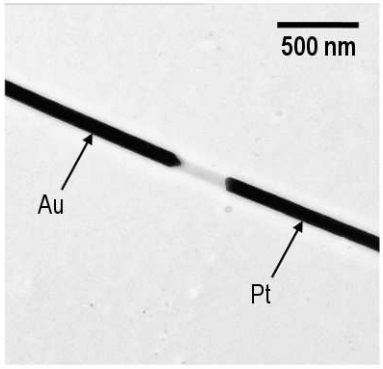

Figure 2.21 *TEM picture of a 90 nm diameter Pt-PPy-Au nanowire.*

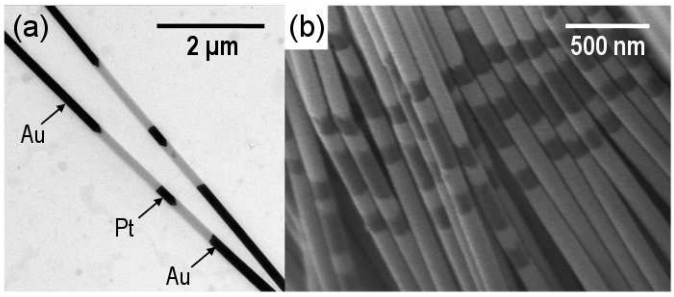

Figure 2.22 *(a) TEM picture of 90 nm diameter Au-PPy-Pt-PPy-Au nanowires. (b) SEM picture of 90 nm diameter multi-PPy junction Pt-PPy-Pt-PPy-Pt-PPy-Pt nanowires.*

c) PPy doping level measurements by XPS[17]

Besides the structure of the metal/polymer interfaces, the PPy doping ratio is another key parameter playing on the electrical transport properties of the hybrid nanowires. X-ray photoelectron spectroscopy (XPS) is a particularly useful tool for gathering information on the doping level of electroactive polymers. We therefore used this technique in order to evaluate and compare the doping ratios of PPy films with the doping ratios of PPy nanostructures grown in similar conditions. This allowed us to highlight the effect of confinement during the electrosynthesis.

PPy nanowires

First, we determined the doping ratio of PPy nanowires by XPS. For that purpose, we synthesized very long (several microns) PPy nanowires to have enough material and so obtain individual elements spectra of sufficient intensity. For this, a surfactant, sodium dodecylsulfate (SDS), was added to the electropolymerization bath. It allows to obtain larger quantities of polymer (in our case longer polymer nanowires) without changing other synthesis parameters. Figure 2.23 shows a wide scan survey of $PPyClO_4^-$ /DS^{2-} nanowires in which the different species can be identified through the main peaks *C1s* (285 eV), *N1s* (400 eV) and *O1s* (532 eV). The dopants, indicated by the presence of *S2p* (169 eV) and *Cl2p* (208 eV), appear less clearly. The presence of a *Si* signal comes from the silicon wafer substrate used to disperse the nanowires. Provided that there are no contaminants in the samples, doping ratios of conjugated polymers are commonly determined by calculating the ratios between atomic percentages of atoms coming from the dopant species and atomic percentages coming from atoms of the polymer chains. So, in our case, we should calculate the (*Cl* + *S*)/ *N* atomic ratios. But, due to the very low intensity of the *Cl2p* and *S2p*, it was not possible to get accurate values by this way.

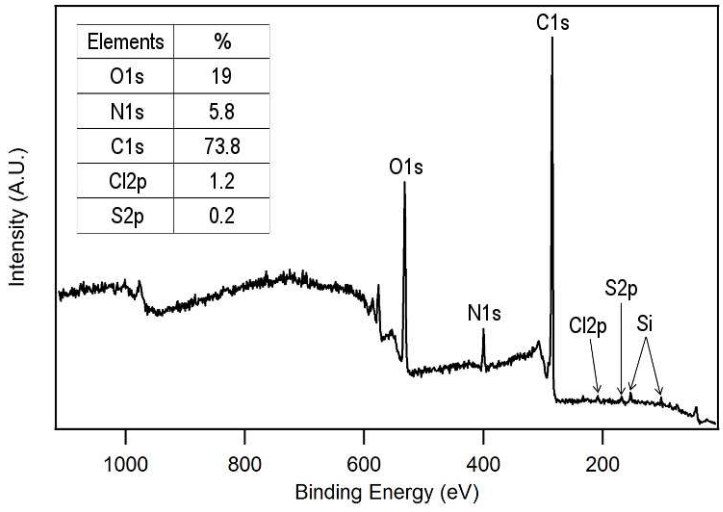

Figure 2.23 *General XPS spectrum of 70 nm diameter $PPyClO_4^-/DS^{2-}$ nanowires.*

Previous XPS works[20,21,22] on PPy demonstrated that the imine defects (=N-), the amine (-NH-) links, and positively charged nitrogen atoms namely (-N+) corresponding to any particular intrinsic oxidation state and protonation level of the polymer can be quantitatively differentiated in the curve-fitted N1s XPS spectra. A typical N1s curve fitted core level spectrum of PPy nanowires is presented in Figure 2.24. The N1s peak was decomposed into two Gaussians. Indeed, the signal intensity was too weak to distinguish more species. The red line centered at 399.8 eV is assigned to the non-protonated nitrogens, while the green line centered at 401.9 eV corresponds to the protonated nitrogens. The doping level in those PPy nanowires, estimated by the $[N^+]/[N]$ ratio, is close to 13% (one protonated nitrogen out of eight). This low doping ratio probably results from a partial reduction of PPy during the electrodeposition of the upper metallic segment. To figure out this phenomenon, we measured the doping level of PPy films submitted to different reducing post-treatments. We performed this study on films rather than on nanowires in order to get sufficient signal and therefore accurate doping level values.

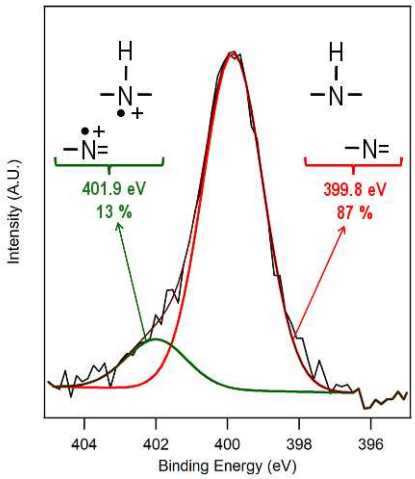

Figure 2.24 *N1s regions for 70 nm diameter $PPyClO_4^-/DS^{2-}$ nanowires.*

PPy films

PPy films were synthesized in conditions similar to those used for the growing of PPy nanowires. Then a potential of -0.2 V vs. RE, was applied for various times. This "post-treatment" reproduced the conditions used for the electrodeposition of the top Pt segment onto PPy in the synthesis of tri-segmented nanowires. A typical N1s XPS spectrum of the as-synthesized PPy films is shown in Figure 2.25.a. Two lines (blue and green curves) representing protonated nitrogens appear at binding energies higher than 400 eV, while two other lines appearing at lower binding energies 399.8 and 397.9 eV correspond to amine-like (red curve) and imine-like (brown curve) nitrogen atoms, respectively. The doping level in the as-synthesized PPy film is close to 22 %, which is a higher value than the doping level found for the 70 nm diameter nanowires. As already reported in literature for conjugated polymer nanotubes[23] , the lower doping value for the template-grown PPy nanowires compared to PPy films results from the electrosynthesis in nanopores (confinement effect). As shown in Figure 2.25 b and c, a progressive decrease of the protonated nitrogen components (blue and green curves) combined with a marked increase of the non-protonated imine-like nitrogen (brown curve) is observed when the potential of -0.2 V is applied to PPy films for 10 or 30 min. This corresponds to a decrease of the doping ratio from 22 to 17 % and further to 14 % after application of reduction conditions for 10 and 30 min, respectively. Based on these XPS experiments done on PPy films and considering the PPy nanowires doping of 13 %, we estimated that in tri-segmented nanowires, the doping ratio of PPy is only a few percents. These results are in good agreement with the values of density of states obtained from the study of transport properties (see next section).

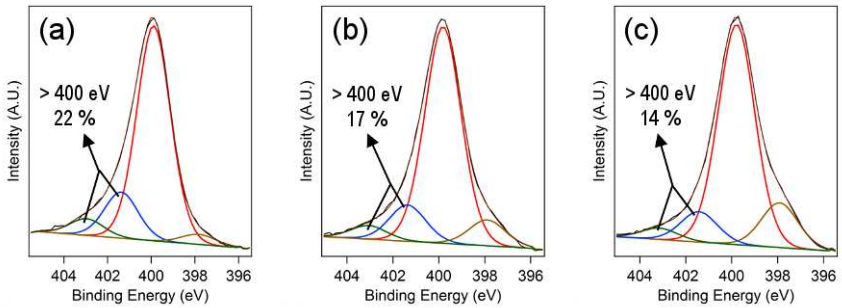

Figure 2.25 *N1s XPS fitted spectra of PPy films: (a) as synthesized, (b) after application of a reduction potential of -0.2 V for 10 min, and (c) after post-treatment of -0.2 V for 30 min.*

d) Electrical transport[18,19]

The study of the electrical properties of multi-segmented nanowires was undertaken in collaboration with the DICE laboratory (in particular, with Loïk Gence and Sorin Melinte) in the framework of the project NANOMOL (Action de Recherche Concertée). First, the current-voltage (I-V) spectroscopy, a powerful technique to gain insight into various transport phenomena such as tunneling and rectification, was used to study tri-segmented Au-PPy-Au nanowires. Variable temperature electrical measurements were carried out over the temperature range from 300 to 4 K. Electrical measurements presented in this part concerned two types of samples, multiple hybrid nanowires (nanowires still embedded in the PC template) and free single nanowires, called M and S, respectively, listed in Table 2.4. Nanowires with diameters covering the 40 to 160 nm range were studied. From the I-V (T) characteristics, resistance values calculated at zero bias as a function of T ($R_{(V=0)}$ (T)) are shown to discuss the transport mechanism. Finally, magnetoresistance measurements are presented.

Table 2.4 *Table reporting the set of presented samples*

Samples	Description
M90A	1st sample of multiple 90 nm diameter nanowires
M90B	2nd sample of multiple 90 nm diameter nanowires
M90-Pt	Multiple 90 nm diameter Pt-PPy-Au nanowires
S70A	1st sample of single 70 nm diameter nanowire
S70B	2nd sample of single 70 nm diameter nanowire
M50	Multiple 50 nm diameter nanowires
M40A	1st sample of multiple 40 nm diameter nanowires
M40B	2nd sample of multiple 40 nm diameter nanowires

Current-Voltage curves

Typical current-voltage characteristics for samples M90A and S70A and for various temperatures are presented in Figure 2.26. In all these studied specimens, the I-V curves present the following common characteristics: they are symmetrical, show no rectification effect and are ohmic between room temperature and a critical temperature T_c ~ 120 K (for samples with a diameter down to 50 nm). As it is displayed in the lower inset of Figure 2.26.a, the Φ = 40 nm category is apart since its ohmic region extended down to lower temperatures. The temperature dependences of the resistance R(T) appearing in the upper insets of Figure 2.26 increases with decreasing temperature, which is a typical behavior of a nonmetallic material. A room temperature conductivity of about 0.04 $S.cm^{-1}$ was obtained for single Au-PPy-Au nanowires, which is comparable with results relative to bulk insulating PPy. This low value was corroborated by the XPS measurements shown in the previous paragraph.

By decreasing the temperature lower than T_c, the non linearity of the I-V plots increases, indicating that a peculiar conduction mechanism occurs at very low temperatures.

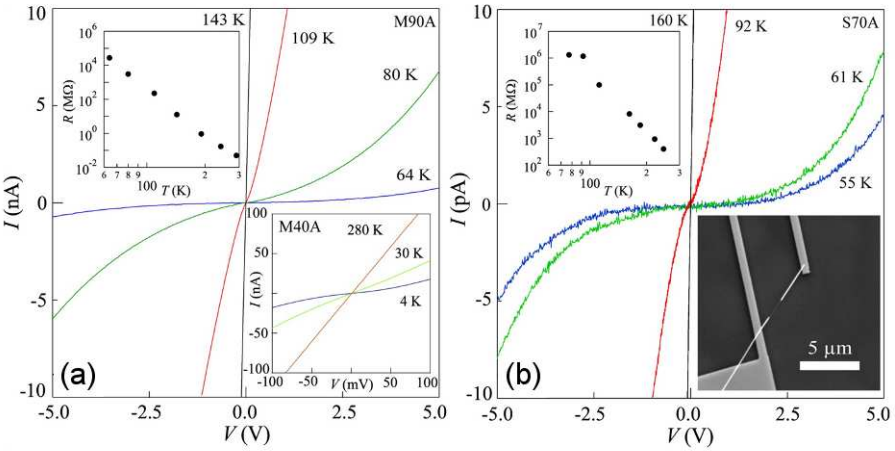

Figure 2.26 *(a) I-V characteristics for sample M90A. Lower inset gives the I-V characteristics of 40 nm diameter sample M40A. (b) I-V characteristics of a single nanowire (sample S70A) at indicated temperatures. Upper inset shows the T dependence of the resistance. Lower inset is a SEM picture of a nanowire placed on two gold leads.*

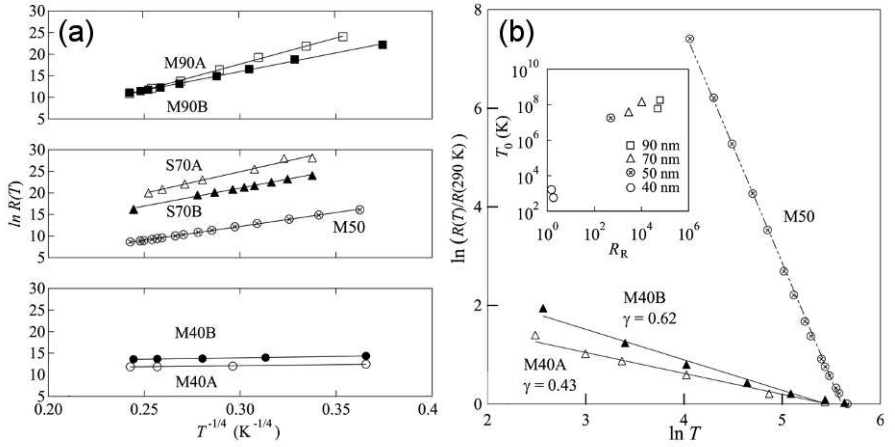

Figure 2.27 *(a) 3D-VRH plots for 90, 70, 50 and 40 nm samples. The solid lines are the 3D-VRH fits to the data. (b) Log-log plot of the resistance with temperature for samples M50, M40A and M40B. The resistance follows a power-law temperature dependence for the 40 nm samples. Solid curves are fit to the data. The dashed curve is guide for the eye. The inset shows T_0 versus R_R (see text) for all samples.*

The electrical transport in our multi-segmented nanostructures can be described by the Mott variable range hopping (VRH), mechanism dominating the electric conduction at low T in insulators. In this model, charge transport corresponds to a tunneling among states localized in a constant density of states in the material. Recent works on PPy and PEDOT nanowires have shown that the three-dimensional (3D) Mott VRH is an adapted model of charge transport in conjugated polymers nanostructures[18,24]. In the 3D-VRH model, the resistance follows the relation $ln[R(T)] \sim (T_0/T)^{1/4}$, where $T_0 = 16\alpha^3/k_B N(E_F)$ is the Mott temperature, k_B is the Boltzmann constant, α^{-1} is the localization length and $N(E_F)$ is the density of states (DOS) at the Fermi energy. The *ln [R(T)] versus* $T^{1/4}$ plots are given in Figure 2.27. The parameter T_0 was extracted from these fits for various samples. The results, listed in Table 2.5, suggest that the charge transport is easier in the narrowest nanowires. The Mott temperature found for Φ = 40 nm specimens are at least four orders of magnitude smaller than other samples. We propose an explanation of the M40 behavior in the last section.

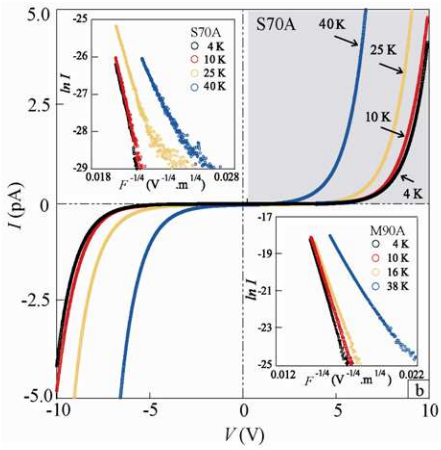

Figure 2.28 *I-V characteristics at temperatures below 40 K for sample S70A. The gray region corresponds to* $\beta >> 1$. *The insets display data for samples S70A and M90A, plotted as ln I versus* $F^{-1/4}$.

Another study to strengthen our conclusions concerning the nature of the charge transport mechanism consists in analyzing the electric field F dependence of the electrical resistance[25,26]. Indeed, the parameter $\beta = eF\alpha^{-}$

$^{1}/k_BT$ defines two different hopping transport regimes. For $\beta << 1$, thermally assisted hopping dominates and for $\beta >> 1$, the electric field-induced hopping regime mainly contributes to the transport. Within the 3D electric-field-induced hopping regime, a $(F_0/F)^{1/4}$ dependence of *ln I* is expected, F_0 being the critical electric field. To reach the $\beta >> 1$ regime, I-V curves have been measured down to 4 K and below. The data are reported in Figure 2.28. The *ln* I versus $F^{1/4}$ fits plotted for samples S70 and M90A at temperatures below 40 K are displayed in the insets of Figure 2.28. The fits are unambiguously linear at the lowest temperatures. This behavior remains valid at further decrease of *T*. The values of the critical electric field F_0 for samples S70, M90A, M90B and M90-Pt have been extracted from the linear fit obtained at the lowest T and are included in Table 2.5. As the parameter F_0 can be expressed as $F_0 = Ck_BT_0/e\alpha^{-1}$ with C = 8/3[26], estimations of localization lengths $\alpha^{-1}(F_0, T_0)$ can be deduced for these same specimens and are reported in Table 2.5. An acceptable agreement is found when these values for samples M90B and M90-Pt are compared with those resulting from the magnetoresistance study (see the following section).

Magnetoresistance measurements

Commonly, the presence of a magnetic field through materials with electrical conduction governed by the VRH mechanism results in a positive magnetoresistance *R*(*B*). In the low-*B* regime, the wave function shrinkage model developed by Shklovskii and Efros[27] predicts that $ln[R(B)/R(0)]=t(B/B_c)^2(T_0/T)^{1/4}$, where *t* is a numerical constant and where $B_c = 6\hbar/[e\alpha^{-2}(T_0/T)^{1/4}$ is the critical magnetic field. In the high-*B* regime ($B >> B_c$), a $B^{1/3}$ dependence is expected.

Magnetic measurements were performed with the magnetic field aligned along the nanowires axis. The plot *ln[R(B)/R(0)]* versus *B* for sample M90B is displayed in Figure 2.29 at T = 11, 5 and 0.5 K. The magnetoresistance was measured close to the $I = 0$ plateau of the I-V curves as it is shown by the arrow in the upper inset of Figure 2.29. Our data presents several noteworthy features. Firstly, as it was expected, a positive magnetoresistance is obtained. Then, the curves are symmetric in magnetic field, in other words $R(B,T) = R(-B,T)$. Lastly, magnetoresistance increases when T is lowered and displays a parabolic like behavior at low *B* at all the investigated

temperatures. These results suggest that the behavior of the magnetoresistance could follow the wave function shrinkage model.

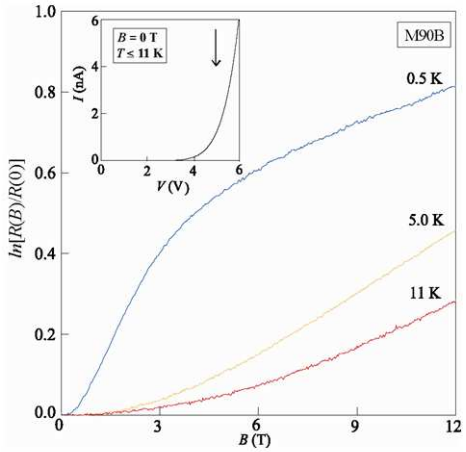

Figure 2.29 *Variation of ln[R(B) /R(0)] with B at indicated temperatures for sample M90B. Inset: below T=11 K, the I-V curves are indistinguishable.*

The T dependence of the critical magnetic field $B_C(T)$ was plotted for samples M90B and M90-Pt to determine the localization lengths α^{-1}. The densities of states $N(E_F)$ were deduced from these values. They are listed in Table 2.5. They are two orders of magnitude lower than typical values found in highly doped PPy films[28]. Nevertheless, these low values corroborates with the low doping level obtained by XPS measurements (see § 2.2.2 c). Recently, a correlation between the doping ratio and $N(E_F)$ in PPy films was reported[29]. A doping level change from 16% to 6% corresponds to a T_0 change of about 4 orders of magnitude. Taking the instance of the lowest doped specimen (6% close to the estimate doping value of PPy in our tri-segmented nanowires), we found $T_0 = 5.10^7$ K, a value in accordance with our results.

It is noticeable that the multi-segmented nanowires Pt-PPy-Au and Au-PPy-Pt-PPy-Au exhibit the same electrical behavior and magnetoresistance.

Size dependence of the transport mechanism[19]

As we saw in the I-V characteristics and the 3D-VRH plots, the case of the Φ = 40 nm class seems to be apart in the population of studied samples. This peculiarity can be highlighted using the empirical parameter $R_R = R(77$

K)/*R*(290 K) frequently used to characterize the extent of disorder in conjugated polymers such as PPy or PEDOT[17,28]. Table 2.5 presents values of R_R parameters for different samples. The parameter R_R obtained for the M40A and M40B specimens is four orders of magnitude smaller than for the Φ = 70 and 90 classes, and still two orders of magnitude smaller than for sample M50. These values suggest that the Φ = 40 nm specimens are very less disordered than the others classes. Another way to highlight the singularity of the Φ = 40 nm class was plotting the Mott temperature as a function of the parameter R_R for all investigated samples. From these plots displayed in the inset of Figure 2.27.b, we can clearly notice that the two samples M40A and M40B are disparate from the group of other samples.

In fact the electric transport occurring in the Φ = 40 nm specimens can be described by a mechanism dominating in materials which belong to an intermediary category between metals and insulators. In this model called the critical regime of the disorder-induced metal-insulator transitions[28], the resistance follows a power-law temperature dependence $R(T) \sim T^{\gamma}$, with $0.3 < \gamma < 1$. The log-log plot of $R(T)$ versus T is given in Figure 2.27.b for samples M40A and M40B. From these fits, found to be much better than the 3D-VRH fits, we obtained for the extracted parameters γ 0.43 and 0.62 respectively. When the sample goes through the transition from the metallic to the insulator side, the exponent γ varies from 0.3 to 1[28]. Consequently, our 40 nm diameter Au-PPy-Au nanowires lie at the limit in the critical regime of a disorder-induced metal-insulator transition when samples with higher diameters are clearly in the insulating side ($\gamma > 1$). From these results, an electric behavior still closer to the metallic side can be expected for lower diameter Au-PPy-Au nanowires (Φ < 30 nm).

Table 2.5 *Table reporting data analysis for the investigated samples. The Mott temperature T_0 was obtained by fitting the ln (R(T)) versus $T^{-1/4}$ plots (all data points shown in Figure 2.27). The parameter $N(E_F)$ is estimated within the 3D-VRH model. The parameter α^{-1} was extracted from the $B_C(T)$ versus $T^{1/4}$ plots obtained from the magnetoresistance measurements. F_0 was extracted from linear fits to ln I versus $(F_0/F)^{1/4}$ data. The parameter $\alpha^{-1}(F_0,T_0)$ is given by the 3D field-induced hopping model.*

Samples	T_0 **(K)**	R_R	$N(E_F)$	α^{-1}	F_0	$\alpha^{-1}(F_0, T_0)$
M90A	1.8×10^{8}	6.17×10^{4}			1.8×10^{13}	0.9
M90B	6.2×10^{7}	4.82×10^{4}	1.1×10^{18}	1.4	1.5×10^{13}	1.0
M90-Pt	7.6×10^{6}		2.6×10^{18}	2.1	0.1×10^{13}	1.8
S70A	1.4×10^{8}	1.04×10^{4}			1.5×10^{13}	2.1
S70B	3.5×10^{7}	0.29×10^{4}				
M50	1.7×10^{7}	0.05×10^{4}				
M40A	580	1.8				
M40B	1608	1.5				

2.3 Conclusions

Owing to the development of the PPy nanowires synthesis by cyclic voltammetry, well-shaped multi-segmented Au(Pt)-PPy-Au(Pt) presenting different in-wire polymeric junction lengths were synthesized by an all-electrochemical process. Characterization of these nanostructures by TEM unambiguously demonstrates the absence of short-circuits and reveals a difference of morphology between the bottom polymer-onto-metal and the upper metal-onto-polymer interfaces. The flat inferior one can be reinforced by using Pt instead of Au for the first metallic segment. The strength of the superior one, initially more robust, can be optimized by adjusting the monomer concentration and/or the scan rate during the electropolymerization step. The electrical behavior of tri-segmented nanowires with diameters between 40 nm and 90 nm was investigated.

Variable temperature measurements have shown that the three-dimensional Mott VRH can explain the transport in PPy nanowires with diameter down to 50 nm. 40 nm diameter samples follow a power-law temperature dependence of the resistance, characteristic of the critical regime of disorder-induced metal-insulator transition, which indicates that a metallic behavior in smaller diameter is possible. XPS measurements realized on PPy films and nanowires allowed to estimate the doping ratio within the polymeric junction of the tri-segmented nanowires at only a few percents, which is in good agreement with the results of the transport study.

2.4 Experimental part

Materials: Ion track-etched membranes of polycarbonate (PC) with a thickness of 21µm, pore densities of 10^8 or 10^9 pores.cm^{-2}, and pore size ranging from 30 to 160 nm were used as templates for the fabrication of nanowires. These nanoporous polymer films, provided by it_4ip and prepared following a procedure developed and patented in POLY Lab [30,31,32], present better properties than other commercially available membranes. In particular, they have cylindrical pore shape (not "cigar-like pore shape"), a very low pore size disparity and smooth pore walls (Figure 2.30). The formation of polymer and metallic nanowires was carried out into the pores of PC membranes by an electrochemical process. All electrochemical experiments were performed using a M273A Potentiostat/Galvanostat (EG&G, Princeton Applied Research) or a CHI660B electrochemical workstation (CH Inc., USA) in a one compartment Teflon cell (Figure 2.31.a) at room temperature with a Pt disk counter-electrode and an Ag/AgCl reference electrode. A thin gold layer evaporated on one side of the membrane served as working electrode (Notice: a very thin chromium layer (~ 20 nm) was deposited prior to gold in order to improve the adhesion of gold on PC) (Figure 2.31.b). Depending on the nature of the deposited material, arrays of nanowires were obtained by filling the pores of the template using either chronoamperommetry or cyclic voltammetry.

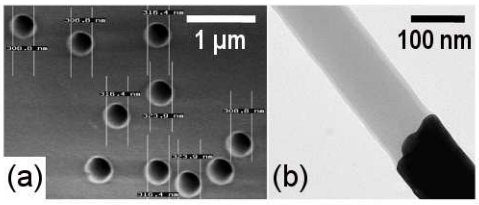

Figure 2.30 *(a) SEM image of the surface of a track-etched polycarbonate membrane. (b) TEM picture of a hybrid nanowire, "negative" of the template. Its morphological qualities show the straightness and the smoothness of the PC membranes pores walls.*

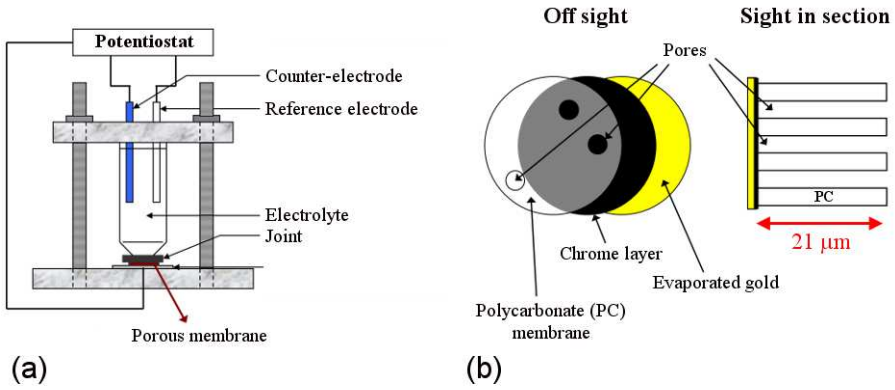

Figure 2.31 *(a) Schematic representation of a gold coated track-etched PC membrane. (b) Schematic representation of the electrochemical device used for the synthesis of nanowires.*

Preparation of Nanowires: Prior to electrodeposition, all solutions were bubbled with nitrogen and the corresponding electrochemical solution was allowed to diffuse for a few minutes into the pores of the template. Gold plating was performed by cycling the potential from 0.7 V to 0 V at 200 $mV.s^{-1}$ using a home-made cyanide free solution containing 0.1 M KCl (Acros), 0.1 M K_2HPO_4 (Acros) and 0.03 M $HAuCl_4.3H_2O$ (Acros) in de-ionized water. Electrodeposition of platinum was carried out in de-ionized water in presence of 0.01 M $Na_2PtCl_6.H_2O$ and 0.5 M H_2SO_4. Pt was electrodeposited potentiostatically at -0.2 V. Electropolymerization of pyrrole was realized by cyclic voltammetry (CV) by repeating scans over the 0 to 0.85 V potential range at different scan rates. The polymer synthesis

onto noble metal segments (Gold (Au) or Platinum (Pt)) was made from an aqueous bath containing 0.1 M $LiClO_4$ (Acros), pyrrole (Acros) in different concentrations (5 to 100 mM range) and eventually 7.10^{-4} M SDS (Acros) used as surfactant. After the synthesis of each nanowire segment, the membrane was removed from the plating solution and immerged into de-ionized water for 30 minutes in order to allow the remaining plating solution diffusing outside the pores of the membrane.

Deposition of SAMs : The deposition of self-assembled monolayers to improve the robustness of the inferior polymer-onto-metal interface was realized by immersing during 18 hours the PC membrane in a solution containing 0.01 M of 3-mercaptopropionic acid (Sigma-Aldrich) or 11-mercaptoundecanoic acid (Sigma-Aldrich) in de-ionized water.

Structural Analysis: Scanning electron microscopy (SEM) images were obtained using a LEO 982 Field emission scanning electron microscope (FE-SEM, Carl Zeiss SMT Inc.). Typical used accelerating voltage was 1 kV. The samples were fabricated as follows. They were fixed on metal holders by putting them in place on carbon double-sided adhesive paper. Then dichloromethane is poured, drop by drop, on the sample to dissolve the PC membrane. The volume of poured solvent must be enough to minimize the quantity of left polycarbonate in the middle of the nanowires network, but not too important to avoid the adhesive dissolution. Generally, a volume of 3 or 4 Pasteur pipettes was sufficient. Transmission electron microscopy (TEM) images were obtained using the LEO 922 transmission electron microscope (Carl Zeiss SMT Inc.). TEM measurements were operated at 200 kV. The preparation of TEM samples is more difficult than the SEM ones because this time after the dissolution of the membrane in dichloromethane, nanowires must be detached from the gold coating used as working electrode without breaking. Two ways were explored to get rid of that metal layer: the first method consists in soaking the sample several times in methanol and de-ionized water. Then the membrane is dissolved by immersion in a CH_2Cl_2 solution, and the suspension is placed in an ultrasonic bath to separate the nanostructures from the Au film evaporated on one side of the membrane. The other method, more efficient, consists in removing the evaporated metal layer with aqua regia solution (mixture formed by concentrated nitric acid

and concentrated hydrochloric acid in a volumetric ratio of 1:3 respectively) and then dissolving in dichloromethane the template ridded of its metal coat, so by avoiding the destroying step of sonication. The specimens for TEM analysis were prepared by placing and letting evaporated a drop of the nanowire suspension on a carbon copper film grid (Agar Scientific Ltd.).

Electrical Characterization: Variable temperature electrical measurements were carried out on two types of samples, nanowires still embedded in PC templates as well as free single nanowires. Measurements on "vertical" multiple-nanowire devices were performed by contacting both sides of the filled membrane with silver paste (Figure 2.32.a). To verify the process efficiency, the resistance of empty templates and templates filled with gold nanowires were measured. They exhibited resistances $R_{empty} > 10^{12}$ Ω and $R_{filled} \sim 50$ Ω, respectively. The planar single-nanowire devices were fabricated as follows. After removing the gold layer from the template by one of the methods described here above, PC membrane was dissolved in CH_2Cl_2. Then nanowires suspension in CH_2Cl_2 was dropped on electrical contacts consisting of 5 and 100 nm of Ti and Au, respectively. The contacts were defined by photolithography on an oxidized silicon substrate with a SiO_2 layer thicker than 100 nm (Figure 2.32.b). No leakage current can be measured between empty contacts (without nanowires) for voltage range used in the experiments.

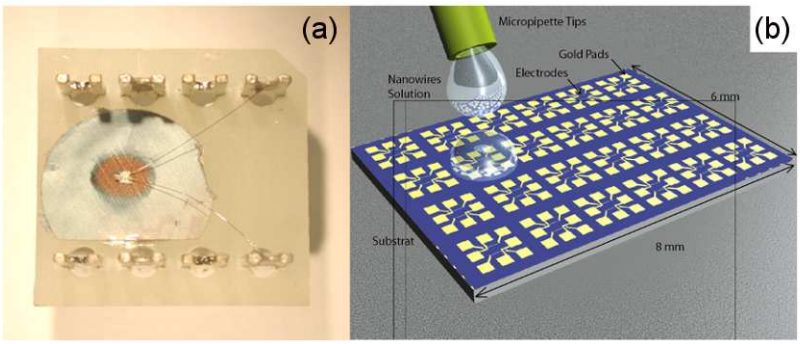

Figure 2.32 *(a) Picture of a multiple-nanowire device. (b) Scheme of the planar single-nanowire device.*

X-Ray Photoelectron Spectroscopy (XPS) : XPS data were collected by a SSX 100/206 photoelectron spectrometer (Surface Science Instruments, USA), equipped with an Al K_α X-Ray source (20 mA, 10 kV) and a quartz monochromator. The pressure during the measurements was always maintained below $1.5x10^{-6}$ Pa. The angle between the normal surface and the axis of the analyzer lens was 55°. Two studies have been carried out. The first one concerned PPy films, the second one 70 nm diameter PPy nanowires. PPy films were electrochemically synthesized on sheets of gold (Goodfellow) and directly analyzed in the spectrometer. The template-grown PPy nanowires were freed from the PC membranes by immersion in CH_2Cl_2 and a drop of the nanowire suspension was deposited on Si wafers. Then the nanowires samples were abundantly rinsed with CH_2Cl_2 to remove to a maximum any contaminant from the nanowire surface. Concerning the XPS analysis, the absolute binding energy scale was obtained by setting the C-(C,H) component of the *C1s* peak of carbon to 284.6 eV. The high resolution *N1s* spectra were fitted to Gaussian components peaks. The position and the intensity of these component peaks were optimized to obtain the best fit to the experimental curve maintaining the same peak widths as the main component.

References

[1] M.S. Wrighton, *Science* **1986**, *231*, 32.

[2] J. W. Gardner, R. N. Bartlett, *Synth. Met.* **1993**, *57*, 3665.

[3] M. Yun, N. V. Myung, R. P. Vasquez, E. Menke, R. M. Penner, *Nano Lett.* **2004**, *4*, 419.

[4] B. Veeraraghaven, J. Paul, B. Haran, B. Popov, *J. Power Sources* **2002**, *109*, 377.

[5] K. Kurachi, H. Kise, *Macromol. Chem. Phys.* **1994**, *196*, 929.

[6] Q. Pei, O. Inganas, *Synth. Met.* **1993**, *57*, 3718.

[7] C. R. Martin, *Acc. Chem. Res.* **1995**, *28*, 61.

[8] J. Duchet, R. Legras, S. Demoustier-Champagne, *Synth. Met.* **1998**, *98*, 113.

[9] T. S. Kang, S. W. Lee, J. Joo, J. Y. Lee, *Synth. Met.* **2005**, *153*, 61.

[10] X. Zhang, S. K. Manohar, *J. Am. Chem. Soc.* **2005**, *127*, 14156.

[11] V. Bocharova, A. Kiriy, H. Vinzelberg, I. Mönch, M. Stamm, *Angew. Chem. Int.* **2005**, *44*, 6391.

[12] S. J. Hurst, E. K. Payne, L. Qin, C. A. Mirkin, *Angew. Chem. Int.* **2006**, *45*, 2672.

[13] C. R. Martin, *Science* **1994**, *266*, 1961.

[14] O. Reynes, S. Demoustier-Champagne, *J. Electrochem. Soc.* **2005**, *152*, D130.

[15] R. Xiao, S. I. Cho, R. Liu, S. B. Lee, *J. Am. Chem. Soc.* **2007**, *129*, 4483.

[16] S. I. Cho, S. B. Lee, *Acc. Chem. Res.* **2007**, *41*, 699.

[17] J.-L. Duvail, Y. Long, S. Cuenot, Z. Chen, C. Gu, *Appl. Phys. Lett.* **2007**, *90*, 102114.

[18] L. Gence, S. Faniel, C. Gustin, S. Melinte, V. Bayot, V. Callegari, O. Reynes, S. Demoustier-Champagne, *Phys. Rev. B* **2007**, *76*, 115415.

[19] L. Gence, V. Callegari, S. Faniel, A. Vlad, C. Dutu, S. Melinte, S. Demoustier-Champagne, V. Bayot, *Phys. Stat. Sol.(a)* **2008**, *205*, N°6, 1447.

[20] P. Pfluger, G. B. Street, *J. Chem. Phys.* **1984**, *80 (1)*, 544.

[21] T. A. Skotheim, M. I. Florit, A. Melo, W. E. O'Grady, *Phys. Rev. B* **1984**, *30*, N°8, 4846.

[22] J. G. Eaves, H. S. Munro, D. Parker, *Polymer Communications* **1987**, *28*, 38.

[23] J.-L. Duvail, P. Rétho, S. Garreau, G. Louarn, C. Godon, S. Demoustier-Champagne, *Synth. Met.* **2002**, *131*, 123.

[24] S. Park, S. W. Chung, C. A. Mirkin, *J. Am. Chem. Soc*. **2004**, *126*, 11772.

[25] D. Shahar, Z. Ovadyahu, *Phys. Rev. Lett.,* **1990**, *64*, 2293.

[26] a) N. Apsley, H. Hughes, *Philos. Mag.* **1974**, *30*, 963. b) N. Apsley, H. Hughes, *ibid.*, **1975**, *31*, 1327.

[27] B. I. Shklovskii, A. L. Efros, *Electronic Properties of Doped Semiconductors* (Springer, Berlin), **1984**.

[28] C. O. Yoon, M. Reghu, D. Moses, A. J. Heeger, *Phys. Rev. B* **1994**, *49,* 10851.

[29] I. N. Hulea, H. B. Brom, A. K. Mukherjee, R. Menon, *Phys. Rev. B* **2005**, 72, 054208.

[30] H. Hanot, E. Ferain, R. Legras, W00149403 **2001**.

[31] E. Ferain, R. Legras, *Nucl. Instrum. Methods Phys. Res. B* **2001**, *174*, 116.

[32] E. Ferain, R. Legras, *Nucl. Instrum. Methods Phys. Res. B* **2003**, *208*, 115.

Chapter 3

Synthesis and characterization of hybrid nanowires based on poly(3,4-ethylenedioxythiophene)

Abstract:

Multi-segmented nanowires (NWs) based on poly(3,4-ethylenedioxythiophene) (PEDOT) and polypyrrole (PPy), are synthesized by an all-electrochemical template method for precise control over segment dimensions. We study the influence of different parameters on the growing process of the PEDOT segment and on the mechanical strength of the conjugated polymer/metal interfaces in tri-segmented Au-PEDOT-Au and tetra-segmented Au-PEDOT-PPy-Au NWs. The co-existence of PEDOT and PPy in tetra-segmented NWs is confirmed by high resolution transmission electron microscopy coupled with energy-dispersive X-ray analysis. We investigate the electrical transport of individual multi-segmented NWs of both types at room temperature. An interesting feature of the tetra-segmented NWs compared to tri-segmented NWs is the switching of their electrical characteristics in function of the redox state of the two conjugated polymer blocks.

A publication was extracted from this chapter:
"Electrochemically template-grown multi-segmented gold-conducting polymer nanowires with tunable electronic behavior", V. Callegari, L. Gence, S. Melinte, S. Demoustier-Champagne, *Chem. Mater.* **2009**, *21*, 4241.

3.1 Introduction

Nanojunctions (metal/molecules or nanoparticles/metal) are of great interest both for improving our fundamental understanding of electrical transport at the nanoscale and for the technological development of novel electronic devices.[1] Impressive progress has been made on carbon nanotubes[2] and low molecular weight organic molecules including alkanethiol monolayers, dithiols, and conjugated oligomers.[3] However, much less reports dealt with the fabrication of nanojunctions by using conducting or semiconducting polymers, though the outstanding opto-electronic properties of conjugated polymers, such as their reversible modulation from metals to insulators by tuning the dopant concentration levels, are well known for more than twenty years.[4] To date, conductive polymer nanotubes and nanowires have been fabricated by various methods[5] that can be divided in three categories: hard template[6], soft template[7] and template free methods.[8] Though all of these methods are commonly used to fabricate one-component systems, only the hard template method offers the ability to generate multi-component nanowires - made from organic and inorganic materials - with a very good control over the composition and spatial distribution of the different nanowire blocks.[9] Based upon this template-based strategy, we have developed an all-electrochemical process, consisting in the sequential deposition of metallic and conjugated polymer segments within the pores of polycarbonate membranes.[10] A major advantage of this all-electrochemical method compared to chemical processes is that it provides excellent control over the length of each nanowire segments, simply by adjusting the amount of charge passed through the system. In our previous work[11], we reported on the synthesis and structural characterization of narrow (40 to 90 nm in diameter) multi-segmented metal (Au or Pt)-Polypyrrole (PPy) nanowires. The study of their electrical properties by variable temperature transport measurements

revealed that both multiple and single nanowires exhibit symmetrical current-voltage characteristics and no rectification effect. Recently, with the aim of studying systems with multi-molecular components, we adapted the template-method for preparing novel hybrid metal-conjugated polymer nanowires (NWs). For the development of nanoscale electronic devices, poly (3,4-ethylenedioxythiophene) (PEDOT) exhibits a number of desirable properties in the oxidized state, including high conductivity and excellent environmental stability.[12] In this respect, a special attention was paid to the optimization of PEDOT-based nanowires synthesis. Herein, we present a highly reproducible route based upon the electrochemical template-based strategy, for preparing well-shaped and mechanically robust tri-segmented Au-PEDOT-Au and tetra-segmented Au-PEDOT-PPy-Au NWs. Remarkably, the tetra-segmented NWs switch their electrical characteristics in function of the redox state of the conjugated polymer blocks.

3.2 Results and discussion

3.2.1 Growth and morphological analysis of Au-PEDOT-Au tri-segmented nanowires

a) Potentiodynamic electropolymerization of EDOT – Optimization of the synthesis parameters

We have carried out a systematic study of the electrochemical growth, by cyclic voltammetry, of hybrid NWs containing PEDOT junctions in polycarbonate membranes. As the mechanical properties of the hybrid nanowires are key for their use as individually addressable electronic components, the effect of several parameters such as the monomer concentration, the potential scan range, and the scan rate, on the morphology and the strength of the metal/polymer interfaces of the resulting tri-segmented nanowires was investigated by SEM and TEM (see Experimental Section). The major results of this study are summarized in Table 3.1.

Table 3.1 *Electropolymerization conditions used in this study for the synthesis of the PEDOT nanowire segment.*

Entry	Concentration (mM)	Potential scan range (V)	Scan rate ($mV.s^{-1}$)	Cycle number
1	14	0.2 – 0.85	400	1000
2	14	0.2 – 0.9	400	1000
3	14	0.2 - 1	400	1000
4	14	0.2 – 1.1	400	1000
5	1	0.2 – 1.1	400	1000
6	5	0.2 – 1.1	400	500
7	14	0.2 – 1.1	400	200
8	14	0.2 – 1.1	200	200
9	14	0.2 – 1.1	800	200

Effect of applied potential

The value of the applied potential is one of the most significant parameters in an electropolymerization process. Therefore, experiments to establish the highest and lowest potential values at which it is possible to obtain well-shaped PEDOT nanowires were first carried out. The upper potential value is conditioned by the fact that the polymer has not to be overoxidised. Based on the work of Du *et al.*[13], we thus decided to select potentials lower than 1.1 V. The 3,4-ethylenedioxythiophene (EDOT) was electropolymerized, from an aqueous solution containing 0.1 M $LiClO_4$ and 14 mM EDOT, by sweeping the potential between 0.2 V and various upper potentials 0.85, 0.9, 1.0 and 1.1 V (Table 3.1, entries 1-4). Figure 3.1 shows typical TEM pictures of the nanowires obtained under these four different electrosynthesis conditions. By sweeping the potential to an upper value less than 0.9 V, a very small amount of PEDOT (segment length $\leq$ 40 nm) is formed on the bottom gold segment, even after 1000 scans (Figure 3.1.a), and none top metal segment can be grown further. Sweeping the potential to higher upper values - from 0.9 to 1.1 V – allowed the subsequent deposition

of Au segments and hence, led to the formation of entire Au-PEDOT-Au NWs (Figure 3.1.b-d), with PEDOT junctions of increasing length. Moreover, for these three upper potential limits, the polymer segment is dense on its whole length. For the upper potential limit of 1.1 V, the polymer/metal interfaces appear stronger, as only less than 25 % of the tri-segmented NWs are broken when freed from the template, while the percentage of broken NWs is around 50 % for upper potential limits of 0.9 and 1.0 V. For that reason, we further carry out EDOT electropolymerization using a fixed potential window from 0.2 to 1.1 V.

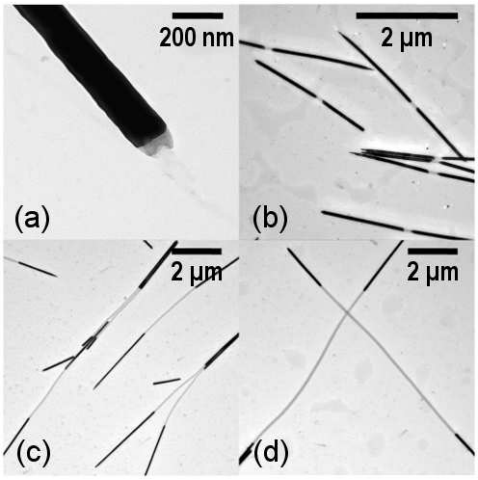

Figure 3.1 *TEM images of PEDOT-based nanowires, where the polymer was synthesized using different upper potential limits: (a) 0.85 V, (b) 0.9 V, (c) 1 V, and (d) 1.1 V.*

Effect of the monomer concentration

As EDOT is poorly soluble in aqueous solutions, low enough concentrations, ranging from 1 to 14 mM, were used in order to guarantee homogeneous media. When using an EDOT concentration equal to 1 mM (Table 3.1, entry 5), no polymer is formed even after a large number of potential scans. By increasing the monomer concentration (Table 3.1, entries 4 and 6), we fabricate high-quality PEDOT segments. Accordingly, the PEDOT growth is cca. 3 times faster when the monomer concentration is increased from 5 to 14 mM.

Effect of the scan rate

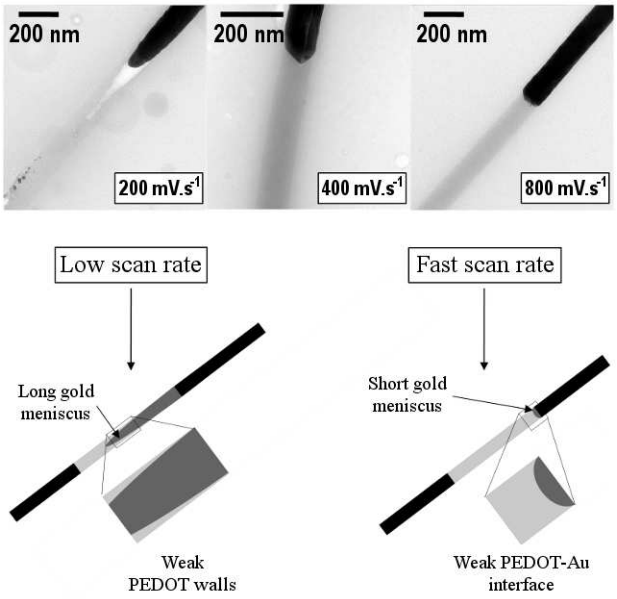

Figure 3.2 *(Top) TEM pictures showing the different morphologies of the Au-onto-PEDOT interface depending on the potential scan rates. Scale bars: 200 nm. (Bottom) Scheme illustrating the shape of the Au-onto-PEDOT interface: (a) at slow potential scan rate and (b) at fast potential scan rate.*

Then, EDOT was electropolymerized from an aqueous solution of 0.1 M $LiClO_4$ and 14 mM EDOT by sweeping the potential between 0.2 and 1.1 V at different scan rates: 200, 400 and 800 $mV.s^{-1}$ (Table 3.1, entries 7-9). As shown by the TEM pictures (Figure 3.2), the potential scan rate has a huge impact on the shape of the Au-onto-PEDOT interface. Indeed, at low scan rate (200 $mV.s^{-1}$), a very long meniscus is formed at the end of the PEDOT nanowire segment. The very thin walls of this PEDOT tubular part are too fragile to strongly maintain the top metal segment, resulting in a high percentage of broken nanowires. When applying a fast scan rate (800 $mV.s^{-1}$), flat Au-onto-PEDOT interfaces are obtained, that also present a very low mechanical strength. Interestingly, at an intermediate scan rate of 400 $mV.s^{-1}$, a conical short gold meniscus soaring into the PEDOT junction is observed, ensuring a strong mechanical link between the polymer and the

top metal section. The different top structures observed for the PEDOT segment (ranging from tubular to full-nanowire structures) in function of the electrochemical growing rate, are in good agreement with the electrochemical synthetic mechanism of PEDOT nanotubes and nanowires formation, recently reported by Lee *et al*.[14]

b) Structural characterization of the tri-segmented Au-PEDOT-Au nanowires

Finally, in order to calibrate the growth of the PEDOT segment, EDOT electropolymerization was carried out, under the optimized conditions (14 mM concentration, 0.2 to 1.1 V scanning potential, and 400 $mV.s^{-1}$ scanning rate), for different scan numbers. SEM micrographs (Figure 3.3.a-b) show that Au-PEDOT-Au nanowires can be grown with various polymer junction lengths and can then be removed intact from the template. Figure 3.3.c shows the evolution of the PEDOT segment length as a function of the number of cyclic voltammetric scans. Each point in the plot was obtained by averaging the lengths of approximately 100 nanowires in TEM images. For each sample, these 100 measured PEDOT lengths are represented by one length interval around the mean value. We observed a linear dependence of the average length of the PEDOT segment on the number of scans, with a mean growth rate of 10 nm/cycle, below 500 voltammetric cycles. Then, for longer deposition periods, the PEDOT growth rate slightly decreases (8 nm/cycle), probably due to a slight increase of the resistivity of very long PEDOT segments. It should however be pointed out that very long PEDOT junction (> 15 μm) can be prepared, while electrode passivation occurred rather earlier with PPy, where the longest electropolymerizable polymer junction was ~ 3 μm.[10] Figure 3.3.d compares the curves of cyclic voltammetry obtained for the electropolymerization of PEDOT and PPy. The current value at the upper potential limit is about three times higher for PEDOT than for PPy. Upon the used conditions of synthesis, PEDOT grows faster than PPy. The choice of a higher upper potential limit also influences the electrical properties of PEDOT nanowires. As in the case of polypyrrole, though the lengths of PEDOT nanowires are locally very homogeneous (Fig. 3.3. a and b), some disparity appears when looking at nanowires grown in different regions of the sample (Fig. 3.3.c.).

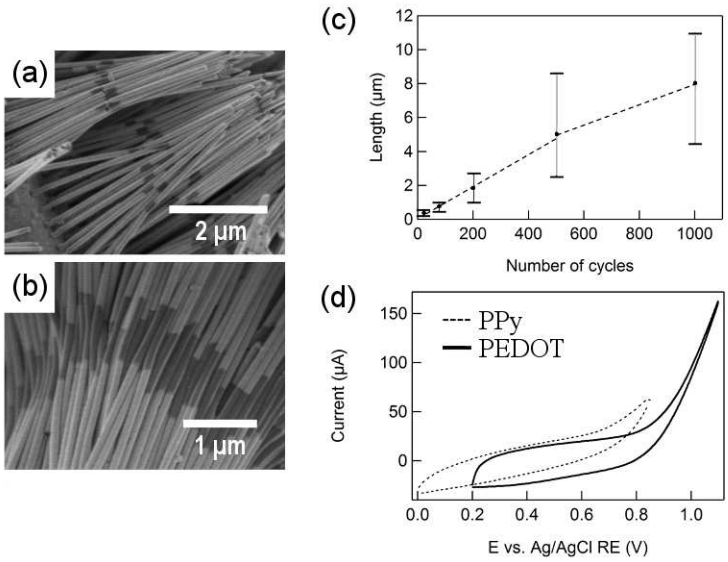

Figure 3.3 *SEM pictures of 110 nm diameter tri-segmented Au-PEDOT-Au nanowires presenting two different polymer junction lengths: (a) 200 nm (20 scans) and (b) 1 µm (100 scans). The good contrast between the metallic and the polymer segments on SEM pictures allows for growth calibration. Scale bars: 1 µm. (c) Length of the PEDOT segment as a function of the number of potential scans between 0.2 and 1.1 V. Each length interval represents all measured PEDOT lengths for 100 observed nanowires. (d) Comparison between cyclic voltammograms recorded during the synthesis of Φ = 110 nm PEDOT and PPy nanowires.*

c) Electroactivity of the PEDOT junctions

During the deposition of the second gold section onto the polymer segment, the observation of the corresponding cyclic voltammogram gives us qualitative information concerning the electroactivity of the polymer. Indeed, in our electrochemical device used for the nanowires synthesis, the matter which fills the pores of the membrane constitutes a continuously modified working electrode. The resistance of gold nanowires being negligible in front of the polymer one and the diameter of the pores being quasi-constant on their whole length, the change recorded for the value of the deposition current associated to the growth of the superior gold segment is a signature of the polymer conductivity, even if no quantified data can be deduced from these observations. Figure 3.4 presents, for two samples of tri-segmented nanowires, a comparison between CV curves recorded during the

formation of the bottom gold segment (black curves) and, during the step following the electropolymerization, the synthesis of the second gold segment (blue curves). The first sample (Figure 3.4.a) corresponds to 62 nm diameter Au-PPy-Au nanowires with a polymer junction of about 3.5 µm and the second one (Figure 3.4.b) to 62 nm diameter Au-PEDOT-Au nanowires with a polymer junction of about 4 µm. While for the Au-PPy-Au sample, a fall of 40% in the deposition current value occurs between the two steps of gold electrodeposition, no fall is recorded for the Au-PEDOT-Au sample, the current holding up at about 200 µA. This indicates that the PEDOT nanowires are more conductive than the PPy ones. This observation, that should be further verified by XPS and electrical measurements, by determining the doping ratio and the conductivity respectively, is in accordance with previous studies that put PEDOT in the category of highly conducting polymers.[15,16]

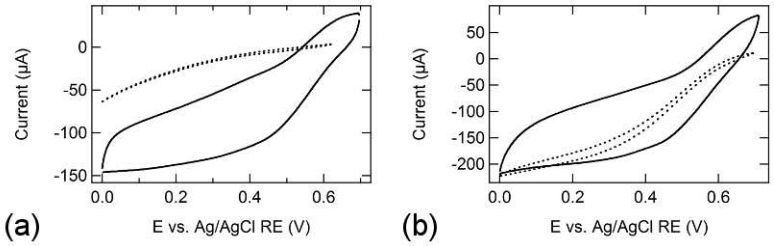

Figure 3.4 *Cyclic voltammograms relative to the growth of the first (black curves) and the second (dashed curves) gold segments in the synthesis of 62 nm diameter (a) Au-PPy-Au (b) Au-PEDOT-Au nanowires.*

d) Mechanical strength of the PEDOT/metal interfaces

Tri-segmented Au-PEDOT-Au nanowires with diameters of 62 and 110 nm and PEDOT junctions of tunable lengths varying from 200 nm to more than 10 µm were synthesized and characterized by TEM (Figure 3.5). Further to the previous works on PPy, our attention was naturally focused on the observation of the two metal/polymer interfaces. As in the case of PPy, the two gold/PEDOT interfaces have a different shape, a relatively flat bottom interface, and an upper interface presenting a metal meniscus. Nevertheless, the Au-PEDOT-Au nanowires freed from the template show no mechanical weakness of the bottom flat interface as numerous entire tri-

segmented nanostructures were observed. The relative strong link ensuring the adhesion between gold and PEDOT at the bottom interface may result from a chemical bonding based on the strong affinity of the sulfur atoms for gold. In previous works, this chemical bonding explained the better contacts obtained between Au or Ag nanoparticles and poly(3-methylthiophene) or PEDOT films than with PPy coatings.[17] For lower diameters ($\Phi < 50$ nm), the risks of breaking are logically more important.

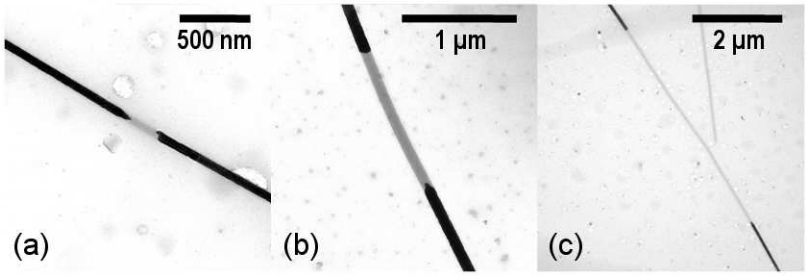

Figure 3.5 *TEM pictures of Au-PEDOT-Au nanowires: (a) Φ = 62 nm, $L_{PEDOT} \approx$ 200 nm. (b) Φ = 110 nm, $L_{PEDOT} \approx$ 1.3 µm. (c) Φ = 62 nm, $L_{PEDOT} \approx$ 5.3 µm.*

e) Formation of gold nanoparticles

Observations by TEM of the first Au-PEDOT-Au samples revealed a phenomenon linked to the insoluble feature of the EDOT. The upper interface of the tri-segmented nanostructures was granular (Figure 3.6). This peculiar shape resulted from the following undesirable reaction occurring between EDOT and $HAuCl_4$[18]:

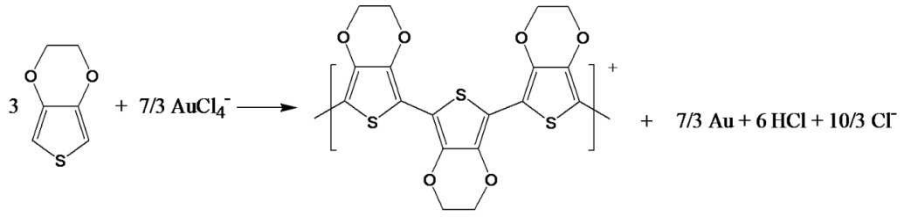

This reaction, used by Shi and co-workers to prepare Au-PEDOT nanocables[19], leads in our case to gold nanoparticles formation. It occurs when the monomer is no entirely dissolved in the electropolymerization solution. EDOT is so insoluble that, even by working under the limit of

solubility as we systematically did, its dissolution in de-ionized water was not complete without sonication. Figure 3.7 illustrates the hypothetical mechanism explaining the formation of gold nanoparticles when no precaution was taken to ensure the complete dissolution of the monomer.

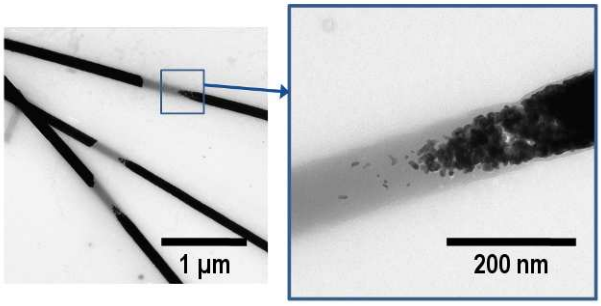

Figure 3.6 *TEM characterization of the upper interface of 110 nm diameter Au-PEDOT-Au nanowires presenting a granular aspect linked to the presence of gold nanoparticles.*

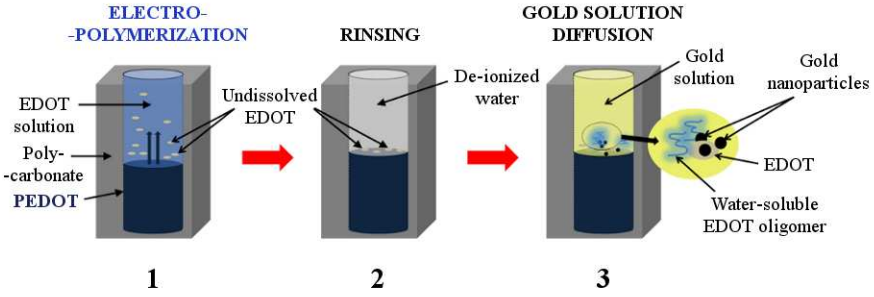

Figure 3.7 *Scheme representing the hypothetical mechanism for the formation of gold nanoparticles at the upper polymer/metal interface of Au-PEDOT-Au nanowires. 1) Even by working under the limit of EDOT solubility in aqueous media, some EDOT molecules remained undissolved if electropolymerization solution is not sonicated. 2) During the intermediary step of rinsing, the undissolved EDOT is not removed from the pores and tends to remain close to the polymer by hydrophobic effect. 3) During the diffusion of gold solution within the pores, the oxidative polymerization of EDOT by $AuCl_4^-$ occurs to form gold nanoparticles located at the future polymer/metal interface. Visually, this undesirable reaction is observed. The gold solution turns from pale yellow to dark blue, which is due to the formation of water-soluble EDOT oligomers.*

This phenomenon only emphasizes that the step of rinsing is essential for the robustness of the nanostructures. Without taking any precaution, the two electrodeposition solutions are put in contact and a reaction occurs between the monomer and metallic salt anions. This remark is equally valid for the pyrrole and the aniline.

3.2.2 Synthesis of hybrid nanowires with a PEDOT-PPy heterojunction

a) Growth of Au-PEDOT-PPy-Au tetra-segmented nanowires

Tetra-segmented nanowires presenting a polymer heterojunction (PEDOT-PPy) were synthesized by the template sequential electrochemical deposition method. In order to get mechanically strong nanowires, the sequence of polymer deposition was determined according to previous observations on the shape and strength of the different metal/polymer interfaces. PEDOT was thus firstly deposited on the Au segment, as the strong chemical bond between Au-S compensates for the weakness of the flat, conjugated polymer-onto-metal bottom interface. PPy was then electrodeposited onto the PEDOT segment, the strength of the metal-onto-PPy interface being ensured by its meniscus shape.[11]

b) Morphological analyses of Au-PEDOT-PPy-Au nanowires

The formation of the PEDOT-PPy heterojunction within Au nanowires was confirmed by high-resolution TEM. Representative Au-PEDOT-PPy-Au nanowires, after removal of the polycarbonate template, are shown in Figure 3.8. A zoom into the PEDOT/PPy interface is presented in the inset of Figure 3.8. On this picture, it appears that one of the two polymers shrank much more than the other one during solvent evaporation in a sampling process. In order to unambiguously distinguish the polymer segments, we employed Energy-dispersive X-ray (EDX) analysis. Figure 3.9.a shows EDX spectra recorded on the four spots marked in Figure 3.9.b. These spectra reveal the presence of sulfur atoms - characteristic for PEDOT, only in the narrow nanowire segment. Therefore, two consecutive segments of PEDOT and PPy were synthesized and the first one could be ascertained by its lower diameter.

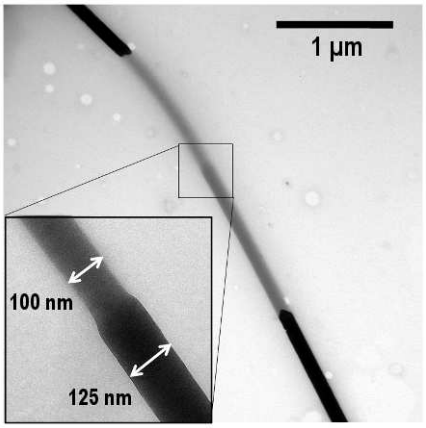

Figure 3.8 *TEM picture of a 110 nm diameter tetra-segmented Au-PEDOT-PPy-Au nanowire. The inset shows a zoom of the heterojunction.*

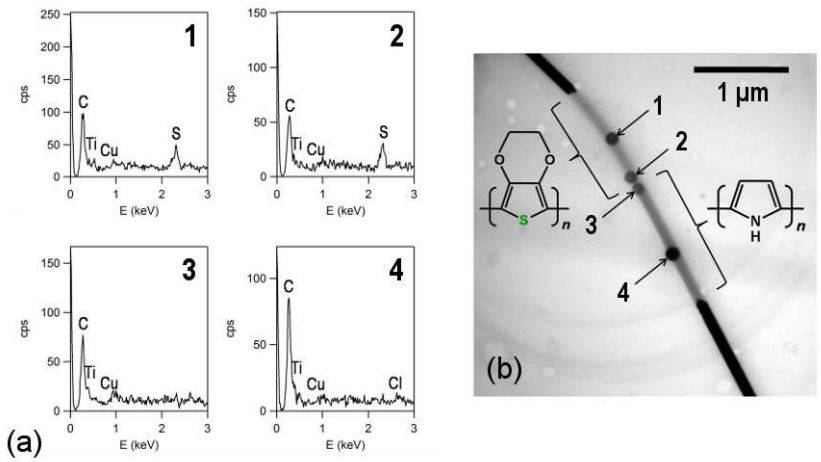

Figure 3.9 *(a) EDX spectra recorded at the extremities of the two polymer segments. The carbon copper grid and the titanium holder explain the presence of Cu and Ti peaks, respectively. (b) TEM picture showing four analyzed areas marked by a dark spot corresponding to the polymer degradation by the electron beam.*

3.2.3 Electrical measurements

a) Electrical characterization of tri-segmented Au-PEDOT-Au nanowires

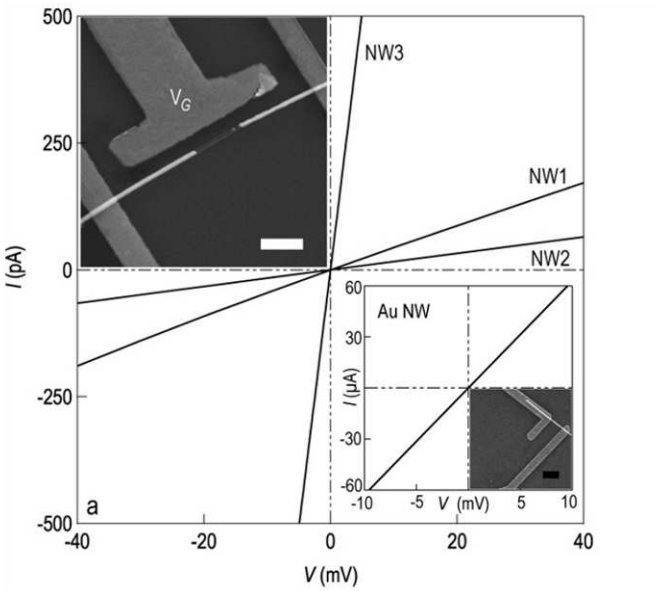

Figure 3.10 *I-V characteristics of tri-segmented Au-PEDOT-Au nanowires. The upper inset is a SEM picture of sample NW2. The nanowire intrinsic conductivity, and not the grid effect, is measured (V_G = 0). The scale bar is 1 μm. The lower inset shows the I-V characteristic measured for the depicted single gold nanowire. The scale bar is 2 μm.*

The electrical transport of single tri-segmented Au-PEDOT-Au nanowires (NWs) has been investigated at room temperature. Figure 3.10 presents the current-voltage (*I-V*) characteristics measured by the two-point technique for three 110 nm diameter as-synthesized samples (NW1, NW2 and NW3) with PEDOT segment lengths of 0.6, 1.2 and 4.5 μm, respectively. Measurements of gold nanowires (see lower inset of Figure 3.10) showed that the unavoidable two-point contact resistance R_c is negligible compared to the resistance R_p of the polymer segment ($R_c < 10^2\ \Omega << R_p \approx 10^6$-$10^7\ \Omega$). The *I-V* plots of Figure 3.10 are symmetrical and linear for the three samples, consistent with ohmic contacts between the gold and PEDOT sections[20,21]. Room temperature conductivities of 4.3, 2.5 and 450

$mS.cm^{-1}$ were found from the slopes of the *I-V* curves. It is assumed that fluctuations in the values of conductivity are due to the post-synthesis processing. The highest values of conductivity for all the Au-PEDOT-Au samples were in the 0.1 – 1 $S.cm^{-1}$ range, which is at least one order of magnitude higher than the two-point values of conductivity found for the tri-segmented Au-PPy-Au nanowires[11]. These results correlate with the comments made in paragraph 3.2.1.c and confirm the higher conductivity of PEDOT compared to PPy.

b) Electrical characterization of tetra-segmented Au-PEDOT-PPy-Au nanowires

Electrical characterization of the tetra-segmented nanowires was performed at room temperature. Measurements were done on as-synthesized samples and on specimens treated with a chemical oxidant. The blue current-voltage (I-V) curve presented in Figure 3.11 shows the symmetrical and linear behavior of a single as-synthesized tetra-segmented Au-PEDOT-PPy-Au nanowire. Note that the current values recorded are much lower compared to those obtained for the tri-segmented specimens. The fact that tetra-segmented specimens are highly resistive is essentially due to the PEDOT-PPy junctions, as previous works demonstrated that the contact resistance between gold and both polymers (PEDOT and PPy) is negligible. Interestingly, after 1 hour of immersion in a 0.5 M $FeCl_3$ solution, the tetra-segmented sample exhibits an asymmetric and highly non linear I-V characteristic (see red curve in Figure 3.11), the gain of current depending on the sign of the bias voltage V (enhancement by a factor of two when switching from a positive to a negative voltage). So, by changing the redox state of the two conjugated polymer segments, the tetra-segmented nanostructures are able to switch their electrical behavior.

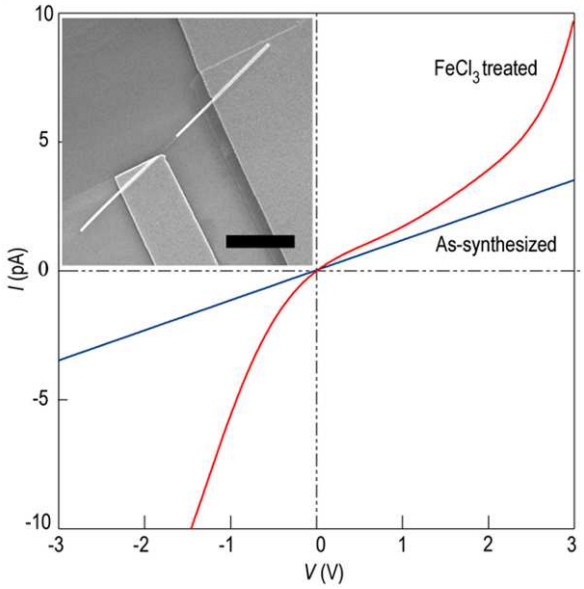

Figure 3.11 *I-V characteristics of a single tetra-segmented Au-PEDOT-PPy-Au nanowire measured before (blue curve) and after (red curve) $FeCl_3$ treatment. Inset shows a connected tetra-segmented nanowire observed by SEM. The scale bar is 10 µm.*

c) Various possible protagonists acting on the electrical transport

To get explanations to the asymmetric non-linear behavior exhibited by the Au-PEDOT-PPy-Au nanowires after treatment with $FeCl_3$, one route forward was to measure independently the intrinsic conductivites of both polymers before and after the same chemical oxidative treatment. The four-point *I-V* characteristics presented in Figure 3.12 and measured for tri-segmented Au-PEDOT-Au nanowires show that, due to the shift in the dopant anion equilibrium within the PEDOT, the conductivity increase occurs in the polymer segment after the $FeCl_3$-treatment. These data demonstrate that the $FeCl_3$ treatment has a dopant effect on PEDOT but is not responsible for the change in the I-V curve shape observed in the PEDOT-PPy heterojunction. The same experiment should be conducted soon for tri-segmented Au-PPy-Au nanowires. Given the electrical measurements already made, we can expect that the chemical oxidative treatment causes a dramatic decrease in the conductivity of PPy, to compensate the conductivity

increase observed in PEDOT after the $FeCl_3$-treatment. We see in the § 3.2.4 that the XPS analysis of PPy electronic structure confirms these predictions.

Generally, electrical measurements were performed on 110 nm diameter tri-segmented Au-PEDOT-Au nanowires in two-point and four-point configurations. For two-point measurements, as shown in Figure 3.10, we observed up to 2 orders of magnitude differences in the room temperature conductivites. For better understanding this disparity and the role of Au-PEDOT interfaces, we also measured the electrical conductivity of electro-deposited single PEDOT nanowires, at various lengths, in a four-point configuration. Figure 3.13 gives the conductivity dependence as a function of the PEDOT length for sample NW 5. An increase of the conductivity is observed with increasing the length of the PEDOT nanowire. On one hand, this behavior partly explains the high conductivities recorded for long PEDOT blocks in tri-segmented nanowires. On the other hand, from the conductivity values observed in single PEDOT nanowires, it appears that the resistance of polymer-metal junctions play a key role in the two-point resistance of tri- and tetra-segmented nanowires. This is further illustrated in Figure 3.14.

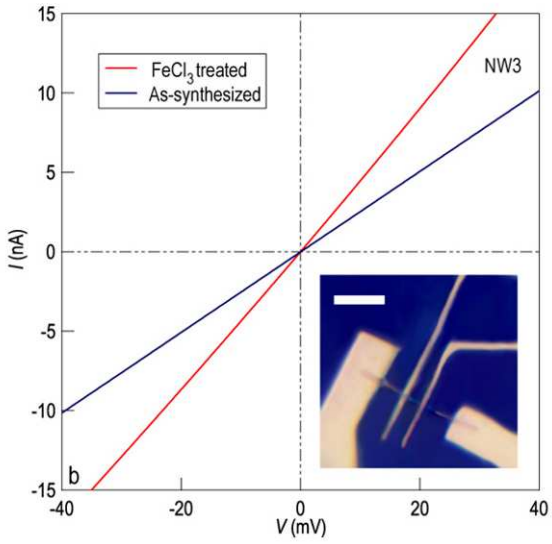

Figure 3.12 *Four-point I-V characteristics of the depicted single Au-PEDOT-Au nanowire before (blue curve) and after (red curve) $FeCl_3$ treatment. The scale bar is 5 µm.*

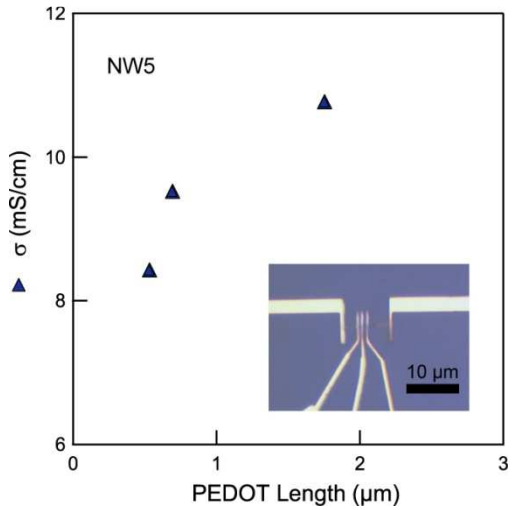

Figure 3.13 *The electrical conductivity of a PEDOT nanowire with several contacts is measured by a four-point technique at various lengths.*

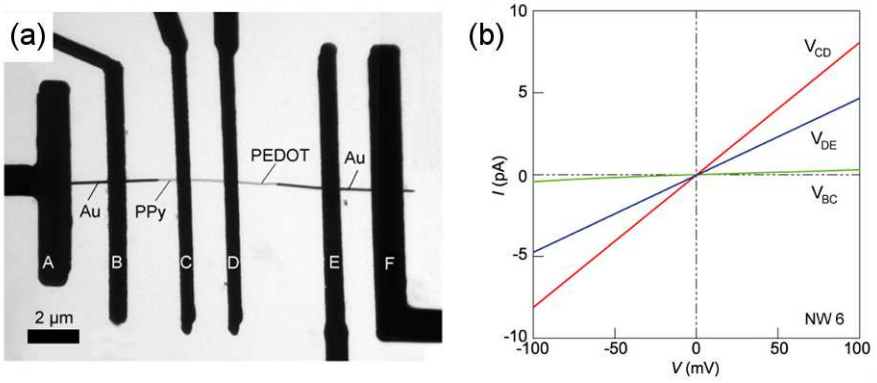

Figure 3.14 *(a) Single tetra-segmented Au-PEDOT-PPy-Au nanowire connected with 6 electrical probes. The current flows from contacts A to F and the voltage is measured across the Au-PPy (voltage probes B-C) and PEDOT-Au (voltage probes D-E) nanojunctions. (b) Room temperature I-V characteristics for voltage probes B-C, D-E and C-D. From this measurement we can infer the following values for the interfacial resistances: 3 x 10^{11} ohm for the Au-PPy nanojunction and 2 x 10^{10} ohm for the PEDOT-Au nanojunction.*

Finally, while common post-synthesis processing such as plasma and solvent cleaning could affect the intrinsic electrical properties of the

electrodeposited polymers (e.g dopant level), the design chosen for device integration also contributes to the different values collected for the nanowire conductivites.

3.2.4 XPS study of as-synthesized and $FeCl_3$-treated PPy and PEDOT films

In order to explain the non-linear behavior displayed by the Au-PEDOT-PPy-Au NWs after treatment with $FeCl_3$, we studied, by XPS, the evolution of the electronic structure and doping ratio of PEDOT and PPy films upon oxidative treatment. The different synthesis and chemical post-treatment conditions used in this study are gathered in Table 3.2 and XPS spectra of the four samples are presented in Figure 3.15.

Table 3.2 *Synthesis and post-treatment conditions of PEDOT and PPy films samples analyzed by XPS.*

Sample names	**Electrosynthesis conditions**	**$FeCl_3$ post-treatment ($[FeCl_3]$ = 0.5 M)**
As-synthesized PEDOT	$[EDOT]$ = 14 mM $[LiClO_4]$ = 100 mM 200 cycles at 400 $mV.s^{-1}$ Potential range: 0.2 – 1.1 V	None
$FeCl_3$-treated PEDOT	$[EDOT]$ = 14 mM $[LiClO_4]$ = 100 mM 200 cycles at 400 $mV.s^{-1}$ Potential range: 0.2 – 1.1 V	1h
As-synthesized PPy	$[Py]$ = 20 mM $[LiClO_4]$ = 100 mM 200 cycles at 400 $mV.s^{-1}$ Potential range : 0 – 0.85 V	None
$FeCl_3$-treated PPy	$[Py]$ = 20 mM $[LiClO_4]$ = 100 mM 200 cycles at 400 $mV.s^{-1}$ Potential range : 0 – 0.85 V	1h

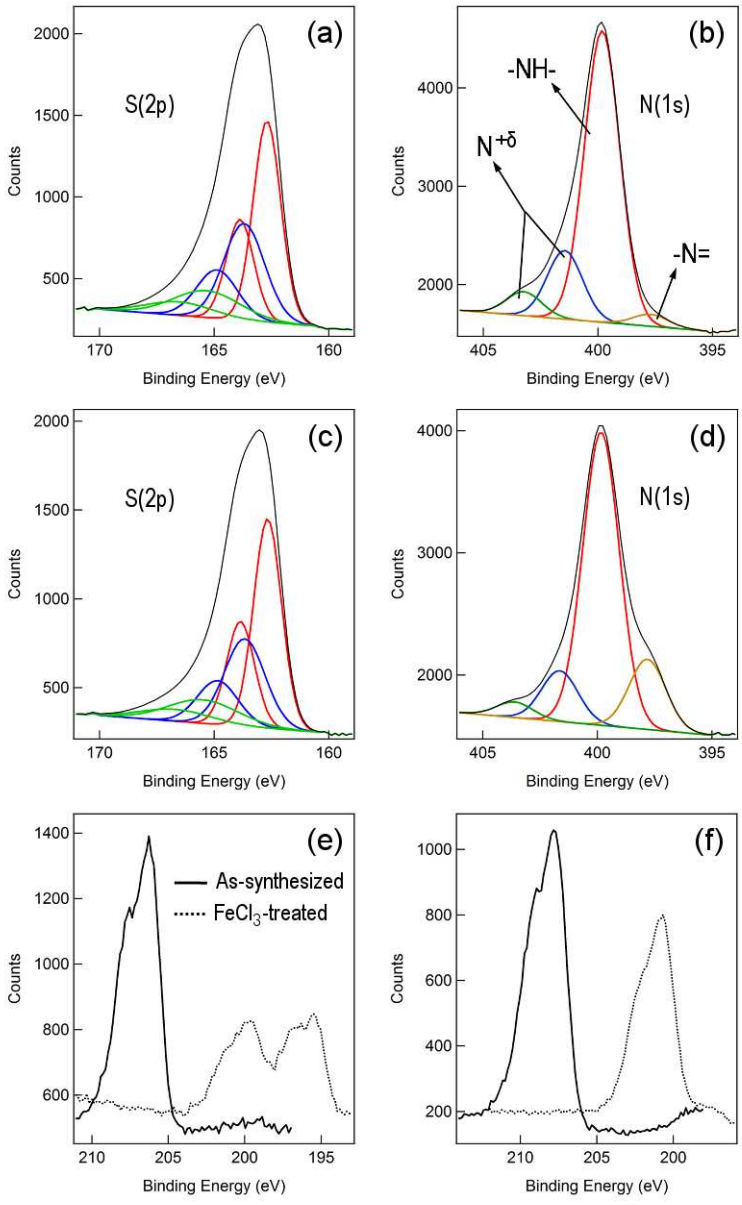

Figure 3.15 *(a) and (b) S2p and N1s XPS fitted spectra of as-synthesized PEDOT and PPy films, respectively. (c) and (d) S2p and N1s XPS fitted spectra of PEDOT and PPy films, respectively, after $FeCl_3$ treatment. (e) and (f) Cl2p XPS spectra of as-synthesized and $FeCl_3$-treated PEDOT and PPy films, respectively.*

The core level *S2p* XPS spectra of the as synthesized PEDOT-ClO_4^- film (Figure 3.15.a) and $FeCl_3$-treated PEDOT (Figure 3.15.c) can be decomposed into two major doublets, at 162.7 and 163.7 eV and at 163.7 and 165.0 eV, that are attributed to the EDOT sulfur atom in the neutral and partially oxidized state [$S^{\delta+}$], respectively. A $\pi \rightarrow \pi^*$ shake-up doublet at high binding energy (> 165 eV) is also introduced, as reported by Tourillon *et al.*.[22] The doping level of the two samples can be determined from the ratio of the positively charged sulfur atoms of EDOT and the total sulfur contribution from PEDOT chains: [$S^{\delta+}$]/[S] ratios.[23] A doping level of 35% is found for the as-synthesized PEDOT and it slightly decreases to 32% after the $FeCl_3$ post-treatment (Table 3.3). The doping levels deduced from the atomic ratios [Cl]/[S] reveal no major changes of value (a slight increase from 32 to 33 % before and after the $FeCl_3$-treatment, see Table 3.3). The *Cl2p* core-level spectra of as-synthesized and $FeCl_3$ PEDOT films (Figure 3.15.e) show clear differences between both samples. Indeed, upon $FeCl_3$ treatment, the characteristic *Cl2p* peak of perchlorate species in the region of 207 eV completely disappears, and two doublets lying at around 196 and 200 eV appear. These binding energy values correspond to the ionic (Cl^-) and covalent (–Cl) chlorine species, respectively.[24] Though the $FeCl_3$-treatment only slightly affects the oxidation state of PEDOT, it has a strong impact on the nature of the counterion, as all the ClO_4^- anions were replaced by chlorine species. So, XPS data revealed that when the PEDOT and the PPy are treated with 0.5 M $FeCl_3$ for 1 hour, an exchange of counterions occurs in the polymers, the perchlorate ClO_4^- anions being totally replaced by chloride Cl^- species. In parallel, electrical measurements showed that the chemical oxidative treatment causes a slightly increase in the current. The influence of anion doping on the properties of the polymer has been widely investigated but most of these studies concern the effect of the counterion used during polymer generation[25,26]. However, in our case, the polymer backbone network remains the one that has been generated with the perchlorate electrolyte. Therefore, it is difficult to establish a clear relationship between the counterion exchange and the change of conductivity observed by referring to the literature. We are in the presence of two inorganic anions with a relatively low difference in radius (0.181 and 0.240 nm for Cl^- and ClO_4^- respectively). Nevertheless, the remarkable difference in shape of these anions (spherical for chloride and tetrahedral for perchlorate) should

have some effect on their strength of ionic interaction with polymer chains, on their mobility in polymer matrix and on the extension of conjugation in polymer backbone as it has been suggested by Tamm and co-workers[27]. Thus, the tetrahedral perchlorate anions have a weaker interaction with the polymer chains and tend to distort the planarity of the chains, therefore, reducing conjugation while the spherical chloride have more suitable geometry but tend to have stronger interaction. Therefore, it is difficult to explain, from their respective properties, the role of the counter-anions in the electrical behavior observed.

Table 3.3 *Doping levels determined by XPS for as-synthesized and $FeCl_3$-treated PPy ($[N^{\delta+}]/[N]$ atomic ratio) and PEDOT ($[S^{\delta+}]/[S]$ and [Cl]/[S] atomic ratios).*

Samples	$[N^{\delta+}]/[N]$ (%)	$[S^{\delta}]/[S]$ (%)	[Cl]/[S] (%)
As-synthesized PPy	23	-	-
$FeCl_3$-treated PPy	15	-	-
As-synthesized PEDOT	-	35	32
$FeCl_3$-treated PEDOT	-	32	33

The *N1s* core-level spectrum of the as-synthesized PPy-ClO_4^- film (Figure 3.16.b) is best resolved into four components whose positions and assignments are in agreement with the literature data.[28] The two peaks above 400 eV can be attributed to positively charged nitrogen species (-NH^+-, abbreviated $N^{\delta+}$), while the amine-like (-NH-) and the imine-like (-N=) structures are located at binding energies of 399.9 and 397.8 eV, respectively. The doping level of the as-synthesized PPy, estimated from the ratio of the positively charged nitrogen atoms and the total nitrogen contribution from PPy chains, $[N^{\delta+}]/[N]$ ratio, is equal to 23%. The treatment with $FeCl_3$ (Figure 3.16.d) results in a strong increase of the imine-like nitrogen (from 3 to 16.5 %, Table 3.4), accompanied by a significant decrease of the *N1s* high binding energy peaks (from 23 to 15%, Table 3.4). Transformation of a part of –NH^+- to –N= groups may be the result of the nucleophilic attack of H_2O and Cl^- anions on the doped PPy.[29,30] The *Cl2p*

core-level spectra of PPy films (Figure 3.16.f) show that upon $FeCl_3$ treatment, all the perchlorate species with a characteristic peak around 207 eV, are replaced by chlorine species (mainly covalent chlorine), as indicated by the appearance of a peak centered at 200 eV. All these XPS data clearly indicate that over-oxidation of PPy occurs during the $FeCl_3$ treatment. This oxidative degradation of PPy is, of course, affecting the electronic properties and electrical conductivity of PPy.

Table 3.4 *N1s component proportions (%) for as-synthesized and $FeCl_3$-treated PPy films.*

Samples	***N1s* component proportions (%)**		
	-N= 397.8 eV	**-NH- 399.9 eV**	**$N^{\delta+}$ > 401 eV**
As-synthesized PPy	3	74	23
$FeCl_3$-treated PPy	16.5	68.5	15

3.3 Conclusions

In this work, we present an effective all-electrochemical template-based method for preparing well-shaped and mechanically robust tri-segmented Au-PEDOT-Au and tetra-segmented Au-PEDOT-PPy-Au nanowires. Our systematic study of the influence of several parameters (monomer concentration, potential scan range, and scan rate) on the electropolymerization process of PEDOT in nanoporous polycarbonate membrane reveals that the morphology and the strength of the metal/polymer interfaces can be tuned by playing on the conducting polymer growth rate. The electrical properties at room temperature of individual multi-segmented NWs were investigated. While the tri-segmented NWs exhibit symmetrical and linear *I-V* characteristics, the tetra-segmented NWs switch to non-linear electrical behavior by exposure to $FeCl_3$. As shown by XPS, this can be attributed to the selective overoxidation of the PPy

segment, leading to strong modifications of its electronic structure and doping ratio.

3.4 Experimental part

Materials: Polycarbonate track-etched membranes with a thickness of 21 μm, a pore density of 10^9 pores.cm^{-2} and an average pore size of 60 or 110 nm, supplied by it4ip, were used as nanoporous templates. Pyrrole (Acros, 99%) was purified immediately before use by passing it through a microcolumn constructed from a Pasteur pipette, glass wool, and activated alumina. The 3,4-ethylenedioxythiophene (EDOT, Sigma-Aldrich), lithium perchlorate ($LiClO_4$, Acros), potassium chloride (KCl, Acros), potassium hydrogenophosphate (K_2HPO_4, Acros), and hydrogen tetrachloroaurate ($HAuCl_4$, Sigma Aldrich, 99,9%), dichloromethane (CH_2Cl_2, Acros) were used without any prior purification. De-ionized water was used to prepare all aqueous solutions. Aqua regia was prepared by carefully adding three volumes of concentrated hydrochloric acid (HCl, Acros) to one volume of concentrated nitric acid (HNO_3, Acros, 63%).

Preparation of Tri-Segmented Au-PEDOT-Au Nanowires: All electrochemical experiments were performed with a CHI660B Electrochemical Workstation (CH Inc.) in a conventional one-compartment cell at room temperature with a Pt disk counter electrode and an Ag/AgCl reference electrode. A 500 nm thick layer of gold evaporated on one side of the polycarbonate membrane served as working electrode. Electrodeposition of Au was performed by cycling the potential of the working electrode from 0.7 to 0 V at 200 mV.s^{-1} using a home-made cyanide free solution (0.1 M KCl, 0.1 M K_2HPO_4, and 0.03 M $HAuCl_4$ in de-ionized water). Electropolymerization of EDOT was carried out by cyclic voltammetry from an aqueous solution containing 0.1 M $LiClO_4$ and various monomer concentrations ranging from 1 to 14 mM. The potential was swept between 0.2 V and different Upper Potential Limit ($0.85 \leq UPL \leq 1.1$ V) with scan rates ranging from 200 to 800 mV.s^{-1}.

Preparation of Tetra-Segmented Au-PEDOT-PPy-Au Nanowires: Electrodeposition of the bottom and top Au segments was performed by cycling the potential of the working electrode from 0.7 to 0 V at 200 $mV.s^{-1}$ using a home-made cyanide free solution (0.1 M KCl, 0.1 M K_2HPO_4, and 0.03 M $HAuCl_4$ in de-ionized water). The electrosynthesis of the PEDOT was carried out by cyclic voltammetry from an aqueous solution containing 14 mM of EDOT and 0.1 M $LiClO_4$. The potential was swept between 0.2 to 1.1 V at a scan rate of 400 $mV.s^{-1}$. Electropolymerization of pyrrole was performed in de-ionized water in presence of 0.1 M $LiClO_4$ and 0.02 M pyrrole, by sweeping the potential between 0 and 0.85 V at a scan rate of 400 $mV.s^{-1}$.

Structural Analysis: The dimensions and morphology of the nanowires were studied by scanning electron microscopy (SEM) and by transmission electron microscopy (TEM) after dissolution of the PC template. SEM pictures were obtained using a LEO 982 Field emission scanning electron microscope (FE-SEM, Carl Zeiss SMT Inc.) at an accelerating voltage of 1 kV. TEM pictures were obtained using a LEO 922 transmission electron microscope (Carl Zeiss SMT Inc.) operating at 200 kV. After removing the evaporated metal layer with aqua regia, and dissolving the template in dichloromethane, two or three drops of the resulting nanowires suspension were placed on a carbon film grid (Agar Scientific Ltd.). Energy dispersive X-ray spectroscopy (EDX) experiments were carried out with the LEO 922 TEM equipped with an INCA x-sight detector (Oxford Instruments).

Electrical Characterization: Single nanowires were measured by a top contact approach briefly described below. After the dissolution of the PC membrane, the nanowires were dispersed in dichloromethane. This solution was dropped onto an oxidized silicon substrate prepared with thick Cr/Au pads defined by photolithography. After drying the solution, the nanowires remain attached to the substrate surface via van der Waals forces; optical and electron microscopies were used to determine the position of isolated nanowires. Nanosized Au electrical probes were subsequently deposited by electron beam lithography (EBL) and lift-off for each nanowire; the probes were defined specifically to fit to the Cr/Au pads design. Prior to the deposition of the Au electrodes, short cleaning oxygen plasma was

performed to remove all PC and resist residues that could remain on the NWs due to the previous processing steps. This ensures a clean nanowire-to-electrode interface, which translates into a good electrical contact. Electrical measurements were performed with an Agilent B1500 Semiconductor Parameter/Device Analyzer equipped with high current resolution (~0.1 fA) Source Measure Units and a Süss-Microtech Probe Station. No measurable leak currents have been observed through the oxide layer or between non-connected pads over the voltage range scanned in the experiments.

XPS: X-ray photoelectron spectroscopy (XPS) data were obtained using a SSX 100/206 spectrometer from Fisons equipped with a monochromatic Al K_α X-ray source powered at 10 kV. The pressure in the analysis chamber was always maintained below $1.5x10^{-6}$ Pa. The energy resolution was set to 1.4 eV and the photoelectron take-off angle was 55^o. PPy and PEDOT films were electrosynthesized on gold sheets (Goodfellow) under similar conditions than those used to grow PEDOT and PPy nanowires and described in Table 3.2 (samples named *as-synthesized films*). Both conjugated polymer films were then immersed, for one hour, in an aqueous solution containing 0.5 M iron(III) chloride ($FeCl_3$, Acros, 98%) and then abundantly rinsed with de-ionized water (samples named *$FeCl_3$-treated films*) before XPS analysis. Data treatment was performed with the CasaXPS program (Casa Software Ltd.). The binding energies were referenced to the *C1s* neutral carbon peak at 284.6 eV. In the analysis of high-resolution XPS spectra, Gaussian curves of variable intensity were used, and the full widths at half-maximum were maintained constant for all components in a particular spectrum.

References

[1] For reviews see; a) S. M. Lindsay, M. A. Ratner, *Adv. Mat.* **2007**, *19*, 23. b) Y. Selzer, D. Allara, *Ann. Rev. Phys. Chem.* **2006**, *57*, 593. c) A. Nitzan, M. A. Ratner, *Science* **2003**, *300*, 1384. d) C. Joachim, J. K. Glimzewski, A. Aviram, *Nature* **2000**, *408*, 541.

[2] a) R. H. Baughman, A. A. Zakhidov, W. A. de Heer, *Science* **2002**, *297*, 787. b) A. Nitzan, M. A. Ratner, *Science* **2003**, *300*, 1384.

[3] a) R. E. Holmlin, R. Haag, M. L. Chabinyc, R. F. Ismaligov, A. E. Cohen, A. Terfort, M. A. Rampi, G. M. Whitesides, *J. Am. Chem. Soc.* **2001**, *123*, 5075. b) D. J. Wold, C. D. Frisbie, *J. Am. Chem. Soc.* **2001**, *123*, 5549. c) D. K. James, J. M. Tour, *Chem. Mater.* **2004**, *16*, 4423. d) R. L. McCreery, *Chem. Mater.* **2004**, *16*, 4477.

[4] a) J. L. Brédas, B. J. C. Scott, K. Yakushi, G. B. Street, *Phys. Rev. B* **1984**, *30*, 1023. b) J. C. Chiang, A. G. MacDiarmid, *Synth. Met.* **1986**, *13*, 193. c) A. J. Epstein, J. M. Ginder, F. Zuo, R. W. Bigelow, H. S. Woo, D. B. Tanner, A. F. Richter, W. S. Huang, A. G. MacDiarmid, *Synth. Met.* **1987**, *18*, 303. d) C. O. Yoon, M. Reghu, D. Moses, A. J. Heeger, *Phys. Rev. B* **1994**, *49*,10851.

[5] a) For recent reviews see: J. Jang, *Adv. Polym. Sci.* **2006**, *199*, 189. b) H. S. Yoon, M. J. K. A. Lee, J. S. Jang, *Macromol. Res.* **2008**, *16*, 85.

[6] a) C. R. Martin, *Adv. Mater.* **1991**, *3*, 457. b) R. Martin, *Acc. Chem. Res.* **1995**, *28*, 61. c) C. R. Martin, *Chem. Mater.* **1996**, *8*, 1739. d) J. Duchet, R. Legras, S. Demoustier-Champagne, *Synth. Met.* 1998, *98*, 113. e) S. Demoustier-Champagne, P. Y. Stavaux, *Chem. Mater.* **1999**, *11*, 829.

[7] Z. X. Wie, M. X. Wan, T. Lin, L. M. Dai, *Adv. Mater.* **2003**, *15*, 136.

[8] a) J. Huang, S. Virji, B. H. Weiller, R. B. Kaner, *Chem.-Eur. J.* **2004**, *10*, 1314. b) J. F. Zang, C. M. Li, S. J. Bao, X. Q. Cui, Q. L. Bao, C. Q. Sun, *Macromolecules* **2008**, *41*, 7053.

[9] a) N. I. Kovtyukhova, T. E. Mallouk, *Chem.-Eur. J.* **2002**, *8*, 4355. b) S. J. Hurst, E. K. Payne, L. Qin, C. A. Mirkin, *Angew. Chem. Int. Ed.* **2006**, *45*, 2672.

[10] O. Reynes, S. Demoustier-Champagne, *J. Electrochem. Soc.* **2005**, *152*, D130.

[11] a) L. Gence, S. Faniel, C. Gustin, S. Melinte, V. Bayot, V. Callegari, O. Reynes, S. Demoustier-Champagne, *Phys. Rev. B* **2007**, *76*, 115415. b) L. Gence, V. Callegari, S. Faniel, A. Vlad, C. Dutu, S. Melinte, S. Demoustier-Champagne, V. Bayot, *Phys. Stat. Sol.(a)* **2008**, *205*, 1447.

[12] a) Q. B. Pei, G. Zuccarello, M. Ahlskog, O. Inganas, *Polymer* **1994**, *35*, 1347. b) L. B. Groenendaal, F. Jonas, D. Freitag, H. Pielartzik, J. R. Reynolds, *Adv. Mater.* **2000**, *12*, 481. c) L. Groenendaal, G. Zotti, P. H. Aubert, J. R. Reynolds, *Adv. Mater.* **2003**, *15*, 855. d) S. Kirchmeyer, K. Reuter, *J. Mater. Chem.* **2005**, *15*, 2077.

[13] X. Du, Z. Wang, *Electrochim. Acta* **2003**, 48, 1713.

[14] a) R. Xiao, S. I. Cho, R. Liu, S. B. Lee, *J. Am. Chem. Soc.* **2007**, *129*, 4483. b) S. I. Cho, S. B. Lee, *Acc. Chem. Res.* **2008**, *41*, 699.

[15] Q. Pei, G. Zuccarello, M. Ahlskog, O. Inganäs, *Polymer*, **1994**, *35*, 1347.

[16] A. Aleshin, R. Kiebooms, R. Menon, A. J. Heeger, *Synth. Met.*, **1997**, *90*, 61.

[17] S. H. Cho, S. M. Park, *J. Phys. Chem. B* **2006**, *110*, 25656.

[18] X. Li, Y. Li, Y. Tan, C. Yang, Y. Li, *J. Phys. Chem. B* **2004**, *108*, 5192.

[19] G. Lu, C. Li, J. Shen, Z. Chen, G. Shi, *J. Phys. Chem.* **2007**, *111*, 5926.

[20] J.-L. Duvail, Y. Long, S. Cuenot, Z. Chen, C. Gu, *Appl. Phys. Lett.* **2007**, *90*, 102114.

[21] Y. Cao, A. E. Kovalev, R. Xiao, J. Kim, T. S. Mayer, T. E. Mallouk, *Nano Lett.* **2008**, *8*, 4653.

[22] G. Tourillon, Y. Jugnet, *J. Chem. Phys.* **1988**, *89*, 1905.

[23] J.-L. Duvail, P. Rétho, V. Fernandez, G. Louarn, P. Molinié, O. Chauvet, *J. Phys. Chem. B* **2004**, *108,* 18552.

[24] E.T. Kang, K.G. Neoh, Y.K. Ong, K.L. Tan, B.T. G. Tan, *Macromolecules* **1991**, *24*, 2822.

[25] S. Kuwabata, J. Nakamura, H. Yoneyama, *J. Chem. Soc., Chem. Commun.* **1988**, 779.

[26] M. Yamaura, T. Hagiwara, K. Iwata, *Synth. Met.* **1988**, *26*, 209.

[27] U. Johanson, M. Marandi, T. Tamm, J. Tamm, *Electrochimica Acta* **2005**, *50*, 1523.

[28] P. Pfluger, G.B. Street, *J. Chem. Phys.* **1984**, *80*, 544.

[29] S. Ghosh , G.A. Bowmaker, R.P. Cooney, J.M. Seakins, *Synth. Met.* **1998**, *95*, 63.

[30] M. Hasik, A. Bernasik, A. Drelinkiewicz, K. Kowalski, E. Wenda, J. Camra, *Surf. Sci.* **2002**, *507-510*, 916.

Chapter 4

Synthesis and characterization of hybrid nanowires based on polyaniline

Abstract:

We investigate the effect of the electrolyte and monomer concentrations, the potential scan range and, the scan rate, on the morphology of polyaniline (PANI) nanostructures grown by cyclic voltammetry in polycarbonate (PC) templates. Decreasing the sweeping rate used for aniline electropolymerization leads to PANI nanowires with a less porous top end. This dependency is consistent with the analysis of current transient data, interpreted in terms of nucleation and growth models. Despite the progress made to improve the quality of the top end of PANI segments, the polymer is not strong enough on its upper part to ensure the mechanical integrity of the top polymer/metal interface in tri-segmented nanowires. Indeed, tri-segmented Pt-PANI-Pt nanowires tend to break at the upper PANI/Pt interface. However, we succeed in preparing robust PANI-conjugated polymer heterojunctions, as illustrated by the successful preparation of tetra-segmented Pt-PANI-PPy-Au nanowires.

4.1 Introduction

Though it is the oldest known synthetic polymer (it was firstly reported in 1862[1]), polyaniline (PANI) has only been intensely studied from the mid-80s as other conjugated polymers. The wide range of interesting properties as its good environmental stability, high electrical conductivity in its oxidized/protonated form and, acid-base properties makes PANI one of the most attractive conducting polymers with potential applications in various fields such as energy storage[2], gas-separation[3,4], anticorrosion coating[5,6] and sensing.[7] Numerous ways of synthesis are reported in the literature for producing PANI one-dimensional (1D) nanostructures. Though several "template-free" methods were developed for avoiding the disadvantages of the post-synthesis process[8], the hard-template synthesis remains the most efficient technique to obtain nanofibers with a good control over the structural, chemical and physical properties.[9] Moreover, it is still the most adapted way to produce hybrid metal-polymer nanostructures. In our previous investigations, we demonstrated the possibility to prepare well-shaped polypyrrole (PPy) nanowires by an electrochemical process and, to integrate them into more elaborated multi-segmented metal-polymer nanostructures.[10,11] More recently, the same technique was successfully applied for preparing nanowires based on PEDOT, in particular tetra-segmented Au-PEDOT-PPy-Au nanowires presenting a switching of their electrical characteristics in function of the redox state of the two conjugated blocks.[12] Among the conjugated polymers, PANI possesses the unique and interesting property of reversible acid-base doping-dedoping between the conducting emeraldine salt and the insulating emeraldine base forms (see the different forms of PANI presented in Figure 4.1). This original reversible chemical doping, makes the integration of PANI in hybrid multi-segmented nanostructures of particularly interest.

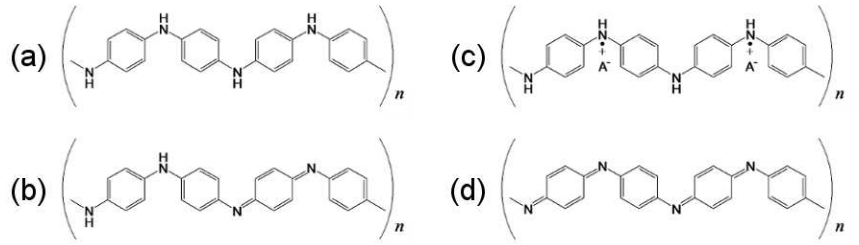

Figure 4.1 *Various forms of polyaniline: (a) the fully reduced "leucoemeraldine", (b) emeraldine base, (c) conducting emeraldine salt, (d) the fully oxidized "pernigraniline" (Adapted from [13]).*

Recently published works[14], dealing with the influence of various parameters on the morphology of electrochemically synthesized PANI nanowires, showed the difficulty of obtaining entirely compact nanostructures of this polymer. Nevertheless, getting a dense morphology is crucial for the integration of PANI in hybrid multi-segmented nanowires. Therefore, in order to electrochemically prepare solid PANI nanowires, we performed a systematic study of the effect of different synthetic parameters on the polymer morphology. Here, cyclic voltammetry was used for the growth of PANI and the current transient data were analyzed in order to find electrosynthesis conditions allowing to avoid the formation of porous PANI nanostructures. Then, the integration of PANI segments in different multi-striped nanowires was tested and a special attention was paid to the analysis, by TEM, of the mechanical robustness of the different interfaces.

4.2 Results and discussion

4.2.1 Growth and morphological analysis of PANI nanowires

As the strength of the metal/polymer interfaces directly depends on the polymer morphology at its ends, it was important before starting the synthesis of multi-segmented nanowires to find optimal electrochemical conditions allowing the deposition of PANI nanowires of good structural quality (compact PANI nanostructures). To reach this aim, we prepared by cyclic voltammetry, different samples of bi-segmented Pt-PANI nanowires

(Φ = 110 nm). Aniline was electropolymerized from aqueous HCl solutions. The effect of different parameters such as, the electrolyte and monomer concentrations, the potential scan range and, the sweeping rate, on the morphology of PANI nanowires was observed by TEM.

a) Effect of the electrolyte concentration

Firstly, to study the influence of the electrolyte concentration, the monomer concentration was fixed at 0.1 M and, various HCl concentrations were used: 0.25, 0.5, 1 and 2 M. Aniline electropolymerization was performed by repetitively cycling the potential between 0 and 0.9 V (vs. Ag/AgCl) at a scan rate of 400 $mV.s^{-1}$. Figures 4.2.a-c show the cyclic voltammograms of aniline electropolymerization obtained with HCl concentrations of 0.25, 0.5 and 1 M, respectively. In the three cases, the broadening of the curve, accompanied by a current increase with increasing cycle number, indicates that polymer is growing. By increasing the electrolyte concentration, the rate of aniline polymerization becomes faster, as indicated by the higher current increase at higher HCl concentrations. Figure 4.2.d shows the two redox systems and the anodic peak appearing in the set of voltamperograms. At the first cycle, an anodic peak P_a^{α}, corresponding to the oxidation of aniline and the generation of free radicals is observed at 0.9 V. Then during the following cycles, a new redox system P^{β}, assigned to the electrochemical response of PANI formed during the oxidation process of aniline. A third redox system P^{γ}, having its redox potential between β and α is also observed. It is generally associated to the electroactivity of degradation products such as, p-benzoquinone and quinoneimine resulting from the polymer hydrolysis.[15] We should notice that this degradation of the formed polymer into hydrolysis products occurs whatever the electrolyte concentration. This phenomenon has already often been observed by other groups when the upper potential exceeds a certain limit.[16]

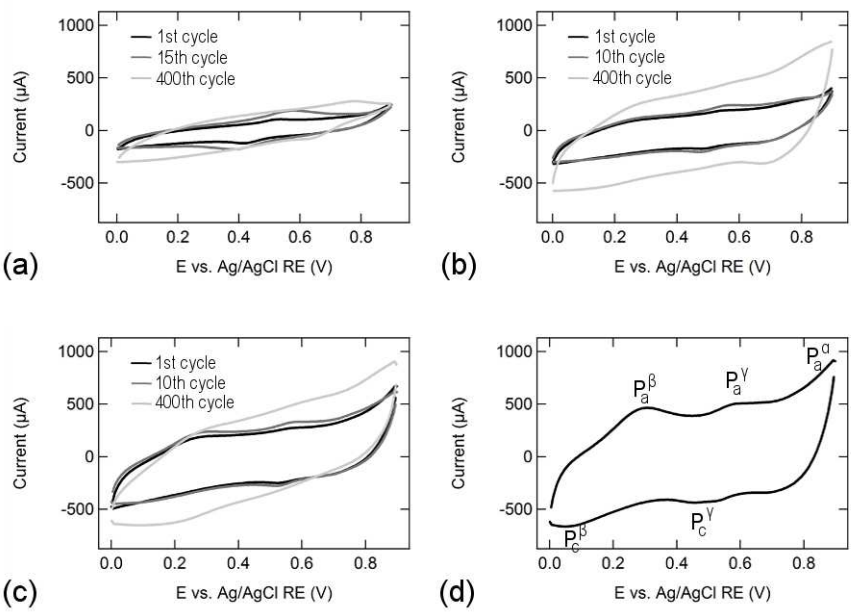

Figure 4.2 *(a), (b) and (c) Cyclic voltammograms of PANI deposition carried out at different HCl concentrations in nanoporous of 110 nm diameter. The monomer concentration was 0.1 M, the scan rate was 400 mV.s^{-1} and the cycle number was 400. The electrolyte concentration was (a) 0.25 M (b) 0.5 M (c) 1 M. (d) Typical cyclic voltammogram of PANI, with its three characteristic oxido-reduction peaks.*

Previous works on the electrochemical synthesis of conjugated polymer films reported that the properties of the resulting electrodeposited materials depend on the nature of the growth.[17] Electrochemists commonly use the current transients of polymerization for probing the nucleation and growth mechanisms of conducting polymers. They consist in following the change in current with time for a fixed potential. In the case of potentiodynamic deposition, this evolution is not directly recorded but, can be deduced from the cyclic voltammograms by taking the current value at the upper potential limit for each cycle. Figure 4.3 illustrates the current-time transients taken at the upper potential limit E = 0.9 V for three of the four tested electrolyte concentrations. We should note that plotting the change in current as a function of time or cycle number is here equivalent, as the potential sweep rate is fixed at 400 mV.s^{-1} for all the samples. In the *[HCl]* 0.25 – 1 M range, all the current-time curves present a similar pattern. After an initial current

drop (Region 1), typical of PANI electropolymerization and, attributed in several studies, to charging current, oxidative electroadsorption of monomers at the electrode surface and substrate passivation[18,19], there is a current increase to a maximum value (Region 2), before a new gradually current decrease (Region 3). However, at electrolyte concentrations higher than 0.5 M, the pattern of the current transient ended by an exponential current increase (Region 4). The current maximum shifts to shorter time and higher current as *[HCl]* increases from 0.25 to 1 M. This trend had already been observed in this electrolyte concentration range[14,20]. It may be attributed to an increase in the diffusion coefficient values (and so a faster diffusion rate of the monomers to the electrode) with the increasing concentration of electrolyte, caused by a change of the hydrodynamic radius of the diffusing species.[21]

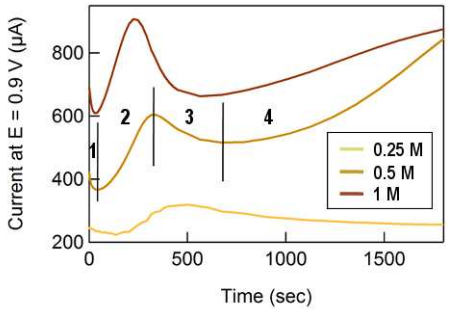

Figure 4.3 *Resulting current transients taken at E = 0.9 V vs. Ag/AgCl for the three different electrolyte concentrations.*

The resulting polyaniline nanostructures grown from electrochemical baths containing different HCl concentration were then observed by TEM (Figure 4.4). Whatever the used electrolyte concentration, we firstly observed that the polymer is more compact and homogeneous near its starting end and, adopts a tubular morphology more inhomogeneous on its growing end (Figure 4.4.d). For the same number of cycles performed during the synthesis (400 cycles), the length of the starting compact part seems to increase with the electrolyte concentration *[HCl]* from 0.25 to 1 M. Moreover, by increasing *[HCl]*, we noticed that the adhesion of PANI onto Pt was better. If for *[HCl]* = 0.25 M, the majority of bi-segmented Pt-PANI nanowires were broken (Figure 4.4.a) at the metal/polymer interface, for

[HCl] ≥ 1M, the quasi-totality of the nanostructures were entire (Figure 4.4 c and d). No structural improvement was, however, observed when increasing the electrolyte concentration from 1 to 2 M. In summary, among the four tested electrolyte concentrations, choosing *[HCl]* = 1 M promotes the polymer growth process leading to compact materials at the detriment of degradation processes leading to more porous materials. For this reason, the electrolyte concentration was further fixed at 1 M.

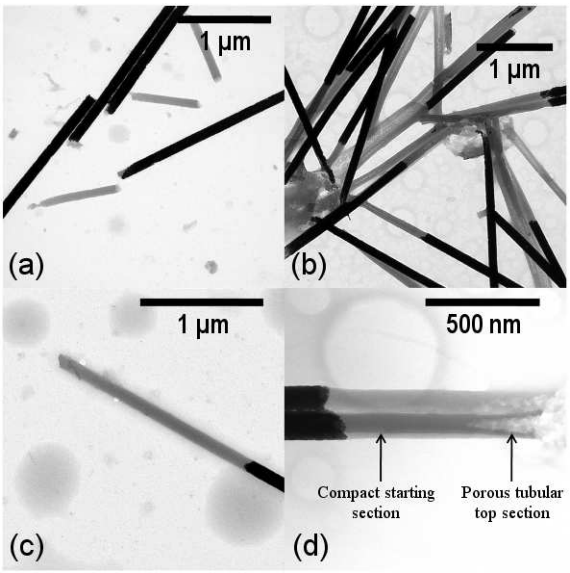

Figure 4.4 *TEM pictures of Pt-PANI nanowires. PANI was synthesized from solutions containing (a) 0.25 M (b) 0.5 M (c) 1 M (d) 2 M of HCl electrolyte.*

b) Effect of the monomer concentration

Different concentrations in aniline, ranging from 0.01 to 0.5 M were then tested for the synthesis of the most compact PANI segments. Even after a larger number of scans, no material was found at 0.01 M aniline concentration. As shown in Figure 4.5.a, some PANI nanofibers with a more or less compact bottom part and a porous upper extremity were observed at 0.05 M aniline concentration but, the majority of the nanowires were of poor quality (Inset of Figure 4.5.a). By increasing the monomer amount into the electropolymerization bath over the 0.1 – 0.3 M concentration range,

smoother and more compact over a few hundred nanometers PANI nanostructures were fabricated (Figure 4.5.b).

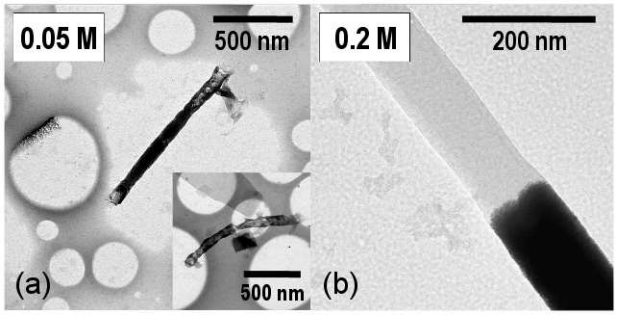

Figure 4.5 *TEM images of Φ = 110 nm PANI nanowires grown from an electrochemical bath containing (a) 0.05 M aniline, and (b) 0.2 M aniline. The other conditions, electrolyte concentration ([HCl] = 1 M), potential scan range (0 - 0.75V), sweep rate (400 mV.s^{-1}) and cycle number (1000), were identical for both samples.*

Based on these results, we further carry out aniline electropolymerization using a fixed monomer concentration of 0.1 M.

c) Effect of the upper potential

The polymerization potential is one of the parameters that have the most dramatic influence on the morphology of the polymer and on its properties. When performing electropolymerization of aniline at high potential, competitive reactions leading to polymer degradation can indeed occur, as shown in section 4.2.1.a. In this study, we thus swept the potential between 0 V and four different upper potential limits: 0.75, 0.8, 0.85 and 0.9 V. Figure 4.6 shows TEM images of Pt-PANI nanowires obtained under these various potential scan ranges. The amount of electrodeposited PANI increased with the value of the upper potential limit. We again deduced from cyclic voltammograms the current transients recorded at the four upper potential limits (Figure 4.7). At upper potential limits lower than 0.8 V, the obtained current profiles are almost flat. These potential values are too low to clearly identify the typical stages of PANI electropolymerization, the growth rate of the polymer being very low. At upper potential limits higher than 0.85 V, we obtain a similar pattern of current variations than the one described

previously. When the upper potential value is increased from 0.85 to 0.9 V, the different steps occur faster. In summary, the growing rate of PANI nanowires increases with the upper potential value, leading to increased amount of electrodeposited polymer. It is interesting to point out that in this study, a very low amount of polymer was deposited on the top of the Pt nanowire when sweeping the potential to an upper limit of 0.75 V (Figure 4.6.a), while Mallouk *et al.*[14] obtained long homogeneous PANI nanowires by galvanostatic deposition at a constant potential of 0.75 V. In contrast, they formed long porous nanowires by fixing the potential at 0.9 V, while we obtained dense PANI segments of more than one micrometer by sweeping the potential up to 0.9 V. If at first sight, these results could seem in contradiction, the differences between our work and the one of Mallouk surely result from several different experimental aspects. Firstly, while they used alumina membranes as templates, we carried out PANI electrodeposition within PC nanoporous membranes and, it is well known that the interactions between the template walls and the growing positively charged polymer have an important impact on the polymer morphology.[22] Secondly, we electrodeposited PANI on flat electrodes (at the top of Pt nanowires), while in Mallouk's investigations, PANI nanostructures were grown from annular base electrodes (the metallic layer deposited on one face of the membrane and serving as working electrode being too thin to fill in the entrance of the pores). However, it was recently reported that the structure (annular or flat) of the working electrode is a critical parameter influencing the polymer growth mechanism.[23] Furthermore, we used a potentiodynamic method for preparing PANI nanostructures, while they used a potentiostatic method. Finally, the last notable difference between the two respective works is the choice of the electrolyte, as we used HCl and not H_2SO_4 aqueous solutions. This parameter can also have a significant impact on the resulting morphology of PANI.

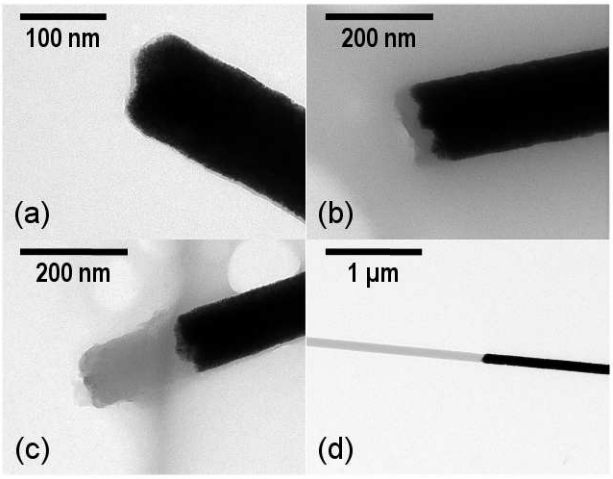

Figure 4.6 *TEM images of Φ = 110 nm Pt-PANI nanowires where PANI was synthesized by sweeping the potential between 0 V and (a) 0.75 V (b) 0.8 V (c) 0.85 V (d) 0.9 V at 200 mV.s^{-1} during 400 cycles.*

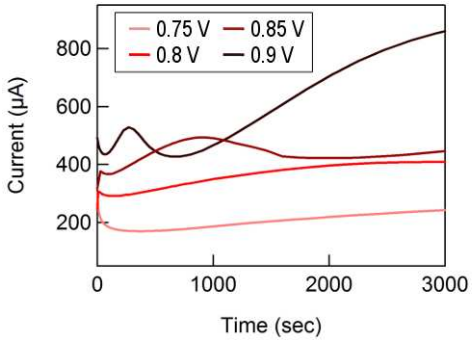

Figure 4.7 *Current transients of PANI synthesized at four different potentials.*

d) Effect of the scan rate

In the potentiodynamic method, the sweeping rate is another determining parameter of the growth mechanism and thus, of the resulting morphology of the polymer.[24] The growth of PANI by cyclic voltammetry have been described as a discontinuous process occurring only in the potential region where aniline is oxidized to PANI (i.e. in our case, roughly in the potential

range of 0.75 to 0.9V).[25] Over the rest of the sweeping potential range, electropolymerization is interrupted but, other essential events occur such as, the electrochemical activation of the polymer[26], the evacuation of the intermediates formed during electropolymerization[27] and the monomer re-supply. Therefore, the properties of electrodeposited PANI depend on the period during which the polymerization is interrupted. From these considerations, it is understandable that PANI morphology greatly depends on the potential scan rate imposed during the electropolymerization process. In the present study, aniline was electropolymerized by sweeping the potential between 0 and 0.9 V at three different sweeping rates: 200, 400 and 800 $mV.s^{-1}$. As shown on the TEM images of Figure 4.8, the quality of the electrodeposited PANI nanowires deteriorates when increasing the scan rate from 200 to 800 $mV.s^{-1}$.

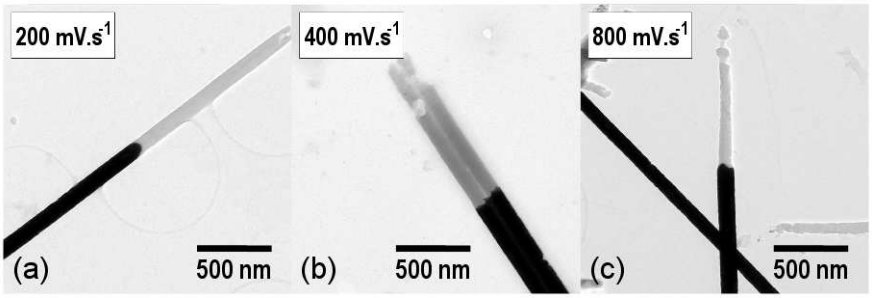

Figure 4.8 *TEM images of Pt-PANI nanowires where the polymer was synthesized at different scan rates.*

To better understand the dependency of the PANI morphology on the scan rate, we carried out a study of the nucleation and growth mechanisms of PANI nanowires from the current transients presented in Figure 4.9.a, corresponding to aniline electropolymerizations performed at 200 and 800 $mV.s^{-1}$. A common way to analyze the nucleation and growth processes is to use the current maximum in current transients. With the coordinates of this singular point, we compared each experimental current-time plot of Figure 4.9.a with theoretical plots corresponding to different modes of PANI nucleation and growth mechanisms. The two theoretical I-t curves characteristics of the two following models: three-dimensional instantaneous nucleation (3DIN) and three-dimensional progressive nucleation (3DPN)

under diffusion control are described by the equations 1 and 2, respectively.[28]

$$\frac{I^2}{I_m^2} = \frac{1.9542}{t/t_m}\left\{1 - exp\left[-1.2564\left(t/t_m\right)\right]\right\}^2 \quad (1)$$

$$\frac{I^2}{I_m^2} = \frac{1.2254}{t/t_m}\left\{1 - exp\left[-2.3367\left(t/t_m\right)^2\right]\right\}^2 \quad (2)$$

where I, t, I_m and t_m are current, time, the maximum current value and the time of its appearance, respectively.

The comparison between our experimental I-t curves, obtained from the experimental data of Fig. 4.9.a and the two theoretical plots is shown in Figure 4.9.b.

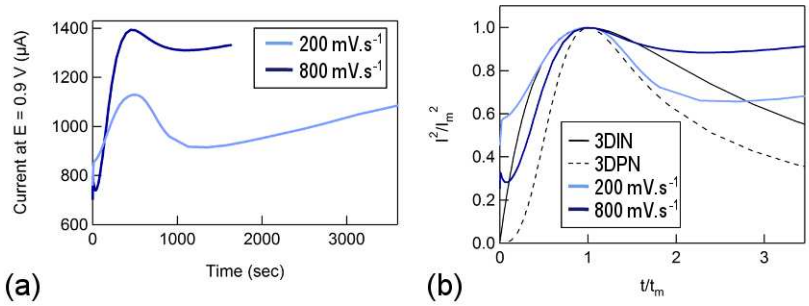

Figure 4.9 *(a) Current transients of aniline polymerization at 200 and 800 mV.s^{-1}. (b) Comparison between the experimental data from Figure 4.9.a with theoretical curves for 3DPN and 3DIN modes.*

After the current maximum, there is a time range during which it is reasonable to assume that PANI growth follows a 3D mechanism. At the scan rate of 200 mV.s^{-1}, the experimental data fall in the region between 3D progressive and instantaneous nucleation, while the experimental data recorded at 800 mV.s^{-1} are in better agreement with the theoretical plot of 3D instantaneous nucleation. As instantaneous nucleation leads to the formation of an inhomogeneous material, this is consistent with the TEM observations where more porous PANI nanowires were observed at higher sweeping rate (Fig. 4.8.c). The further current increase, observed for both experimental current transients, suggests that the PANI growth is governed by a

mechanism different from a 3D mechanism. As the experimental curves are in accordance with the theoretical plots of 3D mechanisms and then tend to increase exponentially, we can suggest that in our case the PANI growth follows a combination of 3D and 1D mechanisms.

4.2.2 Synthesis of multi-segmented nanowires based on polyaniline

a) Synthesis of tri-segmented Pt-PANI-Pt nanowires

Tri-segmented Pt-PANi-Pt nanowires were synthesized by the template sequential electrochemical deposition method, where aniline electropolymerization was performed under the optimal conditions determined previously: *[HCl]* = 1 M concentration, *[aniline]* = 0.1 M, potential sweeping between 0 to 0.9 V at 200 $mV.s^{-1}$. We have indeed shown in the previous sections that these electrosynthesis conditions lead to the formation of PANI nanowires with the shortest top porous section. TEM pictures of Figure 4.10 show the morphology of the resulting Pt-PANI-Pt nanowires. It appears that they present a badly defined upper polymer/metal interface and that the aqueous solution used for growing the top metal segments diffuses into the porous top section of PANI leading to grainy metal-onto-polymer interfaces and even to metallic islands (inset of Figure 4.10.b) within the polymer segment. We should mention that the formation of these weak and badly defined PANI/Pt interfaces leads in most cases to broken nanowires.

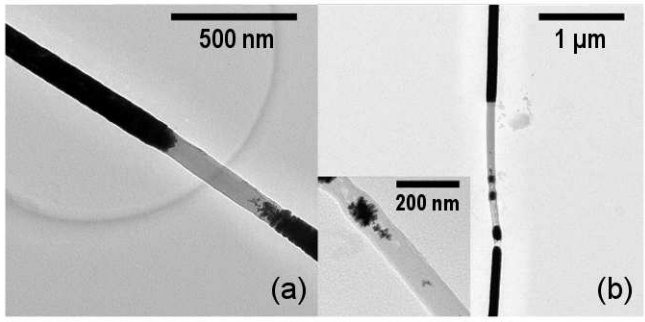

Figure 4.10 *TEM images of (a) an entire Pt-PANI-Pt nanowire (b) a Pt-PANI-Pt nanowire breaking at the weak upper interface. The inset is a magnification of the porous part of the polymer filled with metal nanoparticles.*

b) Synthesis and morphological analysis of Pt-PANI-PPy-Au tetra-segmented nanowires

Though the growing of tri-segmented Pt-PANi-Pt was not fully successful, we tried to prepare tetra-segmented nanowires presenting a polymer heterojunction (PANI-PPy) using a similar sequential template electrochemical strategy. The sequence of polymer deposition has been designed so that the upper end of the PANI segment was not in contact with a metal. Therefore, we firstly electrodeposited PANI onto the first metallic segment and, we further electrodeposited the second conjugated polymer, PPy. The choice of Pt for growing the bottom metallic segment was made according to the high affinity observed between PANI and Pt. Indeed, in the course of the study presented in the first part of this chapter, we rarely observed broken Pt/PANI interfaces. The choice of Au as upper metallic segment was obvious, due the successful growing of PPy/Au interfaces reported previously in the growing of various multi-segmented nanostructures (see chapters 2 and 3).

The formation of PANI-PPy heterojunctions was checked by TEM. A typical picture of the obtained multi-segmented nanostructures is presented in Figure 4.11.a. In this case, a large majority of the Pt-PANI-PPy-Au nanowires was entire. As no chemical element allows distinguishing both polymers, we could not used EDX analysis as we did previously for identifying PEDOT and PPy in PEDOT-PPy heterojunction (see chapter 3). Nevertheless, the high-resolution TEM picture of the upper polymer/metal interface shown in Figure 4.11.b is clearly different from the badly defined PANI/metal interface observed in the tri-segmented metal-PANI-metal nanowires (Figure 4.10) and is more typical of the conical PPy/metal junctions that we often observed in PPy-based multi-segmented nanostructures. This is an indication that a PPy segment has been successfully electrodeposited onto the PANI section. Besides, the high values of current recorded during the two consecutive aniline and pyrrole electropolymerizations confirm that two long successive polymer segments were formed. Based on the preceding observations of interfaces with PANI, we can, however, assume that the interface between the two polymers is not well-defined but, that there is rather a transition area where the two polymers co-exist (with PPy filling the pores of the upper inhomogeneous part of the PANI segment).

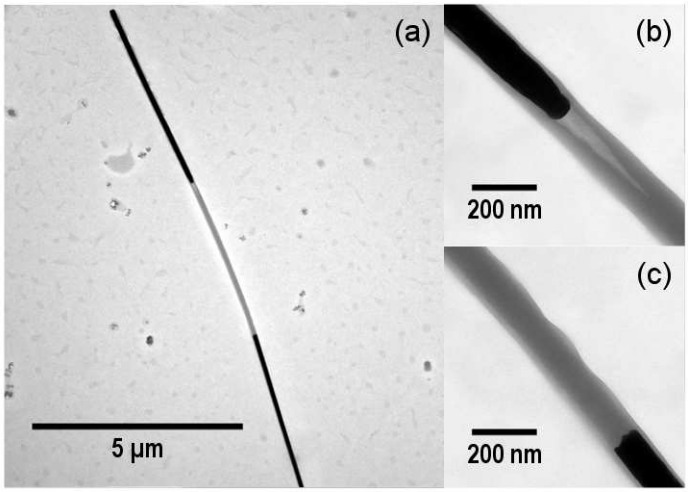

Figure 4.11 *(a) TEM picture of a Φ = 110 nm tetra-segmented Pt-PANI-PPy-Au nanowire. (b) Magnification of the upper PPy/Au interface. (c) Magnification of the bottom Pt/PANI interface.*

Currently, we are considering the preparation by the same way of another kind of tetra-segmented nanostructures: Pt-PANI-PEDOT-Au nanowires. In this case, we will be able to distinguish the two polymers by TEM-EDX, as the two polymers can be identified by the presence or not of sulfur atoms. Moreover, these systems should be very interesting as one can expect to get a reversible switching of their electrical properties by tuning the redox states of both polymers through an acid-base doping-dedoping process.

4.3 Conclusions

We used cyclic voltammetry to prepare PANI nanowires in aqueous HCl solutions. To improve the morphology of the polymer on its top end, we studied the effect of different parameters such as, the monomer and electrolyte concentrations, the potential scan range and the sweeping rate on the electropolymerization process. These investigations revealed that by potentiodynamic method, PANI segments of good structural quality are obtained by sweeping the potential up to a relative high value (0.9 V).

Depending on the applied scan rate (200 to 800 $mV.s^{-1}$), the resulting PANI nanowires were found to be more or less porous when electropolymerization process seems to pass between two 3D diffusion-controlled nucleation and growth mechanism. Current-time transients recorded during electrodeposition suggested that PANI electropolymerization by cyclic voltammetry actually could follow a combination of 3D and 1D mechanisms. Based on the optimized PANI electrosynthesis conditions, robust tetra-segmented Pt-PANI-PPy-Au nanowires were prepared and characterized by transmission electronic microscopy. Taking advantage of the unique acid-base properties of PANI, we expect to obtain original electrical properties from this new kind of multi-segmented nanowires including a conjugated polymer heterojunction. This is currently under investigation.

4.4 Experimental part

Materials: Polycarbonate track-etched membranes with a thickness of 21 μm, a pore density of 10^9 $pores.cm^{-2}$ and an average pore size of 110 nm, supplied by it4ip, were used as nanoporous templates. Aniline (Acros, 99%) and pyrrole (Acros, 99%) were purified immediately before use by passing them through a microcolumn constructed from a Pasteur pipette, glass wool, and activated alumina. Lithium perchlorate ($LiClO_4$, Acros), hydrochloric acid (HCl, Acros), potassium chloride (KCl, Acros) potassium hydrogenophosphate (K_2HPO_4, Acros), hydrogen tetrachloroaurate ($HAuCl_4$, Acros), sodium hexachloroplatinate (Na_2PtCl_6, Aldrich), sulfuric acid (H_2SO_4, Fisher Scientific) and dichloromethane (CH_2Cl_2, Acros) were used without any prior purification. De-ionized water was used to prepare all aqueous solutions. Aqua regia was prepared by carefully adding three volumes of concentrated hydrochloric acid (HCl, Acros) to one volume of concentrated nitric acid (HNO_3, Acros, 63%). The iodine solution was prepared by dissolving 6 g of potassium iodide (KI, Merck) and 1.5 g of iodine (I_2, Sigma-Aldrich) in 60 ml of de-ionized water.

Preparation of Pt-PANI Nanowires: All electrochemical experiments were performed with a CHI660B Electrochemical Workstation (CH Inc.) in a conventional one-compartment cell at room temperature with a Pt disk counterelectrode and a Ag/AgCl reference electrode. A 300 nm thick layer of gold evaporated on one side of the polycarbonate membrane served as working electrode. Electrodeposition of Pt was performed potentiostatically at -0.2 V using a home-made bath (0,01 M $Na_2PtCl_6.H_2O$ and 0,5 M H_2SO_4 in de-ionized water). Electropolymerization of aniline was carried out by cyclic voltammetry from an aqueous solution containing different HCl concentrations ranging from 0.25 to 2 M, different monomer concentration ranging from 0.01 to 0.5 M. The potential was wept between 0 and various Upper Potential Limits ($0.75 \leq UPL \leq 0.9$ V) at sweep rates ranging from 200 to 800 $mV.s^{-1}$.

Preparation of Tetra-segmented Pt-PANI-PPy-Au Nanowires: Electrodeposition of Au segments was performed by cycling the potential of the working electrode from 0.7 to 0 V at 200 $mV.s^{-1}$ using a home-made cyanide free solution (0.1 M KCl, 0.1 M K_2HPO_4, and 0.03 M $HAuCl_4$ in de-ionized water). The electrochemical synthesis of the PANI was carried out by cyclic voltammetry from an aqueous solution containing 0.1 M aniline and 1 M HCl. The potential was swept between 0 and 0.9 V at a scan rate of 200 $mV.s^{-1}$. Electropolymerization of pyrrole was performed in de-ionized water in presence of 0.1 M $LiClO_4$ and 0.02 M pyrrole, by sweeping the potential between 0 and 0.85 V at a scan rate of 400 $mV.s^{-1}$.

Structural Analysis: The dimensions and morphology of the PANI nanowires were studied by transmission electron microscopy (TEM) after dissolution of the PC template. TEM pictures were obtained using a LEO 922 transmission electron microscope (Carl Zeiss SMT Inc.) operating at 120 or 200 kV. After removing the evaporated metal layer with aqua regia or iodine solution, and dissolving the template in dichloromethane, two or three drops of the resulting nanowires suspension were placed on a carbon film grid (Agar Scientific Ltd.).

References

[1] H, Letheby, *J. Chem. Soc.* **1862**, *15*, 161.

[2] K, Rajendra Prasad, N. Munichandraiah, *Journal of Power Sources* **2002**, *112*, 443.

[3] M. R. Anderson, B. R. Mattes, H. Reiss, R. B. Kaner, *Science* **1991**, *252*, 1412.

[4] J. Yang, S. M. Burkinshaw, J. Zhou, A. P. Monkman, P. J. Brown, *Adv. Mater.* **2003**, *15*, 1081.

[5] P. J. Spellane, F. A. Via, *US Patent No 6117558*, 12/09/2000.

[6] D. Sazou, M. Kourouzidou, E. Pavlidou, *Electrochim. Acta* **2007**, *52*, 4385.

[7] a) K. Ramanathan, M. K. Ram, B. D. Malhotra, A. S. N. Murthy, *Mat. Sci. Eng. C* **1995**, *3*, 159. b) J. Huang, S. Virji, B. H. Weiller, R. B. Kaner, *J. Am. Chem. Soc.* **2003**, *125*, 314. c) H. Liu, J. Kameoka, D. A. Czaplewski, H. G. Craighead, *Nano Lett.* **2004**, *4*, 671. d) Z. Matharu, G. Sumana, S. K. Arya, S. P. Singh, V. Gupta, B. D. Malhotra, *Langmuir* **2007**, *23*, 13188.

[8] H. Qiu, M. Wan, B. Matthews, L. Dai, *Macromolecules* **2001**, *34*, 675. b) C. Liao, M. Gu, *Thin Solid Films* **2002**, *408*, 37. c) L. Liang, J. Liu, C. F. Windisch Jr., G. J. Exarhos, Y. Lin, *Angew. Chem. Int. Ed.* **2002**, *41*, 3665. d) Y. Ma, J. Zhang, G. Zhang, H. He, *J. Am. Chem. Soc.* **2004**, *126*, 7097.

[9] M. Delvaux, J. Duchet, P.-Y. Stavaux, R. Legras, S. Demoustier-Champagne, *Synth. Met.* **2000**, *113*, 275.

[10] O. Reynes, S. Demoustier-Champagne, *J. Electrochem. Soc.* **2005**, *152*, D130.

[11] L. Gence, S. Faniel, C. Gustin, S. Melinte, V. Bayot, V. Callegari, O. Reynes, S. Demoustier-Champagne, *Phys. Rev. B* **2007**, *76*, 115415.

[12] V. Callegari, L. Gence, S. Melinte, S. Demoustier-Champagne, *Chem. Mater.* **2009**, *21*, 4241.

[13] D. C. Trivedi, in H. S. Nalwa (Ed), *Handbook of Organic Conductive Molecules and Polymers, vol. 2*, Wiley, **1997**, 509.

[14] Y. Cao, T. Mallouk, *Chem. Mater.* **2008**, *20*, 5260.

[15] L. D. Arsov, *J. Solid State Electrochem.* **1998**, *2*, 266.

[16] E. M. Genies, C. Tsintavis, *J. Electroanal. Chem.* **1985**, *195*, 109.

[17] R. Cordova, M. A. Delvalle, A. Arratia, H. Gomez, R. Schrebler, *J. Electroanal. Chem.* **1994**, *377*, 75.

[18] D. Sazou, M. Kourouzidou, E. Pavlidou, *Electrochim. Acta* **2007**, *52*, 4385.

[19] B. Scharifker, G. Hills, *Electrochim. Acta* **1983**, *28*, 879.

[20] S. Kariuki, H. D. Dewald, *Electroanalysis* **1997**, *9*, 231.

[21] S. Sasaki, *Colloid Polym. Sci.* **1984**, *262*, 406.

[22] C. R. Martin, *Adv. Mater.* **1991**, *3*, 457.

[23] S. I. Cho, S. B. Lee, *Acc. Chem. Res.* **2008**, *41*, 699.

[24] S. K. Mondal, K. R. Prasad, N. Munichandraiah, *Synth. Met.* **2005**, *148*, 275.

[25] S. J. Choi, S. M. Park, *J. Electrochem. Soc.* **2002**, *149*, 26.

[26] D. C. Trivedi, in H. S. Nalwa (Ed), *Handbook of Organic Conductive Molecules and Polymers, vol. 2*, Wiley, **1997**, 504.

[27] S. Y. Cui, S. M. Park, *Synth. Met.* **1999**, *105*, 91.

[28] a) Z. Mandic, L. Duic, F. Kovacicek, *Electrochim. Acta* **1997**, *42*, 1389. b) B. J. Hwang, R. Santhanam, C. R. Wu, Y. W. Tsai, *J. Solid. State. Electrochem.* **2001**, *5*, 280.

Chapter 5

Synthesis and structural characterization of hybrid magnetic metal-conjugated polymer nanowires

Abstract:

A variety of new multi-segmented nanowires based on magnetic metals and conjugated polymers, polypyrrole (PPy) and poly(3,4-ethylenedioxythiophene) (PEDOT), are synthesized by an all-electrochemical template method for precise control over segment lengths. To overcome the major problem occurring when performing direct electrodeposition of PPy or PEDOT on active metals, such as nickel: the concomitant metal oxidation and re-dissolution at the positive potentials required for polymer formation, a two-step chemical process is developed. Prior to electropolymerization, the Ni surface is pre-treated with 3-(pyrrol-1-yl) propanoic acid. This strategy allows the improvement of the polymer adhesion, resulting in the formation of mechanically robust Ni/conjugated polymer interfaces. By this way, we successfully prepare different original tri-segmented nanostructures, such as systems containing one magnetic segment, Ni-PPy-Pt and Ni-PEDOT-Au nanowires and, systems containing two different magnetic metals, Ni-PPy-Co and Ni-PEDOT-Co nanowires. All these one-dimensional multi-component nanostructures present both fundamental interest and potential applications in nano-electronics and in biomedical field.

5.1 Introduction

Due to their unique properties, one-dimensional (1D) nanowires are particularly attractive for sensing and electronics applications. However, to incorporate these nanostructures into devices, it is critically important to be able to control their motion and position. Various approaches for controlling the position and alignment of nanowires or nanotubes have already been reported. Among them, we can cite the use of chemically patterned pre-fabricated electrodes[1] and, the use of electrical or magnetic fields[2]. For performing such type of nanowire manipulation, the nanostructures must contain an adequate material, different than the functional one. For that reason, the design and synthesis of multi-segmented 1D nanowires, containing stripes of different materials that can perform specific functions, have recently received considerable attention.[3] An attractive route for preparing such multi-segmented nanowires involves sequential electrodeposition into a nanoporous membrane, followed by the dissolution of the nanoporous template. However, one of the major issue for the application of multi-component nanowires is the improvement of the mechanical strength of the different in-wire material interfaces, this problem being even more marked in narrow ($\Phi < 120$ nm) diameter nanowires. In chapters 2 and 3, we reported on an effective all-electrochemical template-based method for preparing a variety of well-shaped and mechanically robust tri- and tetra-segmented noble metal (Au or Pt)-conjugated polymer (PPy and PEDOT) nanowires. In the present chapter, our goal was to develop a method allowing the preparation of magnetic metal (Ni or Co)-conjugated polymer based nanowires. However, the electropolymerization of pyrrole or EDOT on active metals is much more difficult than on noble metals. Indeed, the oxidation potentials of these metals are much lower than that of the conjugated monomers and, consequently, dissolution of the metal occurs before electropolymerization begins. To form homogeneous and adherent conjugated polymer layers onto oxidizable metals, it is thus necessary to find synthesis conditions that will strongly passivate the metal without impeding electropolymerization. Although, there is an extensive literature on the electropolymerization of conducting polymers on oxidizable metals, there are very few reports devoted to deposition on nickel[4] and, none on the synthesis of Ni-conjugated polymer based nanowires.

Here, we firstly report on the development of a strategy consisting in a two-step process for preparing Ni-PPy and Ni-PEDOT nanowires with a good adhesion between the polymer and the metal. Prior to electropolymerization, the Ni surface was pre-treated with a bi-functional molecule, which through specific interactions ensures a good adhesion between the two nanowires segments. In a second part, we describe the synthesis and, structural characterization by SEM and TEM, of tri-segmented magnetic metal-conjugated polymer (CP)-noble metal nanowires, typically Ni-PPy-Pt and Ni-PEDOT-Au nanowires. This kind of 1D nanostructures offers various possibilities in terms of self-assembly or functionalization by using the specific surface chemistry of the different segments. Finally, for the first time, we report on the preparation of nanowires composed of a CP junction sandwiched between two magnetic segments of different nature, typically tri-segmented Ni-CP-Co nanowires. The efficiency of the process, in particular the Ni/CP and CP/Co interfaces robustness was checked by observing the different nanostructures by SEM and/or TEM. These fully magnetic multi-segmented nanowires meet all criteria required for tunnel magnetoresistance manifestation: as good organic conductors, conjugated polymers have both relatively long spin relaxation times and a sufficient large conductivity, while the multi-striped geometry offers an inorganic/organic interface quality. This suitable configuration makes them very attractive candidates for fundamental investigations in organic spintronics[5]. A particularly interesting study in this young field could be the determination of the spin relaxation length for these conducting polymers by measuring the magnetoresistance dependence on the organic junction length.

5.2 Results and discussion

5.2.1 Synthesis of magnetic bi-segmented nanowires with a good adhesion between the metal and the conjugated polymer segments

Toward achieving the goal of preparing multi-segmented nanowires containing one or two magnetic metal segments, we first focus our attention

on the development of a synthetic process allowing the preparation of strong Ni/CP interfaces. Our approach consists in a chemical pre-treatment of the active metal substrate with an appropriate bi-functional molecule to form a passivating self-assembled monolayer (SAM)[6] that suppresses or limits the metal re-dissolution without preventing the electrodeposition of the CP. More precisely, for promoting the adhesion of the CP on nickel, we used 3-(Pyrrol-1-yl) propanoic acid (3PPA). This passivating molecule was chosen due to its facile synthesis[7,8], and because it contains two end-functional groups, a carboxylate group at one extremity and a pyrrole group at the other end, that can specifically interact with the Ni substrate and the growing CP, respectively (Figure 5.1). Moreover, the presence of a short alkyl chain between the two reactive groups allows the formation of well-covering monolayer without stopping further electrochemical process at the Ni electrode.

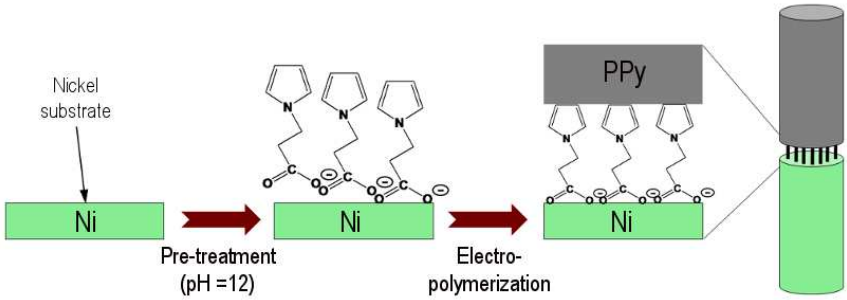

Figure 5.1 *Schematic representation of the chemical pre-treatment of the nickel substrate for the formation of an adherent polypyrrole coating.*

a) SAM deposition on Ni plates

We first investigated the ability of grafting a 3PPA monolayer onto a nickel substrate by using flat nickel surfaces as model systems. The substrates were immersed for 18 hours in basic aqueous solutions of 3PPA of different concentrations, rinsed abundantly with de-ionized water, and dried under nitrogen flux. The formation of a more or less dense layer was highlighted by cyclic voltammetry using a redox probe (Figure 5.2).

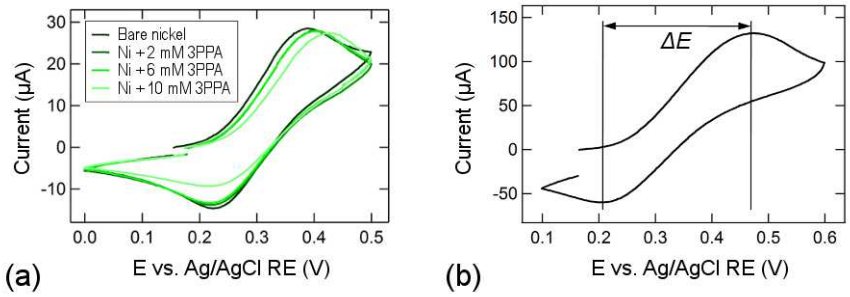

Figure 5.2 *Cyclic voltammograms of differently chemically pretreated Ni electrodes recorded in aqueous solutions containing 0.1 M $LiClO_4$, 7.10^{-4} M sodium dodecylsulfate (SDS) and 2.5 mM of $K_4Fe(CN)_6.3H_2O$. (a) 3PPA molecule concentration in the pre-treatment bath ranging from 2 to 10 mM. (b) [3PPA] = 50 mM; the parameter ΔE used to compare different cases is represented on the cyclic voltammogram. Scan rate is 50 mV.s^{-1}.*

Table 5.1 *Evolution of the anodic peak (E_{PA}), cathodic peak (E_{PC}) and, $\Delta E = E_{PA} - E_{PC}$ of the redox probe Fe^{III}/Fe^{II} in function of the [3PPA] used for the formation of a SAM onto the Ni electrode.*

[3PPA] (mM)	**E_{PA} (mV)**	**E_{PC} (mV)**	**ΔE (mV)**
0 (Bare Ni)	389	225	164
2	403	220	183
6	403	220	183
10	428	215	213
50	473	203	270

The electrochemical activity of the redox couple Fe^{III}/Fe^{II} using different chemically modified nickel substrates as working electrodes was followed by sweeping the potential between 0 and 0.5 V for *[3PPA]* ranging from 2 to 50 mM (Figure 5.2.a). From these curves, it clearly appears that the 3PPA concentration used in the pre-treatment solution has a significant impact on the electrochemical activity of the redox couple. Indeed, the higher the *[3PPA]* is, the larger the gap between the oxidation and reduction peak potentials (ΔE, Figure 5.2.b) is (Table 5.1). This transition towards a less reversible system can be explained by the decrease of the electron transfer

rate, resulting from the grafting of a progressively denser monolayer onto the Ni electrode.

b) Synthesis of Ni nanowires

Membrane-based technology has already been successfully used to fabricate nanowires of magnetic metals such as Ni and Co[9,10,11]. Here, we used the template electrochemical method for preparing smooth, homogeneous and narrow Ni nanowires (Fig. 5.3). Nickel was electrodeposited by chronoamperommetry at E = -1.05 V (Fig. 5.4.a) within the pores of a polycarbonate membrane (Φ = 110 nm) from an electrochemical bath containing Ni sulfate hexahydrate ($NiSO_4.6H_2O$) and boric acid (H_3BO_3)[12]. As shown in Figure 5.4.b, the length of the Ni nanowires can be easily controlled by the electrodeposition time.

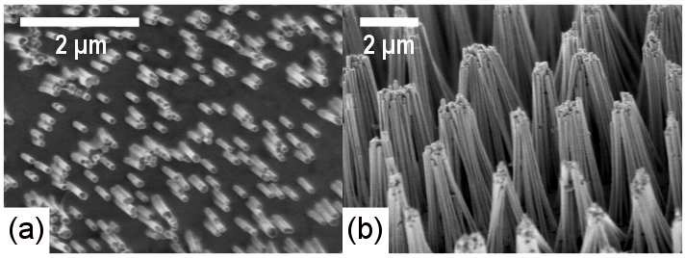

Figure 5.3 *SEM pictures of Ni nanowires after dissolution of the template membrane (a) electrodeposition time = 200 seconds (L_{Ni} ≈ 800 nm), (b) electrodeposition time = 600 seconds (L_{Ni} ≈ 5 µm).*

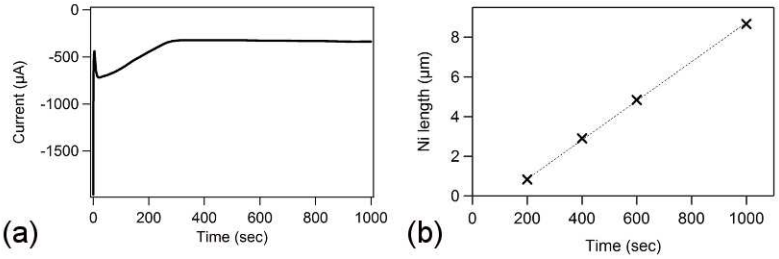

Figure 5.4 *(a) Current-time curve recorded during Ni electrodeposition within the pores of a 110 nm diameter PC membrane. (b) Length of the Ni nanowires in function of electrodeposition time.*

c) Synthesis of Ni-PPy nanowires

Assuming that the chemical pre-treatment of Ni by 3PPA molecules is also efficient in confined environment, the adhesion of the polymer segment on Ni nanowires should depend on the homogeneity and compactness of the deposited monolayer. In order to determine the optimal *[3PPA]* to be used for the formation of a SAM that will efficiently slow down the oxidation and re-dissolution of the nickel without stopping the electropolymerization process, we carried out pyrrole electropolymerization on Ni nanowires, which were previously treated with 3PPA solutions of four different concentrations 2, 10, 50 and 250 mM. In all cases, the Ni nanowires, embedded in the PC membrane, were immersed in the 3PPA solution for 18 hours and then, an aqueous solution containing 0.02 M pyrrole and 7.10^{-4} M sodium dodecylsulfate (SDS) was used for the electrosynthesis of the polymer. According to the calibration curve presented in Figure 5.4.b, 8-10 µm nickel nanowires were prepared. Polypyrrole (PPy) nanowires were deposited by sweeping the potential between 0 and 0.85 V at a scan rate of 400 $mV.s^{-1}$ during 1000 cycles. The morphological observations performed by TEM on this series of samples are gathered in Figure 5.5.

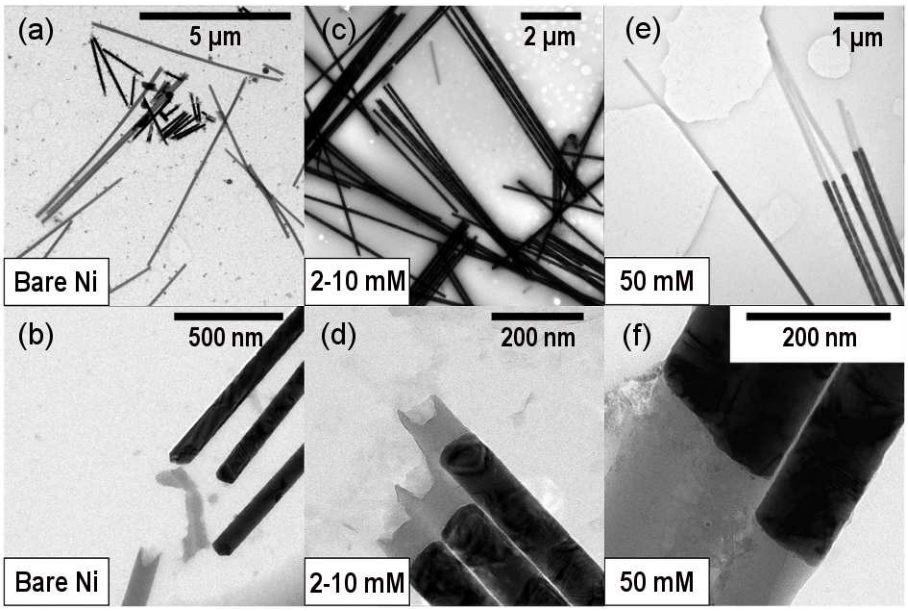

Figure 5.5 *TEM images of Ni-PPy nanowires synthesized using different [3PPA] for the SAM deposition.*

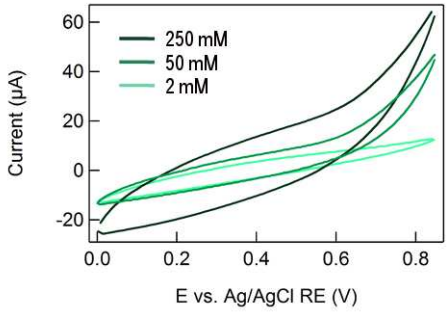

Figure 5.6 *Effect of the [3PPA] on the last potential cycle performed during electropolymerization.*

When the electropolymerization of pyrrole was directly carried out on bare nickel nanowires, only one-component PPy nanowires and one-component Ni nanowires were found, but no bi-segmented Ni-PPy nanowires (Figure 5.5 a and b). This observation surely results from Ni oxidation and partial re-dissolution occurring during the electropolymerization process. As this phenomenon is particularly important at the beginning of the polymer electrosynthesis, it leads to the formation of very fragile Ni/PPy interfaces and consequently to nanowires broken at the metal/polymer interface. When using a 2 or 10 mM 3PPA solution for the formation of a SAM at the top of the Ni nanowire before starting PPy electropolymerization, a few entire Ni-PPy nanowires are obtained, but in most cases, with very short PPy segments bound to Ni nanowires (Figure 5.5 c and d) Moreover, a large number of one-component PPy nanowires are still present, demonstrating the weakness of the metal/polymer interface. By increasing the *[3PPA]* to 50 mM, a much larger number of unbroken Ni-PPy bi-segmented nanowires were obtained (Figure 5.5 e and f), though we did not succeed in reaching results as good as those obtained previously when using noble metals. Indeed, no adhesion improvement was achieved at a higher *[3PPA]* of 250 mM. Therefore, we further used a 3PPA concentration of 50 mM for monolayer deposition.

We also compared the cyclic voltammetry (CV) curves recorded for the various polymer syntheses of Figure 5.5 and, found that the SAM compactness had an influence on the pyrrole electropolymerization rate. The CV curves presented in Figure 5.6 correspond to the last cycle completed

during pyrrole electropolymerization for 2, 50 and 250 mM *[3PPA]*. We can notice that the current intensity in the potential range corresponding to efficient pyrrole electropolymerization (~ 0.6 to 0.8 V) increases with the *[3PPA]* used for the SAM deposition. That means that by increasing the homogeneity and compactness of the organic barrier onto the Ni, PPy growth is less hindered by Ni re-dissolution and is therefore faster. This trend can be correlated with the TEM observations that the length of PPy segment grown in similar conditions, increases with increasing *[3PPA]*.

To demonstrate the ability of the 3PPA monolayer in reducing the nickel oxidation and re-dissolution occurring at the positive potentials applied for polymer formation, pyrrole electropolymerization on bare and chemically pre-treated nickel nanowires was followed, at different steps of the process, by cyclic voltammetry (Figure 5.7). In the first cycle recorded during electropolymerization on bare Ni nanowires, nickel oxidation starts at a potential situated around + 0.3 V, while in the following sweeping cycles, it appears at higher potentials (~ + 0.5 V). This indicates the formation of an oxide layer that partially passivates the Ni electrode toward oxidation but does not suppress it completely. As a consequence, the interface with PPy is based on metal oxide – polymer mixture, that leads, as already shown by TEM, to a very poor adhesion between PPy and Ni and, consequently to the formation of broken nanowires. For comparison, the CV curves recorded during electropolymerization of pyrrole onto 3PPA pre-treated Ni segments are presented in Figure 5.7.b. Though in the first cycle a weak nickel oxidization peak (lower oxidation current than on bare Ni) still appears at a potential around + 0.5 V, the phenomenon does not occur anymore during the following cycles. Moreover, in this case, the recorded CV cycles look like typical curves recorded during electropolymerization of pyrrole on noble metals.

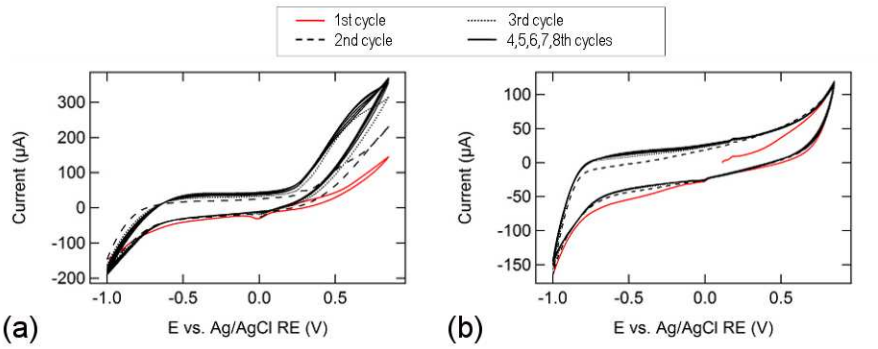

Figure 5.7 *Cyclic voltammograms recorded during electropolymerization of pyrrole on (a) 90 nm diameter bare Ni nanowires, (b) 3PPA-modified Ni nanowires. Scan rate = 50 mV.s^{-1}.*

5.2.2 Synthesis of magnetic tri-segmented nanowires

a) A noble metal as upper segment – Synthesis of Ni-CP-Noble metal nanowires

With the aim of producing tri-segmented nanowires containing one magnetic segment, we considered the synthesis of two types of nanostructures: Ni-PPy-Pt and Ni-PEDOT-Au nanowires. This choice was based on the observed particular affinities between PPy and Pt and between PEDOT and Au (see chapters 2 and 3). The aimed nanostructures were elaborated following the process schematically illustrated in Figure 5.8.

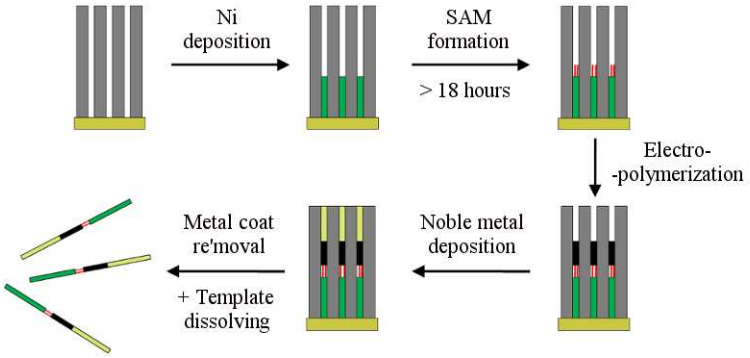

Figure 5.8 *Scheme describing the synthesis of tri-segmented Ni-CP-Noble metal nanowires.*

The resulting Ni-PPy-Pt and Ni-PEDOT-Au nanostructures were characterized by SEM and TEM. As shown in Figure 5.9, entire nanowires are observed for both types of nanostructures. Nevertheless, the percentage of unbroken nanowires remains low compared to the tri-segmented nanowires containing only noble metals, reported in the previous chapters. Tri-segmented nanowires including polymer and metal segments of various lengths were then prepared. When the length of the conjugated polymer segment and the top noble metal segment are increased, the strength of the chemically modified Ni/CP interface is subjected to increasing strain. This leads for Ni-PPy-Pt nanostructures to the breaking of the bottom magnetic metal/polymer interface, while the Ni/PEDOT interfaces withstand this strain and, entire very long Ni-PEDOT-Au nanowires can be obtained (Figure 5.9.c). This higher strength of the Ni/PEDOT interfaces might be due to the fact that the PEDOT segment is more flexible than the PPy one, and could easily bend as illustrated in Figure 5.9.d.

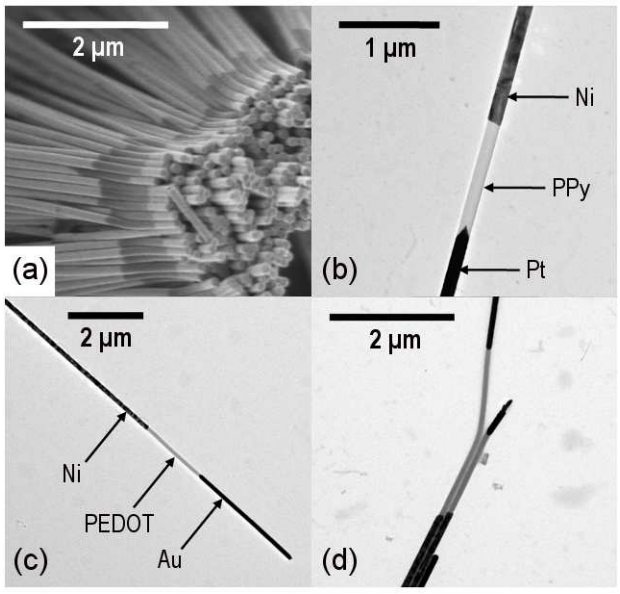

Figure 5.9 *(a) SEM picture of 110 nm diameter tri-segmented Ni-PPy-Pt nanowires. (b) TEM picture of a 110 nm diameter tri-segmented Ni-PPy-Pt nanowire. (c) TEM pictures of Ni-PEDOT-Au nanowires (d) with a bended polymer junction.*

It is important to note that in this study, the CP segments were prepared under quasi-identical or identical electrosynthesis conditions than those used in chapters 2 and 3. But, we know that some parameters such as, the addition of the 3PPA molecule in the solution of electropolymerization, the scanning rate or the value of the upper potential limit used in cyclic voltammetry, could have a strong impact on the polymer adhesion to the Ni nanowires. This should be further investigated if we want to increase the number of resulting unbroken long tri-segmented nanowires including a Ni segment. However, the results obtained up to now, allow us to go a step further and try to prepare tri-segmented nanowires including two different magnetic segments.

b) A magnetic metal as upper segment – Synthesis of Ni-CP-Co nanowires

Our next objective was then to develop a process allowing the preparation of tri-segmented nanowires containing a very short polymer junction sandwiched between two magnetic segments of different nature, typically Ni-CP-Co nanowires. To obtain a magneto-resistance effect in these tri-segmented nanostructures, all three components should satisfy a requirement of length, as illustrated in Figure 5.10.a: a long Ni segment, to give rise to a magnetization of type “form”, directed along the axis of the nanowire, an organic junction of limited thickness (≤ 100 nm), and a short Co segment with a magnetization of type “magneto-crystalline”, directed perpendicular to the axis of the nanowire. A magneto-resistance effect can then occur, as shown in Figure 5.10.b: at zero magnetic field (H = 0), the current does not cross the organic junction. Applying a magnetic field (H = sat) aligns the magnetization of Co in the axis of the nanowire, which strongly decreases the resistance of the system.

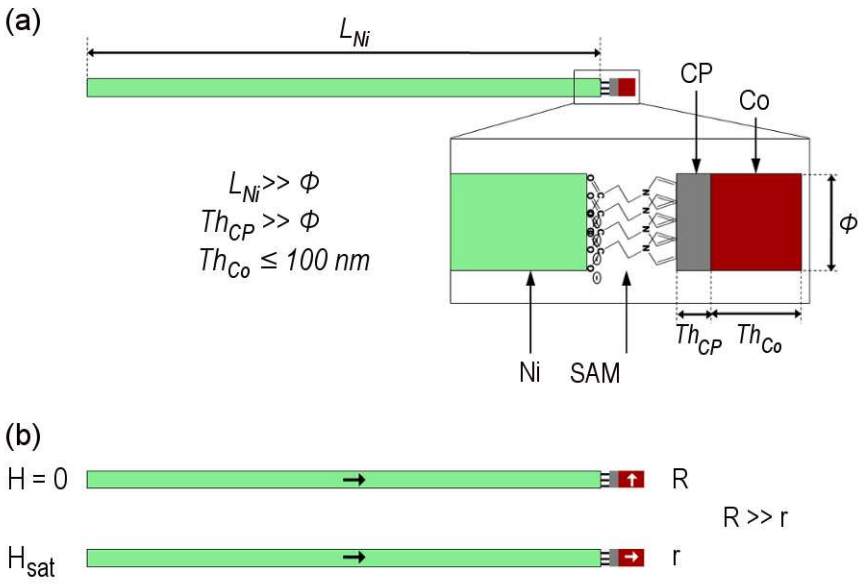

Figure 5.10 *(a) Schematic representation of the aimed tri-segmented Ni-PPy-Co nanowire. (b) Principle of the aimed magneto-resisance effect in the tri-segmented Ni-CP-Co nanowires: 1) At zero magnetic field, magnetizations of the two magnetic materials are perpendicular and the nanowire is strongly resistive. 2) Applying the magnetic field aligns the magnetization of the two materials, which strongly decreases the resistance of the nanowire.*

Here, we report our first results on the preparation of Ni-PPy-Co and Ni-PEDOT-Co nanowires synthesis by an all-electrochemical process. First, in order to evaluate the feasibility, tri-segmented nanowires with magnetic metal and polymer segments of different lengths were prepared. SEM and TEM pictures of typical resulting nanostructures are gathered in Figure 5.11. The SEM picture on Figure 5.11.a shows bundles of PPy-based nanostructures with some entire tri-segmented Ni-PPy-Co nanowires, but a majority of bi-segmented Ni-PPy nanowires. TEM picture on Figure 5.11.b confirms what was largely observed for Ni-PPy-Co nanowires: breaking at the PPy/Co interfaces and, never at the Ni/PPy ones. The situation was quite different when using PEDOT as CP segment. Indeed, even with long PEDOT segments, entire Ni-PEDOT-Co nanowires were observed (Figure 5.11.c). On this figure, which corresponds to a TEM image of a freshly prepared Ni-PEDOT-Co nanowire sample (observation made on the day of

the synthesis), the contrast between the cobalt and the polymer is enough high to easily distinguish the two materials. However, when observing the same sample ten days after the synthesis (Figure 5.12.a), it is much more difficult to unambiguously distinguish these two material (Co and PEDOT) segments. This lost of contrast, accompanied by the apparition of dark "spheres", as illustrated in Figure 5.12.b, results from the fast oxidation and degradation of Co when kept in air. In order to confirm the segmented composition of the nanowires, we performed TEM-EDX analysis. As illustrated on Figure 5.12.c, EDX unambiguously reveals the presence of the characteristic element for each of the three segments (Ni, S for PEDOT and, Co). The traces of sulfur and chlorine found in the Co segment are probably due to the formation of Co complexes with sulfate and chlorine ions, coming from cobalt and PEDOT electroplating solutions, respectively.

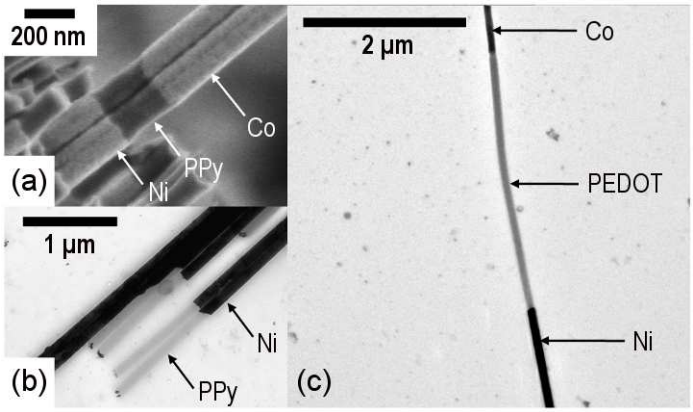

Figure 5.11 *(a) SEM pictures of 110 nm diameter Ni-PPy-Co nanowires. (b) TEM picture of 110 nm diameter Ni-PPy-Co broken at the PPy/Co interfaces. (c) TEM picture of a 110 nm diameter Ni-PEDOT-Co nanowire.*

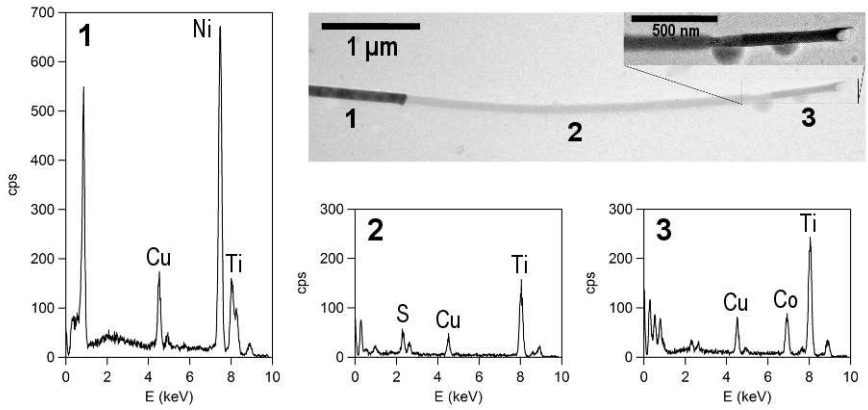

Figure 5.12 *EDX analysis of a Φ = 110 nm Ni-PEDOT-Co nanowire: (a) TEM picture of the analyzed tri-segmented nanowire. (b) Zoom on the cobalt segment. (c) EDX spectra recorded on each segment of the tri-segmented nanowire. Only the K_α X-rays of the elements that identify each material are indicated. The presence of Ti and Cu elements with K_α X-rays at 4.5 and at 8 keV comes from the titanium holder and the copper grid.*

The next step in our work on the Ni-CP-Co nanowires was to reduce the length of the polymer in order to obtain tri-segmented nanostructures presenting the configuration illustrated in Figure 5.10: a very short polymer junction sandwiched between the two different magnetic segments. In order to produce polymer junctions of very short length, the potential scan rate used for the electropolymerization was increased. This synthesis parameter change has two interesting effects: on the one hand, it allows obtaining nanowires of more uniform length and, on the other hand, the upper part of the polymer junction is flatter (and not a meniscus as previously observed). So, by sweeping the potential at 800 $mV.s^{-1}$ instead of 400 $mV.s^{-1}$ and, by adjusting the number of performed cycles, we succeeded, for the first time, to prepare entire Ni-PPy-Co nanowires (Figure 5.13) presenting a very short polymer junction (≈ 20 nm) without any short-circuit.

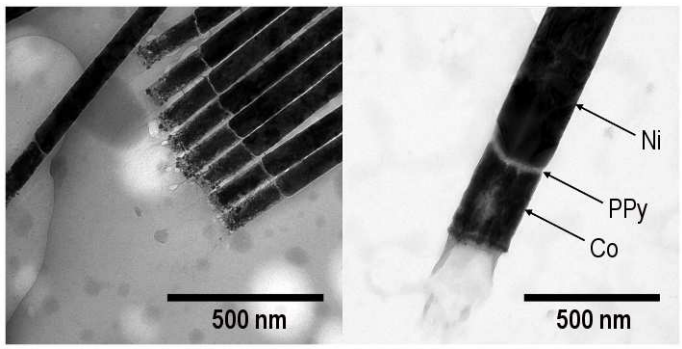

Figure 5.13 *TEM pictures of Ni-PPy-Co nanowires with a very short polymer junction.*

As PPy/Co interface is a second zone of weakness in the tri-segmented Ni-Polymer-Co, the electrodeposition of a quite short Co segment onto the polymer junction is preferable. Up to now, Co nanowires were synthesized by chronoamperometry at an applied potential of - 0.95 V. Upon these synthesis conditions, the growing of Co nanostructures is rather fast as shown in the current-time curve presented in Figure 5.16. This I-t curve corresponds to the electrodeposition of the Co segments ($L_{Co} \approx 300$ nm) appearing on the TEM pictures of Figure 5.14. Based on this chronoamperogram, we estimated the growth rate of Co nanowire in nanopores of 110 nm to about 12 nm.s^{-1}. Despite this fast Co growth rate, it is possible to obtain relatively short Co segments by reducing the duration of the electroplating to only a few seconds.

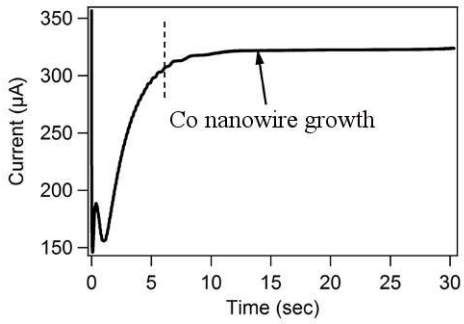

Figure 5.14 *Current-time curve recorded during the electrodeposition of Co at E = -0.95V vs. Ag/AgCl within nanopores of 110 nm.*

5.3 Conclusions

In this work, we present the use of a template-based method for the electrochemical synthesis of a variety of new magnetic-conjugated polymer nanowires of controlled dimensionality through the sequential synthesis of the multiple segments. In order to deposit PPy and PEDOT onto an active metal such as Ni and, get mechanically robust interfaces, we developed a strategy consisting in a two-step process. Prior to the polymer electropolymerization, an organic monolayer of 3PPA was deposited on the Ni surface. Though, the process could still be improved, it already allows, as proved by SEM and TEM, the preparation of various magnetic conjugated polymer based nanostructures: Ni-PPy-Pt, Ni-PEDOT-Au, Ni-PPy-Co, Ni-PEDOT-Co. All these multi-component nanostructures present interesting potential applications. On the one hand, Ni-conjugated polymer-noble metal nanowires, where each segment possesses unique physical and chemical properties (the noble metal offers excellent conductivity, the conjugated polymer brings stimuli-sensitivity and, the ferromagnetic nickel segment imparts the possibility to magnetically position and align the nanowires on a device) could be useful multi-functional nanostructures in the field of biosensors. On the other hand, the successful synthesis of tri-segmented Ni-PPy-Co nanowires with a very short PPy junction and a small Co segment paves the way to interesting investigations in organic spintronics. These studies are currently carried out.

5.4 Experimental part

Materials: Polycarbonate track-etched membranes with a thickness of 21 μm, a pore density of 10^9 pores.cm^{-2} and an average pore size of 60 or 110 nm, supplied by it4ip, were used as nanoporous templates. Pyrrole (Acros, 99%) and the 3,4-ethylendioxythiophene (EDOT, Sigma-Aldrich) were purified immediately before use by passing it through a microcolumn constructed from a Pasteur pipet, glass wool, and activated alumina. The lithium perchlorate ($LiClO_4$, Acros), sodium dodecylsulfate (Acros), boric acid (H_3BO_3, UCB), nickel (II) sulfate hexahydrate ($NiSO_4.6H_2O$, Acros),

cobalt (II) sulfate heptahydrate ($CoSO_4.7H_2O$, Sigma-Aldrich), potassium chloride (KCl, Acros), potassium hydrogenophosphate (K_2HPO_4, Acros), hydrogen tetrachloroaurate ($HAuCl_4$, Sigma Aldrich, 99,9%), and dichloromethane (CH_2Cl_2, Acros) were used without any prior purification. De-ionized water was used to prepare all aqueous solutions. The iodine solution was prepared by dissolving 6 g of potassium iodide (KI, Merck) and 1.5 g of iodine (I_2, Sigma-Aldrich) in 60 ml of de-ionized water.

Magnetic Nanowires Fabrication: Nickel and cobalt segments were deposited in de-ionized water from solutions containing 0.5 M boric acid (H_3BO_3, UCB) and respectively nickel (II) sulfate hexahydrate (0.85 M $NiSO_4.6H_2O$, Acros) and 0.85 M cobalt (II) sulfate heptahydrate ($CoSO_4.7H_2O$, Sigma-Aldrich). Nickel was electrodeposited at a constant potential of -1.05 V. The electrodeposition of Co nanowires was carried out by chronoamperommetry at a potential of -0.95 V.

Synthesis of the 3-(Pyrrol-1-yl)Propanoic Acid (3PPA)[7,8]: 25 g (0.2 mol) of N-(2-Cyanoethyl)-pyrrole ($C_7H_8N_2$, Acros) and 60 mL of a solution of potassium hydroxide 6.7 M were brought to the reflux until the organic phase disappeared (about 5 hours). To the resulting cooled amber transparent solution, 18 mL of water was added. Then the solution was acidified until a pH of 5 with hydrochloric acid 8 M. The crude product was extracted five times with diethyl ether. The resulting organic phase was dried with sodium sulfate anhydrous and evaporated under reduce pressure to lead to a beige product. Re-crystallization was then carried out in hot n-heptane (90-100°C). Nucleic magnetic resonance (NMR) was used to identify the product. NMR spectra were recorded at 300 MHz for ^1H and 75 MHz for ^{13}C on a Bruker Avance with a 5 mm BBFO probe gradients-z. ^1H NMR ($CDCl_3$): δ 2.84 (t, J = 6.9 Hz, 2H); 4.20 (t, J = 6.9 Hz, 2H); 6.15 (t, J = 2.1 Hz, 2H); 6.70 (t, J = 2.1 Hz, 2H). ^{13}C NMR ($CDCl_3$): δ 36.2 (CH_2-COOH); 44.5 (CH_2-N); 108.6 (C_β); 120.5 (C_α).

Verification of the SAM Grafting on Nickel: More or less compact monolayers of 3-(Pyrrol-1-yl)propanoate were deposited on freshly prepared nickel plates by immersing the substrates during 18 hours in aqueous solutions containing the molecule 3-(Pyrrol-1-yl)propanoic acid in various

concentrations from 2 to 50 mM (pH fixed at about 12[*]). Electrochemical probe used to confirm the monolayer deposition on nickel was the Fe^{III}/Fe^{II} redox couple. Warning bath contained 2.5 mM potassium ferrocyanide (II) trihydrate ($K_4Fe(CN)_6.3H_2O$, Acros) and 0.1 M lithium perchlorate ($LiClO_4$, Acros) in de-ionized water.

[*] Different concentrations in NaOH were used to adjust the pH of the solutions for the monolayer deposition. Their values were calculated as follows. C_o is the concentration of 3-(Pyrrol-1-yl)propanoic acid (3PPAH). We first considered the acid-base reaction occurring when 3-(Pyrrol-1-yl)propanoic acid (3PPAH) is dissolved in a solution of NaOH:

$$3PPAH + OH^- \text{ give } 3PPA^- + H_2O$$

The conservation of matter requires: $[3PPAH] + [3PPA^-] = C_o$ (1)

The solution is electrically neutral: $[H_3O^+] + [Na^+] = [3PPA^-] + [OH^-]$ (2)

We write the definition of the acidity constant of the couple ($3PPAH/3PPA^-$):

$$K_a = [3PPA^-] [H_3O^+] / [3PPAH] \quad (3)$$

As the sodium ions are chemically inert, their concentration provides access to the concentration of NaOH necessary to adjust the pH. By combining the equations (1), (2) and (3), the concentration of NaOH is expressed as a function of concentration of 3PPAH and pH:

$$[NaOH] = [Na^+] = C_o / (1 + [H_3O^+] / K_a) + K_e / [H_3O^+] - [H_3O^+] \quad (4)$$

With $K_e = [H_3O^+] [OH^-]$ the ionic product of water.

The pK_a of the couple ($3PPAH/3PPA^-$) is supposed close to that of acetic acid (≈4.8).

At pH = 12, the equation (4) simplifies to:

$$[NaOH] \# C_o + 10^{pH-14} = C_o + 0.01$$

The table below reports the concentrations of NaOH used to adjust the pH to 12 for the different tested concentrations of 3PPAH.

Table 5.2 *Table reporting the composition of different solutions used for the SAM deposit on nickel.*

C_o (mM)	[NaOH] (M)
2	0.012
6	0.016
10	0.02
50	0.06
250	0.26

Preparation of Tri-segmented Ni-PPy-Pt, Ni-PEDOT-Au, Ni-PPy-Co and Ni-PEDOT-Co nanowires: All electrochemical experiments were performed with a CHI660B Electrochemical Workstation (CH Inc.) in a conventional one-compartment cell at room temperature with a Pt disk counter electrode and a Ag/AgCl reference electrode. A 300 nm thick layer of gold evaporated on one side of the polycarbonate membrane served as working electrode. Magnetic nanowires were prepared as described above. Electropolymerization of pyrrole was carried out by cyclic voltammetry from an aqueous solution containing 0.1 M $LiClO_4$, 0.02 M pyrrole and 7.10^{-4} M SDS. The potential was swept between 0 and 0.85 V with a scan rate, if it is not mentioned, of 400 $mV.s^{-1}$. Electropolymerization of EDOT was performed by using an electrolyte containing 0.1 M $LiClO_4$ and 0.014 M EDOT and by sweeping the potential between 0.2 and 1.1 V at a scan rate of 400 $mV.s^{-1}$. Electrodeposition of Au was performed by cycling the potential of the working electrode from 0.7 to 0 V at 200 $mV.s^{-1}$ using a home-made cyanide free solution (0.1 M KCl, 0.1 M K_2HPO_4, and 0.03 M $HAuCl_4$ in de-ionized water). Electrodeposition of Pt was accomplished potentiostatically at -0.2 V using a home-made bath (0.01 M $Na_2PtCl_6.H_2O$ and 0.5 M H_2SO_4 in de-ionized water).

Structural Analysis: The dimensions and morphology of the nanowires were studied by transmission electron microscopy (TEM) after dissolution of the PC template. TEM pictures were obtained using a LEO 922 transmission

electron microscope (Carl Zeiss SMT Inc.) operating at 200 kV. After removing the evaporated metal layer with iodine solution, and dissolving the template in dichloromethane, two or three drops of the resulting nanowires suspension were placed on a carbon film grid (Agar Scientific Ltd.). Energy dispersive X-ray spectroscopy (EDX) experiments were carried out with the LEO 922 TEM equipped with an INCA x-sight detector (Oxford Instruments).

References

[1] N. I. Kovtyukhova, T. E. Mallouk, *Chem. Eur. J.* **2002**, *8*, 4354.

[2] M. A. Bangar, C. M. Hangarter, B. Yoo, Y. Rheem, W. Chen, A. Mulchandani, N. V. Myung, *Electroanal.* **2008**, *21*, 61.

[3] a) B. R. Martin, D. J. Dermody, B. D. Reiss, M. Fang, L. A. Lyon, M. J. Natan, T. E. Mallouk, *Adv. Mater.* **1999**, *11*, 1021. b) S. Park, S.-W. Chung, C. A. Mirkin, *J. Am. Chem. Soc.* **2004**, *126*, 11772. c) S. J. Hurst, E. K. Payne, L. Qin, C. A. Mirkin, *Adv. Mater.* **2006**, *45*, 2672. d) X. Wang, C. S. Ozkan, *Nano Lett.* **2008**, *8*, 298.

[4] a) T. Zalewska, A. Lisowska-Oleksiak, S. Biallozor, V. Jasulaitiene, *Electrochimica Acta* **2000**, *45*, 4031. b) F. Lallemand, D. Auguste, C. Amato, L. Hevesi, J. Delhalle, Z. Mekhalif, *Electrochimica Acta* **2007**, *52*, 4334. c) F. Lallemand, F. Plumier, J. Delhalle, Z. Mekhalif, *Appl. Surf. Sci.* **2008**, *254*, 3318.

[5] a) S. Pramanik, C.-G. Stefanita, S. Patibandla, S. Bandyopadhyay, K. Garre, N. Harth, M. Cahay, *Nature Nanotech.* **2007**, *2*, 216. b) W. J. M. Naber, S. Faez, W. G. van der Wiel, *J. Phys. D Appl. Phys.* **2007**, *40*, R205. c) S. Sanvito, *Nature Mater.* **2007**, *6*, 803.

[6] Z. Mekhalif, J. Delhalle, P. Lang, F. Garnier, J.-J. Pireaux, *Synth. Met.* **1998**, *96*, 165.

[7] S. Maeda, R. Corrada, S. P. Armes, *Macromolecules* **1995**, *28*, 2905.

[8] S. Roux, P. Audebert, J. Pagetti, M. Roche, *New J. Chem.* **2000**, *24*, 877.

[9] T. M. Whitney, J. S. Jiang, P. C. Searson, C. L. Chien, *Science* **1993**, *261*, 1316.

[10] R. Ferré, K. Ounadjela, J. M. George, L. Piraux, S. Dubois, *Phys. Rev. B* **1997**, *56*, 14066.

[11] T. N. Narayanan, M. M. Shaijumon, L. Ci, P. M. Ajayan, *Nano. Res.* **2008**, *1*, 465.

[12] L. Piraux, A. Encinas, L. Vila, S. Mátéfi-Tempfli, M. Mátéfi-Tempfli, M. Darques, F. Elhoussine, S. Michotte, *J. Nanosci. Nanotechnol.* **2005**, *5*, 372.

Chapter 6

General conclusions and prospects

6.1 General conclusions

The first main objective of this thesis was to develop the synthesis of solid nanowires (NWs) of different conjugated polymers (CPs) with a sufficiently good structural quality that allows their integration into more complex one-dimensional (1D) multi-segmented nanostructures. A special attention was thus paid to the optimization of the synthesis parameters of CPs nanowires in order to improve the mechanical robustness of the various metal/CP interfaces prepared in this work. In this manuscript, we successively described the preparation of various multi-striped systems combining various metals (gold (Au), platinum (Pt), nickel (Ni) and cobalt (Co)) and different CPs (polypyrrole (PPy), poly(3,4-ethylenedioxythiophene) (PEDOT) and polyaniline (PANI)). Given the specific properties of each material, these multi-component NWs are interesting systems for different potential applications, in particular, in the field of nano-electronics. In this respect, a study of the electrical transport properties of a large variety of these multi-segmented NWs has been carried out, in collaboration with our colleagues, Loïk Gence and Sorin Melinte from UCL-DICE lab.

6.1.1 Synthesis and structural characterization aspects

Although numerous and diverse synthetic routes exist for synthesizing nanostructures, the template electrosynthesis method presents several advantages and, remains the only efficient technique for preparing multi-segmented NWs. As demonstrated all along this work, one major advantage of the exclusively electrochemical process for preparing hybrid nanowires is that the length of each segment as well as the total length of the hybrid nanowires can be easily varied from a few microns to only a few nanometers and, adjusted at the desired length. Numerous works showed that the electrosynthesis of PPy, PEDOT or, PANi by chronoamperometry, naturally leads to the formation of nanotubes.[1] Therefore, in order to get solid CP nanowires, one originality of our study was to resort to another electrochemical technique, cyclic voltammetry, for electrodepositing the CPs

[1] a) C. R. Martin, *Science* **1994**, *266*, 1961. b) J. Duchet, R. Legras, S. Demoustier-Champagne, *Synth. Met.* **1998**, *98*, 113.

within nanoporous membranes. We showed that the CP morphology strongly depended on several electrosynthesis parameters.

More precisely, in the case of PPy and PEDOT (chapters 2 and 3), it appeared that by varying the potential scan rate used during the electropolymerization, the structure of the growing end of the polymer segment could be tuned from a long meniscus shape to a more flat one. This top-end morphology had, of course, a strong impact on the strength of the interfaces between the conjugated polymer and the top metallic segment deposited on it. Therefore, by optimizing the electrosynthesis conditions, we succeeded in forming strong conjugated polymer/metal interfaces by embedding the metal into the conical end of the polymer segment. When preparing tri-segmented metal-CP (PPy or PEDOT)-metal nanowires, it appeared that the bottom metal/CP interface was always flat and that its strength depends on the nature of the metal used (e.g. Au/PEDOT interfaces were strong due to the specific and strong interactions between Au and the S atoms in PEDOT) and, on the diameter of the nanowires. Thanks to the improvement of the mechanical strength of each materials interface, we were able to prepare very narrow multi-segmented nanostructures ($\Phi < 50$ nm) based on noble metals and Ppy, as well as, tetra-segmented NWs including a polymer heterojunction (Au-PEDOT-PPy-Au NWs) that present different electrical properties than larger NWs (see § 6.1.2).

Electropolymerization of pyrrole and EDOT on active metals, such as nickel, was much more difficult than on noble metals, because the oxidation potentials of these metals are much lower than that of the conjugated monomers. Consequently, dissolution of the metal occurs before electropolymerization begins. Therefore, in order to form homogeneous and adherent CP layers onto oxidizable metals, we developed a strategy based on a chemical pre-treatment of the nickel segment prior to pyrrole or EDOT electropolymerization (Chapter 5). By this way, we successfully prepared different original tri-segmented nanostructures, such as systems containing one magnetic segment, Ni-PPy-Pt and Ni-PEDOT-Au nanowires and, for the first time, systems containing two different magnetic metals: Ni-PPy-Co and Ni-PEDOT-Co nanowires.

As reported in Chapter 4, the synthesis of PANI nanowires was rather complex. Indeed, the porosity that characterizes the upper part of PANI NWs, leading to bad quality CP/metal interfaces was a big problem that we

did not succeed to fully solve. Nevertheless, our careful study of the influence of various electrosynthesis parameters, such as monomer and electrolyte concentrations, potential scan range and sweeping rate, allows us to identify experimental conditions for successfully preparing some tetra-segmented PANI-based nanostructures, such as Pt-PANI-PPy-Au nanowires.

6.1.2 Electrical properties aspects

For physicists, 1D nanostructures are ideal systems for elucidating transport mechanisms and for studying structure-properties relationships in conducting materials. In collaboration with the DICE Lab, the electrical transport properties on single multi-segmented nanowires of various compositions have, therefore, been studied (or are still under investigation). In the present work, we mainly focus our attention on the systems based on noble metals and PPy and/or PEDOT.

In particular, the electrical behavior of Au-PPy-Au tri-segmented nanowires with diameters ranging between 40 and 90 nm was investigated. On one hand, variable temperature measurements have shown that the three-dimensional Mott variable range hopping model can explain the transport in PPy nanowires with diameter down to 50 nm. On the other hand, 40 nm diameter samples follow a power-law temperature dependence of the resistance, characteristic of the critical regime of disorder-induced metal-insulator transition, which indicates that a metallic behavior in smaller diameter is possible (Chapter 2).

Tri-segmented NWs based on PEDOT are, on average, an order of magnitude more conductive than the tri-segmented NWs based on PPy (0.4 and 0.04 $S.cm^{-1}$ as maximum values of conductivity, respectively). But, while the tri-segmented NWs exhibit symmetrical and linear *I-V* characteristics, tetra-segmented Au-PEDOT-PPy-Au present a more original electrical behavior. Indeed, we showed that their transport characteristics could be switched by changing the redox state of the two conjugated polymer blocks (Chapter 3).

6.2 Prospects

Given the enhanced electrical properties found for low diameter multi-segmented nanostructures, it should be very interesting to go on with the synthesis of robust sub-40 nm diameter NWs. Based on the whole results presented in this thesis, it appears that the best polymer candidate for very low diameter organic junction based systems should be PEDOT. Indeed, we think that its elastic properties (as illustrated in chapters 3 and 5) tend to decrease the tension at the metal/polymer interfaces and, consequently, reduce the risks of NWs breaking.

The mechanical strength of multi-segmented nanowires at the interfaces is a key point in the synthesis of these nano-objects. In this study, the estimation of their mechanical properties was carried out empirically, through the observation by electronic microscopy of fracture or not of the interfaces. Investigations on the mechanical properties of the multi-segmented nanowires using methods based on the atomic force microscopy should be considered.

Although there are still some problems to solve for preparing highly dense PANI NWs, the successful synthesis of tetra-segmented Pt-PANI-PPy-Au NWs paves the way to the preparation and characterization of other interesting tetra-segmented NWs, such as NWs based on a PANI-PEDOT polymer heterojunction. Taking advantage of the unique reversible acid-base properties of PANI, we can indeed expect to obtain original electrical properties from this new kind of multi-segmented nanowires

CPs are also known to be good candidates for different biological and biomedical applications. CPs functionalization was not discussed in this thesis manuscript, but the incorporation of bioactive molecules, either by entrapment or by covalent attachment, inside the polymer junctions of the multi-segmented NWs, may be considered to build biosensors. For that purpose, Ni-conjugated polymer-noble metal nanowires, where each segment possesses unique physical and chemical properties (the noble metal offers excellent conductivity, the conjugated polymer brings stimuli-sensitivity and, the ferromagnetic nickel segment imparts the possibility to magnetically position and align the nanowires on a device) could be particularly useful multifunctional nanostructures.

Finally, the successful synthesis of tri-segmented nanowires based on two different magnetic segments, such as Ni-PPy-Co NWs, with a very short PPy junction (down to 20 nm) paves the way to potential interesting applications in spintronics.

Appendix

Release process of the nanowires

A.1 Introduction

The hybrid multi-segmented nanowires are nano-objects with potential in many applications. The mechanical strength of these nanostructures is essential if we wish to use them as nano-components in electronic devices. To increase the chances of obtaining entire nanowires, a lot of efforts was focused on improving the strength of metal/polymer interfaces, as reported throughout this manuscript. In parallell to this study, technical progresses were made to improve the release of the nanowires from the polycarbonate membrane. Indeed, the state in which the nanowires are observed depends above all on this critical step during which the nanostructures are separated from the template but also from the metal layer serving as a working electrode during the electrochemical synthesis.

The different methods that were successively used to improve the nanowires release protocol are reviewed in this appendix.

A.2 An interface to weaken

With their quasi-1D geometry, the nanowires have original and attractive properties. But this high aspect ratio makes them subject to mechanical fractures. For the multi-segmented nanowires, areas of weakness are located at the interfaces joining materials most often of a different nature. However, in the system formed by the nanowires still embedded into the polycarbonate membrane coated with a metal layer, there is another area of potential weakness : the interface that the metal layer forms with the first metal segment of the nanowire. Figure A.1 represents the system formed by tri-segmented metal-polymer-metal nanowires still embedded in PC membrane coated with the chromium-gold layer. The different areas of weakness, rated "I" as "interface", are show on this scheme : I_1 is the metal coat/first metal segment interface and I_2 and I_3 correspond to the bottom metal/polymer and top polymer/metal interfaces, respectively.

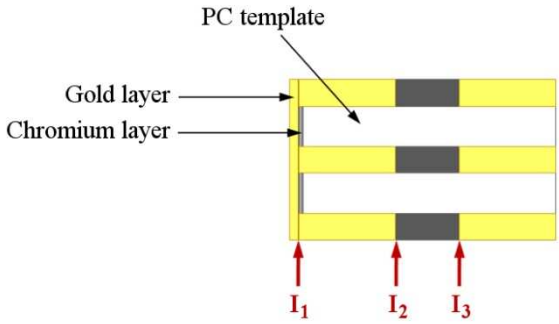

Figure A.1 *Schematic representation of the system formed by tri-segmented metal-polymer-metal nanowires still embedded in the PC membrane. I_1, I_2 and I_3 are the three interfaces described in the text.*

In such a system, the nanowires may break first or only at their most fragile interface. However, the chances of getting entire nanowires increase if the interface I_1 is weaker than the weakest interface of the tri-segmented nanowire (e.g. I_2 in the case of nanowires based on PPy or PEDOT). Otherwise (I_1 stronger than I_2), the recovered nanowires have a missing segment, the bottom metallic section, as this part remains attached to the base metal layer, forming a "brush" of metallic nanowires. Figure A.2 illustrates these two cases.

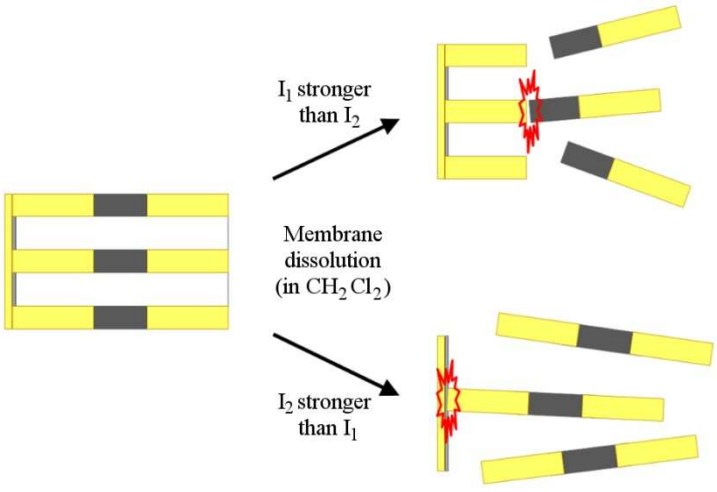

Figure A.2 *Schematic representation of the two observed cases after the PC membrane dissolution depending on the relative strength of the interfaces.*

Therefore, in addition to our efforts to improve the strength of the metal/polymer interfaces, our objective was to find an effective route to weaken the interface I_1 prior to the dissolution of the PC template. In this respect, various methods were tested and are presented in the following section.

A.3 The different routes to release the nanowires

Three different methods were successively suggested to perform the release of the nanowires from the template. Chronologically, there was a first process that we called "the membrane swelling/unswelling". Then, the use of a sacrificial foot was considered. Finally, the chemical destruction of the evaporated metal layer was tested.

A.3.1 The "membrane swelling/unswelling" process

This first method involves immersing alternately and repeatedly the sample in methanol and de-ionized water. When soaked in methanol, the PC membrane swells, which has the effect of bending the layer of evaporated gold to which the template is bound. Then the water has the opposite effect, ie a shrinking of the template (Figure A.3). Thus, from a bath to another, the layer of evaporated gold undergoes deformations which tend to weaken it. As it is shown in Figure A.4, this degradation logically depends on the thickness of this gold coating, and therefore on the pore diameter of the membranes. If for pores of diameter 30 nm, the gold layer is usually easily detached from the PC membrane, the process is less efficient and more random for larger diameters. For diameters larger than or equal to 100 nm, the gold layer often remains precisely in the area where the nanowires were electrodeposited (Figure A.4.c).

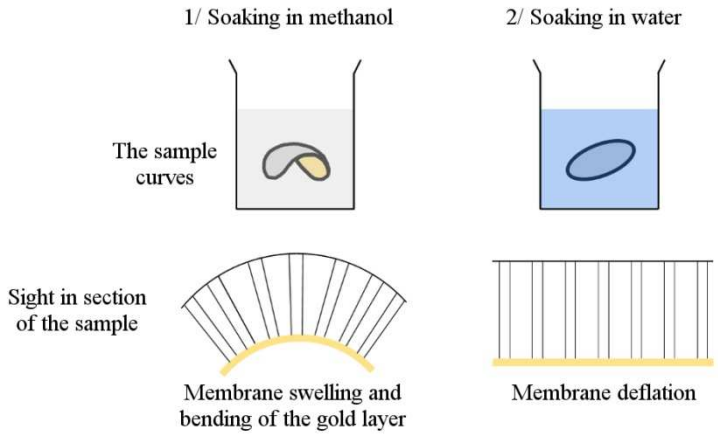

Figure A.3 *Principle of the "Membrane swelling/unswelling" process.*

Figure A.4 *Pictures of the evaporated gold layer after the process for different diameters: (a) 30 nm, (b) 70 nm, (c) 100 nm. For each of the three samples, the underwent treatment was as follows: soaking in methanol (10 min) and soaking in de-ionized water (10 min) (x3).*

A.3.2 Use of a sacrificial foot

As the method described above does not provide full satisfaction, we considered the use of a sacrificial foot to release the nanowires. The principle of the sacrificial foot has already been used to release multi-segmented nanowires.[1] This process usually consists in specifically

[1] (a) D. J. Peña, J. K. N. Mbindyo, A. J. Carado, T. E. Mallouk, C. D. Keating, B. Razavi, T. S. Mayer, *J. Phys. Chem. B* **2002**, *106*, 7458. (b) X. Wang, C. S. Ozkan, *Nano Lett.* **2007**, *8*, 398.

destroying the sacrificial material in order to break the link between the desired nanowires and the metallic electrode. In the case of small diameter noble metal-polymer nanowires, it was difficult to find a material whose chemical destruction would be carried out without damaging any of the materials constituting the nanowires. Therefore, we considered the synthesis of a very short sacrificial foot of polymer which would form the most possible fragile interfaces with the evaporated gold layer or, in the best of cases with the nanowire synthesized afterwards (Interfaces called in $I_1^{'}$ and $I_2^{"}$ in Figure A.5, respectively). Depending on whether the break occurs on one or other of these interfaces, the nanowires are recovered with or without the sacrificial polymer foot as shown in Figure A.5.

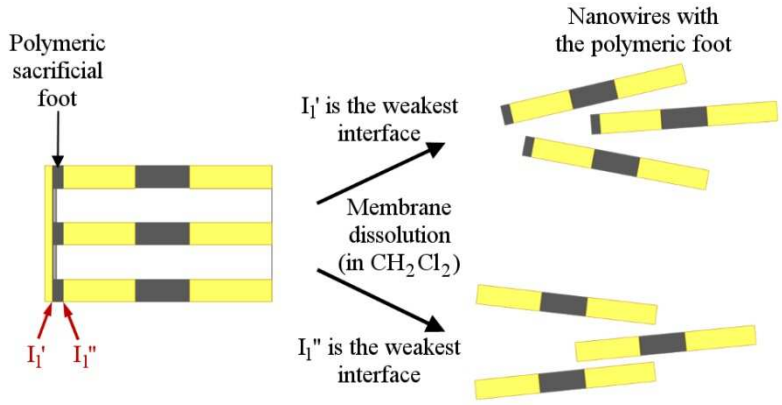

Figure A.5 *Schematic representation of the two cases found after the process of nanowire release using a polymeric sacrificial foot.*

To increase the chances of breaking at the interface $I_1^{"}$, the parameters for the electropolymerization must be chosen such that this interface is as flat as possible. In our investigations, we saw that this could be achieved in particular by playing on the potential scanning rate. The use of a polymeric sacrificial foot to release the nanowires was used for some samples, but the percentage of entire nanowires obtained by this route was generally large (> 50%). However, this process has the disadvantage of introducing an additional step in the synthesis.

A.3.3 Chemical destruction of the gold coating

The last technique we considered to release the nanowires is to chemically destroy the gold layer before dissolving the PC membrane in dichloromethane (See Figure A.6). For this, two types of oxidizing solutions were used. The first one is a solution of aqua regia (nitric acid HNO_3 + hydrochloric acid HCl) which quickly attacks the noble metals, and almost instantaneously oxidized metals. If the nanowires contain nickel or cobalt, a second oxidizing bath, a solution of iodine (I_2 + KI), which more specifically attacks gold, should be used. As some of the materials used in the composition of the nanowires are of the same nature as the layer to eliminate, the sample should not stay for a too long time in contact with the oxidizing solution to avoid damaging the nanowires themselves. Typically, for 100 nm diameter tri-segmented gold-polymer-gold nanowires, which corresponds to a 300 nm-thick gold layer to eliminate, about one minute and half into contact with aqua regia is sufficient to destroy the gold coat. The base of the first metallic segment comprising the tri-segmented nanowire is usually attacked by the oxidizing solution. As this first metal segment is shortened as a result of the chemical treatment, its length is generally provided greater.

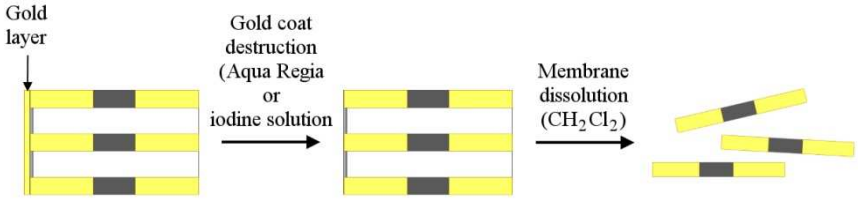

Figure A.6 *Shematic representation of the nanowire release process performed by chemically attacking the gold layer coated on the PC membrane.*

Of the three tested methods, this method of chemical attack of the gold coating was the most effective. For instance, the tri-segmented Au-PPy-Au nanowires, which were the first investigated systems presenting problems of interface strength, were systematically recovered with at least 50 % of entire nanowires when using this release route.

A.4 Conclusions

Different methods to release the nanowires from the template were tested during our investigations. The first one, which involves alternately soaking the sample in a solution of methanol and water prior to the dissolution of the PC membrane, is too uncertain for pore diameters above 70 nm. Indeed, for these diameters, the evaporated gold layer is too thick and can be hardly removed. Consequently, the nanowires usually break at the weakest of their metal/polymer interfaces. The use of a polymer sacrificial foot has proven quite effective, but requires an additional step in the synthesis. The chemical destruction of the evaporated gold layer prior to the template dissolution remains the most effective method for obtaining entire nanowires.

Curriculum Vitae

Vincent Callegari was born in Valence (France) in 1979. He obtained his Master in "Chimie Inorganique et Bio-Inorganique" at the Université Joseph-Fourier, Grenoble, in June 2004. In September 2004, he started his Ph. D program in the Laboratoire des Hauts-Polymères (POLY) at the Université Catholique de Louvain, Belgium, under the supervision of Professor Sophie Demoustier-Champagne. His thesis topic involved the synthesis and the characterization of multi-segmented metal-conjugated polymer nanowires as well as improving their mechanical strength. The results of this research are presented in this manuscript.

Publications

V. Callegari, L. Gence, S. Melinte, S. Demoustier-Champagne, "Electrochemically template-grown multisegmented gold-conducting polymer nanowires with tunable electronic behavior", *Chem. Mater.* **2009**, *21*, 4241.

D. Magnin, V. Callegari, S. Mátéfli-Tempfli, M. Mátéfli-Tempfli, K. Glinel, A. M. Jonas, S. Demoustier-Champagne, "Functionalization of magnetic nanowires by charged biopolymers", *Biomacromolecules* **2008**, 9, 2517.

L. Gence, V. Callegari, S. Faniel, A. Vlad, C. Dutu, S. Melinte, S. Demoustier-Champagne, V. Bayot, "Size related transport mechanisms in hybrid metal-polymer nanowires", *Phys. Stat. Sol.* (a) **2008**, 205, 1447.

V. Callegari, L. Gence, O. Reynes, S. Melinte, V. Bayot, S. Demoustier-Champagne, "Template electrosynthesis and structural characterization of hybrid metal-polymer nanowires", *Polymer Preprints ACS* **2007**, 48, 53.

L. Gence, S. Faniel, C. Gustin, S. Melinte, V. Bayot, V. Callegari, O. Reynes, S. Demoustier-Champagne, "Structural and electrical characterization of hybrid metal-polypyrrole nanowires", *Phys. Rev. B* **2007**, 76, 115415.

C. C. Buron, V. Callegari, B. Nysten and A. M. Jonas, “Resistance of poly(ethylene oxide)-silane monolayers to the growth of polyelectrolyte multilayers”, *Langmuir* **2007**, 23, 9667.

V. Callegari, C. Bucher, J.-C. Moutet, G. Royal, E. Saint-Aman, J. Pécaut, “Electrochemically induced motion in copper complexes of tetraferrocene-cyclam” *J. Solid State Electrochem.* **2005**, 9, 758.